THE EARTHQUAKE RESPONSE OF DETERIORATING SYSTEMS

Thesis by

Nathan Craig Gates

In Partial Fulfillment of the Requirements

for the Degree of

Doctor of Philosophy

California Institute of Technology

Pasadena, California

1977

(Submitted on March 29, 1977)

ACKNOWLEDGMENTS

For everything involved during my pursuit of a Ph.D., I praise and thank my Lord Jesus Christ. I gratefully acknowledge the special support and encouragement He has given me through His followers at Lake Avenue Congregational Church and in the Caltech Christian Fellowship.

I am especially grateful for my advisor, Professor W. D. Iwan, who has provided constant encouragement and guidance throughout my graduate studies. His example as a Christian, a scientist and an engineer means a great deal to me.

I want to thank the entire Faculty of Applied Mechanics and Civil Engineering for the excellent instruction I received. My thanks and appreciation are extended to all the secretaries in Thomas Laboratory for their gracious assistance. Special thanks to Sharon Vedrode for typing this. The assistance of Chuck Krousgrill in some of the computer calculations is also gratefully acknowledged.

My thanks to the National Science Foundation for their financial support of my graduate studies and all of the research presented herein.

The moral support of my entire family and especially Cal and Jean Goodrich has meant a great deal to me. The constant prayer support of my parents, Halsted and Wanda Gates, is greatly appreciated. I also want to acknowledge the importance to me of the excellent examples they provide both as Christians and as

scholars. Another model I gratefully acknowledge is my brother, Bill Gates, whose pursuit of structural engineering kindled my own interest. His continued encouragement and advice throughout my research at Caltech is greatly appreciated.

Finally I want to thank my wife, Janet, to whom this thesis is dedicated, for her love, prayers, encouragement, help and patience throughout our marriage and the pursuit of my Ph.D.

ABSTRACT

This thesis is concerned with the earthquake response of deteriorating systems. A model for stiffness degrading or deteriorating systems is used to describe six different single-degree-of-freedom systems. A numerical investigation of the response of these six systems is performed using an ensemble of twelve earthquakes. The response is studied at nine nominal periods of oscillation. The numerical results are presented as response spectra corresponding to six different ductilities.

An approximate analytical method for calculating the earthquake response of deteriorating systems from a linear response spectrum is presented. The method, called the average stiffness and energy method, is based upon the premise that a linear system may be defined which is in some sense equivalent to the deteriorating system. The criterion for equivalence in this method is that the average stiffness of the deteriorating system be equal to the stiffness of the linear system and the average energy dissipated by the linear system be the same as the average energy dissipated by the deteriorating system.

The new analytical method is compared to existing methods. Comparison with the numerical results is also made. Based upon these comparisons, it is concluded that the average stiffness and energy method represents a significant improvement over currently available methods for predicting the earthquake response of deteriorating and nondeteriorating systems.

TABLE OF CONTENTS

TABLE OF CONTENTS (CONTINUED)

TABLE OF CONTENTS (CONTINUED)

TABLE OF CONTENTS (CONCLUDED)

CHAPTER I

INTRODUCTION

There have been numerous studies of the earthquake response of linear, elasto-plastic, bilinear hysteretic and simple yielding systems and many of the results of these studies have now been incorporated into design manuals and codes. There has been far less attention devoted to the study of the dynamic behavior of deteriorating systems. Deterioration here refers to changes in a structure which result in loss of stiffness and reduced energy absorbing capacity with cyclic loading.

Many investigations have demonstrated the existence of deterioration or "stiffness degradation" in structural elements [1-9]. Some work has been done to develop a simple model for deteriorating systems [9-24]. A particularly useful model for deteriorating was proposed by Iwan [23,24] and will be used in this investigation because of its ability to approximate a wide class of deteriorating systems.

The use of linear response spectra in earthquake design criteria is well established. Despite some opposition [25,26], the use of inelastic response spectra derived from linear response spectra is also gaining wide acceptance [27-33]. There are two methods by which an inelastic response spectrum may be obtained from a linear response spectrum. The first method is to develop a set of rules based upon empirical observations. An example of such a method is the widely accepted method of Newmark and Hall [33]

for the elastoplastic system. The second method involves an analytical approach to defining a linear system which will in some sense be "equivalent" to the nonlinear system. The second method is more easily generalized to a variety of systems. The second method also gives greater insight into the manner in which variations in system behavior affect the earthquake response.

Much of the work in the area of defining an equivalent linear system for a nonlinear system has been devoted to nonlinear elastic, elasto-plastic, bilinear hysteretic and simple yielding systems [34-49]. The little work that has been done in the area of deteriorating systems has been associated with a rather specialized model for deterioration [19-22]. The method presented in this investigation is applicable to general deteriorating systems. Comparison with numerical results for six different systems is also presented.

The ultimate goal of this investigation is to present an analytical method for obtaining the nonlinear or inelastic response spectrum from a linear response spectrum for general deteriorating systems.

In Chapter II, existing methods for determining the effective linear system parameters for nondeteriorating systems are discussed. A new method, the average stiffness and energy method, which is applicable to general deteriorating systems is also presented. The predictions of the various methods are compared for a simple bilinear hysteretic system.

In Chapter III a model for stiffness degrading systems [23, 24] is presented. Six particular systems used in the numerical section of this investigation are presented and their behavior is discussed in detail.

In Chapter IV the results of a numerical investigation of the earthquake response of deteriorating systems are presented. The six systems of Chapter III are considered along with an ensemble of twelve earthquakes. Nine nominal periods of oscillation are used to define the response spectrum of the nonlinear system; a range of values of relative amplitude of excitation to strength of the nonlinear system is used to obtain values of spectral displacement corresponding to six values of ductility ratio. The numerical results are compared with linear response spectra and an effective linear period and damping are determined for each nonlinear system.

In Chapter V the approximate methods of Chapter II are used to calculate effective linear system parameters and spectral displacements. Comparison is made with the numerical results and conclusions are drawn concerning the relative merit of the various methods. It is concluded that the average stiffness and energy method is superior to the other methods considered not only because it is applicable to deteriorating systems, but also because it gives a better estimate of the spectral displacement for nondeteriorating systems.

CHAPTER II

APPROXIMATE ANALYTICAL METHODS

2.0 Introduction

The response history of deteriorating structures such as reinforced concrete can be simulated by analytical models which specify in detail the changes in hysteretic response. Such models require considerable computational expense. Therefore, an approximate analytical method for estimating the earthquake response of deteriorating systems is desirable.

In this chapter the existing approximate analytical methods for estimating the earthquake response of nonlinear systems will be summarized. First, methods applicable to harmonic excitation will be discussed. Then, methods for stationary random excitation and finally methods for earthquake excitation will be examined.

Only the average stiffness and energy method in section 2.5.2 is applicable to a general deteriorating system. Although the substitute damping method in section 2.5.1 is applicable to deteriorating systems, the model for deterioration used by that method is very specialized. The other methods discussed in this chapter are not applicable to deteriorating systems.

The approach that will be used throughout this chapter is to define a linear system which is equivalent in some sense to the nonlinear system. The equivalent linear system will be described in terms of two effective or equivalent linear parameters; an effective period T_e and an effective fraction of viscous damping ζ_e.

The peak earthquake response of a nonlinear system may be obtained by calculating the peak response of the linear system specified by T_e and ζ_e.

2.1 Terminology and Definitions

In this section some basic concepts which will be used throughout the chapter will be defined and explained.

2.1.1 Nature of the System

The system investigated is a single-degree-of-freedom oscillator which can be represented as in Fig. 2.1. For conceptual purposes, the system may be considered to consist of a mass m_0 supported by flexible members whose generalized restoring force is $k_0 f(x)$ and which also provides viscous damping $c_0 \dot{x}$. The system is excited by a base acceleration a(t). It is further assumed that

$$\lim_{x \to 0} \frac{df(x)}{dx} = 1 \qquad (2.1)$$

k_0 and c_0 are the nominal stiffness and nominal damping coefficient of the system, respectively. f(x) is a normalized restoring force function which could be linear, nonlinear elastic, hysteretic or deteriorating as indicated in Fig. 2.2. In this chapter only hysteretic restoring forces will be discussed, although the methods are equally applicable to elastic restoring forces.

For hysteretic systems the generalized restoring force f(x) is generally defined in terms of a scaling parameter x_y called the yield level. The specification of this parameter is somewhat

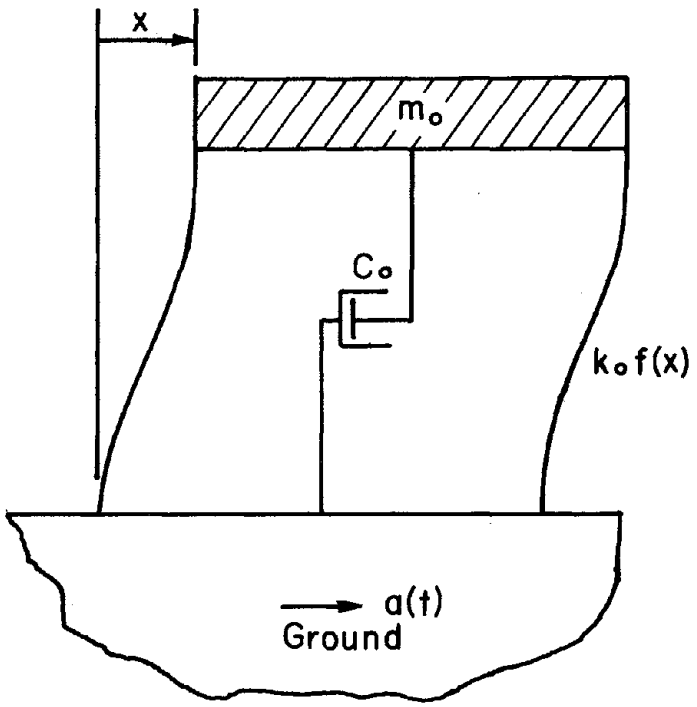

Figure 2.1. Single-Degree of Freedom Oscillator.

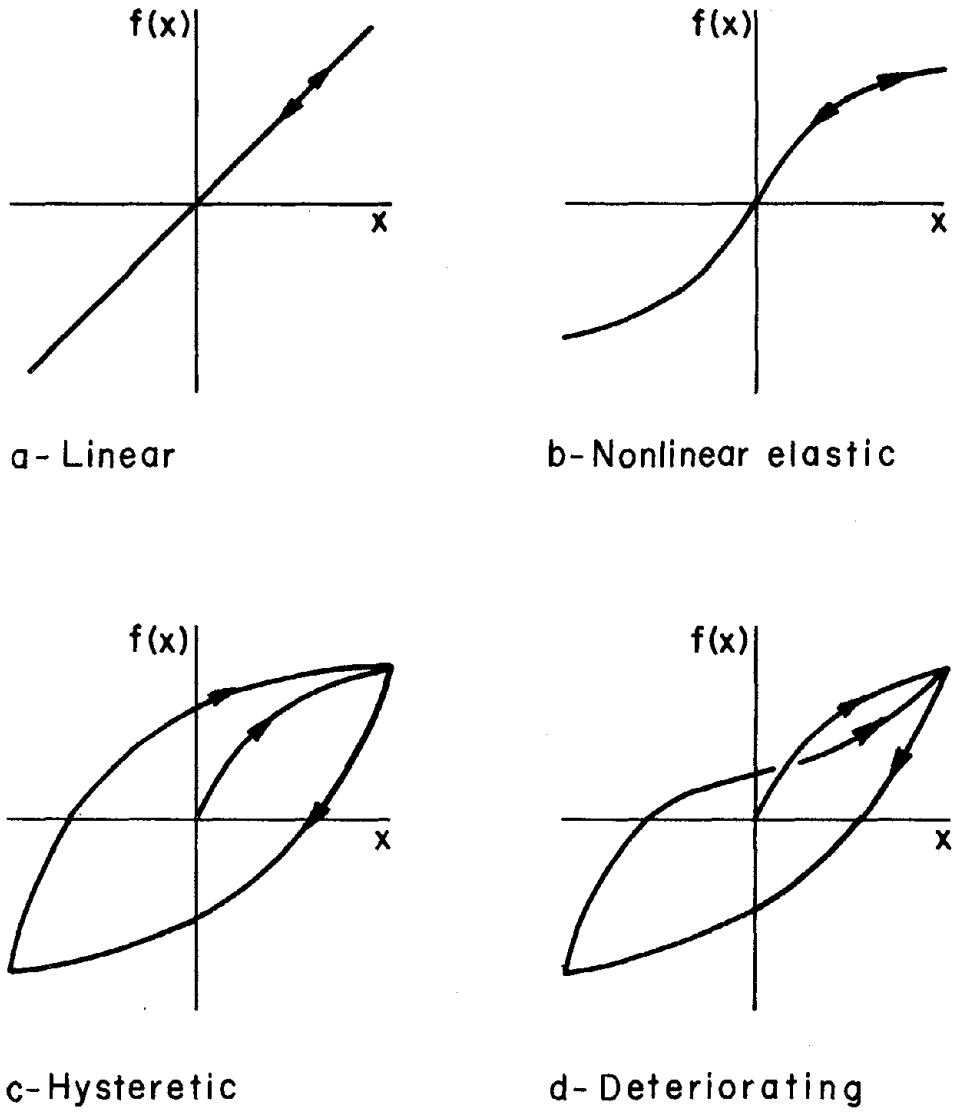

Figure 2.2. Restoring Force Diagrams.

arbitrary but it is usually taken to be the generalized displacement at which significant reduction in stiffness is obtained. If x_m is the absolute maximum displacement obtained during a particular time history of excitation of a hysteretic system, the parameter $\mu = x_m/x_y$ is referred to as the ductility ratio of the response. This parameter is frequently used to indicate the degree of yielding of a hysteretic system.

2.1.2 Viscous and Hysteretic Damping

In a single-degree of freedom oscillator with hysteresis, energy is dissipated in two ways; viscous damping and hysteresis. Let V represent the energy dissipated by viscous damping. Then, for harmonic oscillations of amplitude x_m the viscous energy dissipated per cycle of oscillation may be represented by the area of the ellipse in Fig. 2.3b and may be written as

$$V(x_m) = 2\pi\zeta k x_m^2 \qquad (2.2)$$

where $\zeta = c/2\sqrt{km}$ is the fraction of critical damping.

Let H represent the energy dissipated by hysteresis. For harmonic oscillations of amplitude x_m the hysteretic energy dissipated per cycle of oscillation is denoted by $H(x_m)$ and is represented by the area of the hysteresis loop in Fig. 2.3a.

The total energy dissipated is the sum of the energy dissipated by hysteresis and the energy dissipated by viscous damping. Let ΔW denote the total energy dissipated. Then

$$\Delta W = H + V \ . \qquad (2.3)$$

2.1.3 Secant Stiffness

In several methods of analysis the secant stiffness will be used. The secant stiffness $k(x_m)$ is defined as the slope of a line from the origin of the restoring force diagram to the turnaround point for cyclic loading to amplitude x_m. Fig. 2.3a shows the secant stiffness for a hysteretic system.

2.1.4 Skeleton Curve and Loci of Response Maxima

The skeleton curve of a hysteretic system is defined as the load deflection relation for monotonic loading from a virgin state. Fig. 2.3a shows the skeleton curve for a general nondeteriorating hysteretic system. For such a system the maximum of the response for cyclic loading with a slowly varying amplitude generally lies on the skeleton curve. In this case, the skeleton curve may also be referred to as the locus of response maxima.

For a deteriorating system two or more loci of response maxima may exist. If such a system is loaded cyclically from a virgin state with gradually increasing amplitude, the locus of response maxima will correspond to the skeleton curve. However, if the amplitude of cyclic response is gradually decreased and subsequently increased, the locus of response maxima will normally lie below the skeleton curve. This lowering of the locus of response maxima is tied directly to the reduction in stiffness and energy dissipation of the deteriorating system which takes place after significant yielding has occurred. In this case, the skeleton

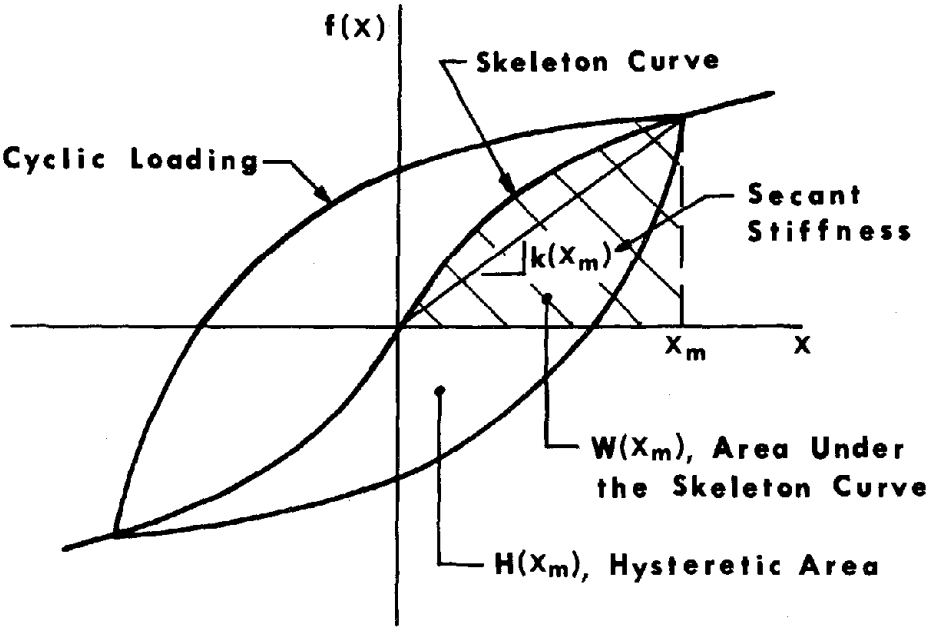

Figure 2.3a. Hysteresis Loop for Nondeteriorating System.

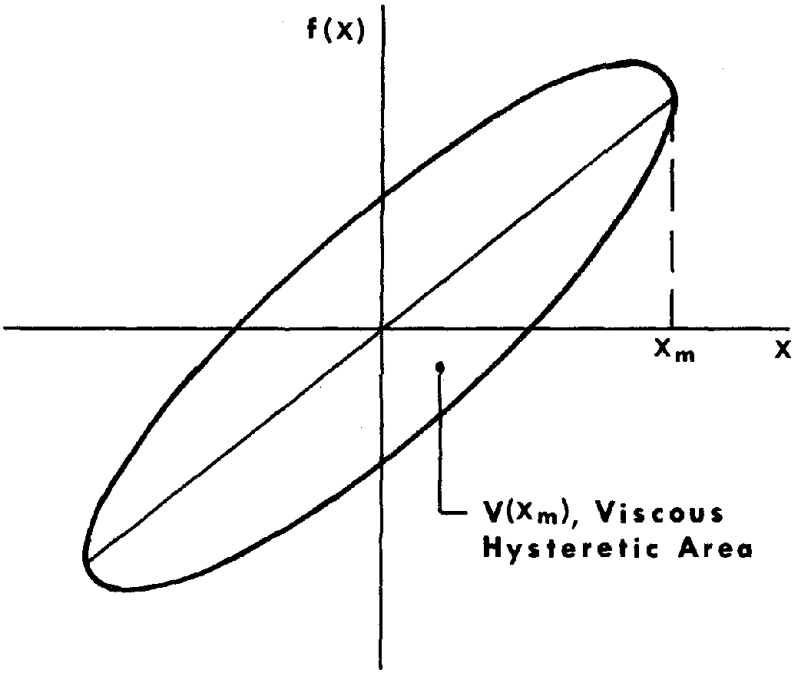

Figure 2.3b. Hysteresis Loop for Viscous Damped Linear System.

curve as given by the initial loading curve provides only an upper bound on the loci of response maxima.

In many deteriorating systems a unique lower locus of response maxima can be identified as shown in Fig. 2.4. All the points on the lower locus of maxima are potential turnaround points for cyclic loading after a maximum displacement x_{max} has been experienced.

2.2 Equation of Motion

The equation of motion for the single-degree-of-freedom oscillator shown in Fig. 1 may be written as

$$m_0\ddot{x} + c_0\dot{x} + k_0 f(\dot{x}) = -m_0 a(t) \quad . \tag{2.4}$$

This equation may be rewritten in the form

$$\ddot{x} + \beta_0\dot{x} + \omega_0^2 f(x) = -a(t) \tag{2.5}$$

where

$$\beta_0 = 2\zeta_0\omega_0 \tag{2.6a}$$

$$\omega_0^2 = \frac{k_0}{m_0} = \left(\frac{2\pi}{T_0}\right)^2 \tag{2.6b}$$

Then, ζ_0 is the nominal fraction of critical damping, ω_0 is the nominal frequency and T_0 is the nominal period of the system.

As mentioned in section 2.0, the approach used in the chapter involves defining an effective linear system with system parameters ζ_e and T_e. Thus, the linearized equation of motion may be written as

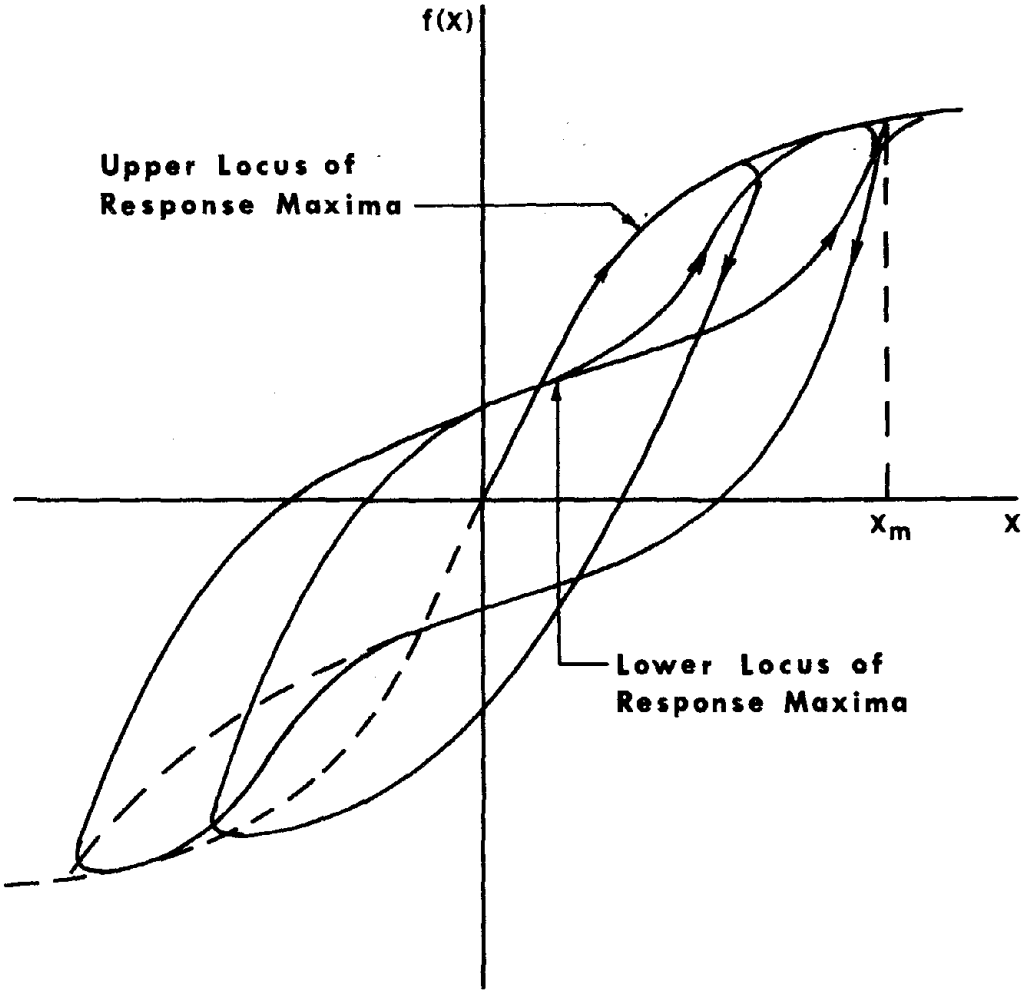

Figure 2.4. Repeated Loading of a Deteriorating System.

$$\ddot{x} + \beta_e \dot{x} + \omega_e^2 x = -a(t) \tag{2.7}$$

where

$$\beta_e = 2\zeta_e \omega_e \tag{2.8a}$$

$$\omega_e^2 = \frac{k_e}{m_e} = \left(\frac{2\pi}{T_e}\right)^2 . \tag{2.8b}$$

Note that most effective linear system parameters will be a function of the amplitude of response of the nonlinear system. If x_m is the amplitude of response, then $\mu = x_m/x_y$ is the ductility ratio and the effective linear parameters may be written as functions of μ.

2.3 Nondeteriorating Systems with Harmonic Excitation

The ultimate goal of this chapter is to examine methods for estimating the peak earthquake response of deteriorating systems. However, before investigating deteriorating systems, methods applicable to nondeteriorating systems will be discussed. For small amplitudes of excitation and for short duration of strong ground motion, the deteriorating features of a system may have little effect on the response. Hence, in some cases deteriorating systems may be modeled adequately as nondeteriorating systems.

Before examining techniques applicable to earthquake-like excitation, consideration will be given to excitations which can be more precisely described mathematically. First harmonic and then stationary random excitation will be discussed.

Structural testing employing forced harmonic excitation is frequently used to gain information about the nature of the structure

and to define structural parameters such as period and damping. Also, the response of a structure to earthquake excitation is often very nearly harmonic in character. Hence, an understanding of the steady-state harmonic response of hysteretic structures is useful.

2.3.1 Harmonic Equivalent Linearization (HEL)

In the method of equivalent linearization the difference between the nonlinear equation of motion (2.5) and the linear equation of motion (2.7) is minimized with respect to the parameters β_e and ω_e^2 for all solutions of the form

$$x(t) = A \cos(\omega t - \varphi) = A \cos\theta \tag{2.9}$$

where A is the amplitude of steady-state oscillation, ω is the forcing function frequency and φ is the shift in phase angle. The difference between the two equations may be written as

$$\delta = \beta_0 \dot{x} + \omega_0^2 f(x) - \beta_e \dot{x} - \omega_e^2 x \ . \tag{2.10}$$

Minimization of this difference may take several forms. However, in the method of equivalent linearization for harmonic response, the mean square value of the difference over one cycle of oscillation is minimized. Let

$$\overline{\delta}^2 = \frac{1}{T} \int_0^T \delta^2 \, dt \ . \tag{2.11}$$

A necessary condition for the minimization will be

$$\frac{\partial}{\partial \beta_e}(\overline{\delta}^2) = \frac{\partial}{\partial \omega_e^2}(\overline{\delta}^2) = 0 \quad . \tag{2.12}$$

Substituting for x from equation (2.9) and performing the specified differentiations yields the following expressions for β_e and ω_e^2

$$\beta_e = \beta_0 - \frac{\omega_0^2}{\omega_e} \frac{S(A)}{A} \tag{2.13a}$$

$$\omega_e^2 = \omega_0^2 \frac{C(A)}{A} \tag{2.13b}$$

where

$$S(A) = \frac{1}{\pi} \int_0^{2\pi} f(A \cos \theta) \sin \theta \, d\theta \tag{2.14a}$$

$$C(A) = \frac{1}{\pi} \int_0^{2\pi} f(A \cos \theta) \cos \theta \, d\theta \quad . \tag{2.14b}$$

The function S(A) is related to the energy dissipated by hysteresis in the following manner

$$S(A) = - \frac{H(A)}{\pi k_0 A} \tag{2.15}$$

where H(A) is the energy dissipated by hysteresis per cycle of oscillation of amplitude A. The function C(A) is related to the strain energy per cycle of oscillation. For a linear system with slope k_0

$$S(A) = 0 \qquad \text{and} \qquad C(A) = k_0 A \quad .$$

2.3.2 Resonant Amplitude Matching (RAM)

In this method, the shift in period of the yielding system is not taken into account. The mass and stiffness of the equivalent linear system are taken to be the mass and nominal stiffness of the yielding system. Thus,

$$T_e = T_0 \qquad \forall\ A \ . \tag{2.16}$$

The resonant response amplitude of the equivalent linear system is set equal to the resonant response amplitude of the yielding system and the effective viscous damping is chosen so that the two systems dissipate the same amounts of energy at resonance. Thus

$$\Delta W_e(A) = \Delta W(A) \qquad \forall\ A \tag{2.17}$$

where $\Delta W(A)$ is the energy dissipated by the yielding system per cycle of oscillation of amplitude A. For the linear system $\Delta W_e(A)$ is given by (2.2) which can be rewritten as

$$\Delta W_e(A) = V_e(A) = 2\pi\zeta_e k_e A^2 \ . \tag{2.18}$$

In this case $k_e = k_0$, $\forall$ A. Thus, (2.17) and (2.18) give

$$\zeta_e = \frac{\Delta W(A)}{2\pi k_0 A^2} \ . \tag{2.19}$$

This is easily interpreted as the ratio of two areas; the area of the hysteresis loop in Fig. 2.3a and the area of the ellipse in Fig. 2.3b.

2.3.3 Dynamic Mass (DM)

Another physically motivated approach is the dynamic mass method. In this method, the stiffness of the equivalent linear system is taken to be the nominal stiffness of the yielding system and the mass of the equivalent linear system is varied so as to match the observed period shift in the resonance response of the yielding system. Thus, the effective period calculated by this method is the same as that calculated by harmonic equivalent linearization. As in the resonant amplitude matching method, the resonant amplitudes and energies dissipated per cycle by the yielding and equivalent linear systems are set equal to each other. Thus, for a system with purely hysteretic energy dissipation, resonant amplitude matching and dynamic mass give the same effective viscous damping.

2.3.4 Constant Critical Damping (CCD)

It is possible to define an equivalent linear system in such a way that the critical damping factor ($c_c = 2\sqrt{km}$) remains constant, while modeling the period shift of the yielding system. This is done by setting

$$k_e m_e = k_0 m_0 \tag{2.20a}$$

and

$$\frac{k_e}{m_e} = \omega_e^2 \tag{2.20b}$$

where ω_e^2 is given by (2.13b). Thus, the effective period is the

same as in harmonic equivalent linearization and dynamic mass. As in the resonant amplitude matching and dynamic mass approaches, the resonant amplitudes and dissipated energies of the linear and nonlinear systems are equated. Since $k_e \neq k_0$, the effective viscous damping calculated using this method is not the same as that given by (2.19). Hence,

$$\zeta_e = \frac{\Delta W(A)}{2\pi k_e A^2} \tag{2.21}$$

which differs from (2.19) by the replacement of k_0 by k_e.

2.3.5 Geometric Stiffness (GS)

In all the previous methods with the exception of the resonant amplitude matching method, the period of the equivalent linear oscillator matches the resonant period of the yielding oscillator. In the geometric stiffness method, the stiffness of the equivalent linear oscillator is specified by the geometry of the hysteresis loop. Berg [34], and Rosenblueth and Herrera [49] have used this approach for hysteretic systems and have chosen the equivalent stiffness to be the secant stiffness shown in Fig. 2.3a. Equating the mass, resonant amplitude and energy dissipated for the hysteretic and equivalent linear oscillators implies that ζ_e is given by (2.21) and

$$T_e = T_0 \sqrt{\frac{k_0}{k_e}} \tag{2.22}$$

where k_e is taken to be the secant stiffness. Since k_e in this

method is the secant stiffness, both T_e and ζ_e will be different from any T_e and ζ_e obtained in previous methods.

2.3.6 Geometric Energy (GE)

Another geometric method of approximating the equivalent viscous damping for the steady-state harmonic response of hysteretic structures has been proposed by Jacobsen [44]. In this approach the geometry of the skeleton curve and the hysteresis loop as shown in Fig. 2.3a are used to calculate the effective viscous damping. Let W(A) be the maximum strain energy during a cycle of oscillation of amplitude A. Note that W(A) is the area under the skeleton curve as shown in Fig. 2.3a. For a linear system, the energy dissipated by viscous damping is given by equation (2.2) and the maximum strain energy is

$$W(A) = \tfrac{1}{2} kA^2 \quad . \tag{2.23}$$

Hence, by analogy to the linear system the effective linear viscous damping for the yielding system may be written as

$$\zeta_e = \frac{1}{4\pi} \frac{\Delta W(A)}{W(A)} \tag{2.24}$$

where $\Delta W(A)$ is the energy dissipated per cycle of oscillation by the yielding system and W(A) is the maximum strain energy per cycle of oscillation stored in the yielding system. The geometric energy method does not provide an effective period.

2.4 Nondeteriorating Systems with Stationary Random or Earthquake Excitation

In this section the response of nondeteriorating systems will be investigated further. The methods in this section are of two types. The first type assumes the excitation to be a stationary random process. The second type assumes the excitation to be an earthquake. In the harmonic methods the response of the system was assumed to be fixed at one amplitude so that $A = x_m$. In the methods of this section, the response is assumed to vary in amplitude and x_m will represent the peak value of the response amplitude while A will continue to represent the amplitude of a cycle of harmonic oscillation.

2.4.1 Stationary Random Equivalent Linearization (SREL)

The method of equivalent linearization has been applied to stationary random excitation by many investigators since first formulated by Booton [50] and Caughey [51]. The development of the method proceeds just as in the case of harmonic excitation except that minimization of the difference term δ in equation (2.10) must be interpreted in a statistical sense. If the response is an ergodic process, time averages may be replaced by ensemble averages. The minimization condition in this case may be written as

$$\frac{\partial}{\partial \beta_e} E[\delta^2] = \frac{\partial}{\partial \omega_e^2} E[\delta^2] = 0 \qquad (2.25)$$

where $E[\cdot]$ denotes the expected value or ensemble average.

Substituting for δ from (2.10), interchanging the order of differentiation and expectation yields

$$\beta_e = \beta_0 + \omega_0^2 \frac{E[\dot{x}f(x)]}{E[\dot{x}^2]} \tag{2.26a}$$

$$\omega_e^2 = \omega_0^2 \frac{E[xf(x)]}{E[x^2]} \tag{2.26b}$$

where it is assumed that x and $\dot{x}$ are jointly stationary.

In the development of this method, two basic assumptions about the response of the oscillator are made. First, the response is assumed to be a narrow band process. Thus, it is assumed that

$$x(t) = A(t) \cos [\omega t - \varphi(t)] = A(t) \cos \theta \tag{2.27}$$

where A(t) and $\varphi(t)$ are slowly varying random functions of time. Second, the response is assumed to be Gaussian. These assumptions are valid for a linear system with small damping and Gaussian excitation but for large nonlinearities the response is neither narrow band nor Gaussian. However, Iwan and Lutes [37] have found that even though these assumptions are not strictly valid for large nonlinearities, the results of this analysis are surprisingly good.

For hysteretic systems eqns. (2.26) must be modified by substituting (2.27) into (2.26) and averaging over one cycle of oscillation to yield

$$\beta_e = \beta_0 - \frac{\omega_0^2}{\omega_e} \frac{E[AS(A)]}{E[A^2]} \tag{2.28a}$$

$$\omega_e^2 = \omega_0^2 \frac{E[AC(A)]}{E[A^2]} \tag{2.28b}$$

where S(A) and C(A) are defined by eqns. (2.14).

Since the response process has been assumed to be narrow band and Gaussian, the probability density function of the response amplitude A may be approximated by a Rayleigh distribution. Hence,

$$E[g(A)] = \int_{-\infty}^{\infty} \frac{Ag(A)}{\sigma^2} \exp\left[-\frac{A^2}{2\sigma^2}\right] dA \tag{2.29}$$

where g(A) is any arbitrary function of A and σ is the rms value of the response.

Substituting (2.29) into (2.28) yields β_e and ω_e as functions of σ rather than μ or x_m. However, these may be written as functions of x_m by assuming some relationship between x_m and σ. The simplest relationship is a linear one such as

$$x_m = \lambda\sigma \ . \tag{2.30}$$

Since x_m is the peak response, λ must be greater than one. As λ is increased the probability that x_m is exceeded decreases as is shown in Fig. 2.5. Liu [52] has suggested the use of $\lambda = E[x_m] = \sqrt{\pi/2}$. This value for λ would imply that the probability that x_m is exceeded would be 0.45 which is large. On the other hand, $\lambda = 5$ would imply that there is only a 4×10^{-6} probability that x_m is exceeded. The upper bound on values of λ is dependent

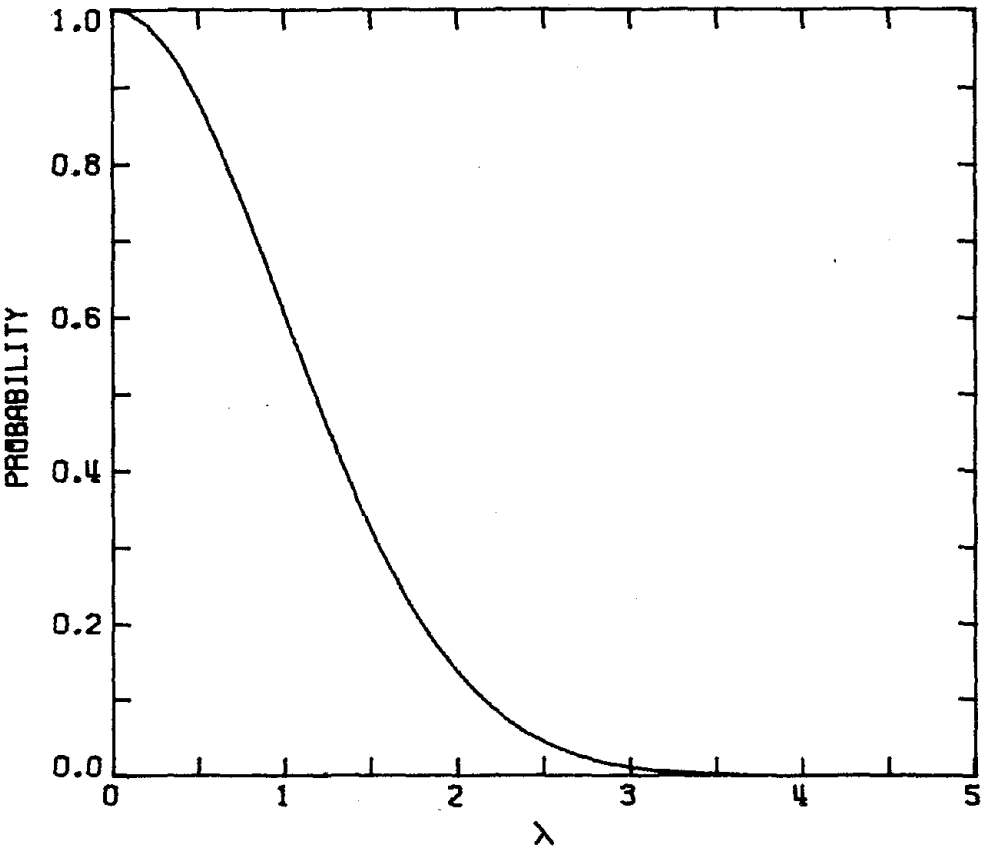

Figure 2.5. Probability that x_m is exceeded where $x_m = \lambda\sigma$.

on how realistic the resulting system parameters are. Further discussion of λ will be reserved until section 2.6.7.

2.4.2 Extended Equivalent Linearization (EEL)

The method of equivalent linearization has been extended by Kobori, et al. [53] to include three parameters as randomly distributed variables. In this approach the location of the center of hysteresis, the amplitude of hysteretic oscillation and the frequency of hysteretic oscillation are all randomly distributed variables. This method yields stationary random equivalent linearization, if both the scatter of frequency and fluctuation of the center of hysteretic oscillation are neglected.

The extended equivalent linearization method is sufficiently complex to make its application to the problem of the earthquake response of a hysteretic system very difficult. To begin with, it is necessary to specify the probability density function for the three random variables of the model. This involves additional assumptions about the nature of the response which may not be valid in the case of a strongly nonlinear system. Therefore, this method will not be discussed further here.

2.4.3 Average Period and Damping (APD)

Newmark and Rosenblueth [54] present a general approximate method of analysis for the earthquake response of nonlinear systems. This method of analysis is applicable to all single-degree-of-freedom systems with generalized force displacement curves which are

symmetric about the origin, subject only to the condition that the system does not deteriorate.

This approach defines the effective linear system to be the average of all the linear systems, based on the geometric stiffness method, corresponding to amplitudes less than or equal to x_m. Let T_e' be the effective period and ζ_e' the effective viscous damping for harmonic oscillations of amplitude A. Hence, T_e' is given by eqn. (2.22) and ζ_e' is given by eqn. (2.21) where k_e is the secant stiffness. The average period and damping are given by

$$T_e = \frac{1}{x_m} \int_0^{x_m} T_e'(A)\,dA \qquad (2.31a)$$

$$\zeta_e = \frac{1}{x_m} \int_0^{x_m} \zeta_e'(A)\,dA \ . \qquad (2.31b)$$

2.5 Deteriorating Systems with Earthquake Excitation

In this section two approximate analytical methods applicable to deteriorating systems will be presented. The first method by Shibata [19] is applicable only to a specialized model for deterioration. The method called the average stiffness and energy method is presented here for the first time. This latter method is applicable to general deteriorating systems. Both methods assume earthquake excitation of the deteriorating system.

2.5.1 Substitute Damping (SD)

The substitute damping method first suggested by Gulkan and Sozen [5] and further modified by Shibata and Sozen [19-22] was

developed as a vehicle to interpret the response of reinforced concrete. This method assumes that the deteriorating system can be modeled using Takeda's [9] hysteresis rule as shown in Fig. 2.6.

In this method

$$T_e = T_0 \sqrt{\hat{\mu}} \tag{2.32a}$$

$$\zeta_e = \zeta_0 + \frac{1}{5}(1 - 1/\sqrt{\hat{\mu}}) \tag{2.32b}$$

where $\hat{\mu} = x_m/x_y$ = ductility in early formulations and $\hat{\mu} = k_0/k_e$ = damage ratio in later formulations. Since k_e is taken to be the secant stiffness, the difference between the two formulations disappears if the skeleton curve has zero slope after yielding.

According to Gulkan and Sozen [5], quantitative values for this substitute damping were distilled from results of dynamic tests of one-story, one-bay frames. This was done by assuming that the energy input was entirely dissipated by an imaginary viscous damper.

The empirical basis and special model for the deteriorating system restricts the usefulness of this method. In particular, this method cannot be used to estimate the response of a nondeteriorating system.

2.5.2 Average Stiffness and Energy (ASE)

The average stiffness and energy method is not restricted to any special model for the deteriorating system. In this method two

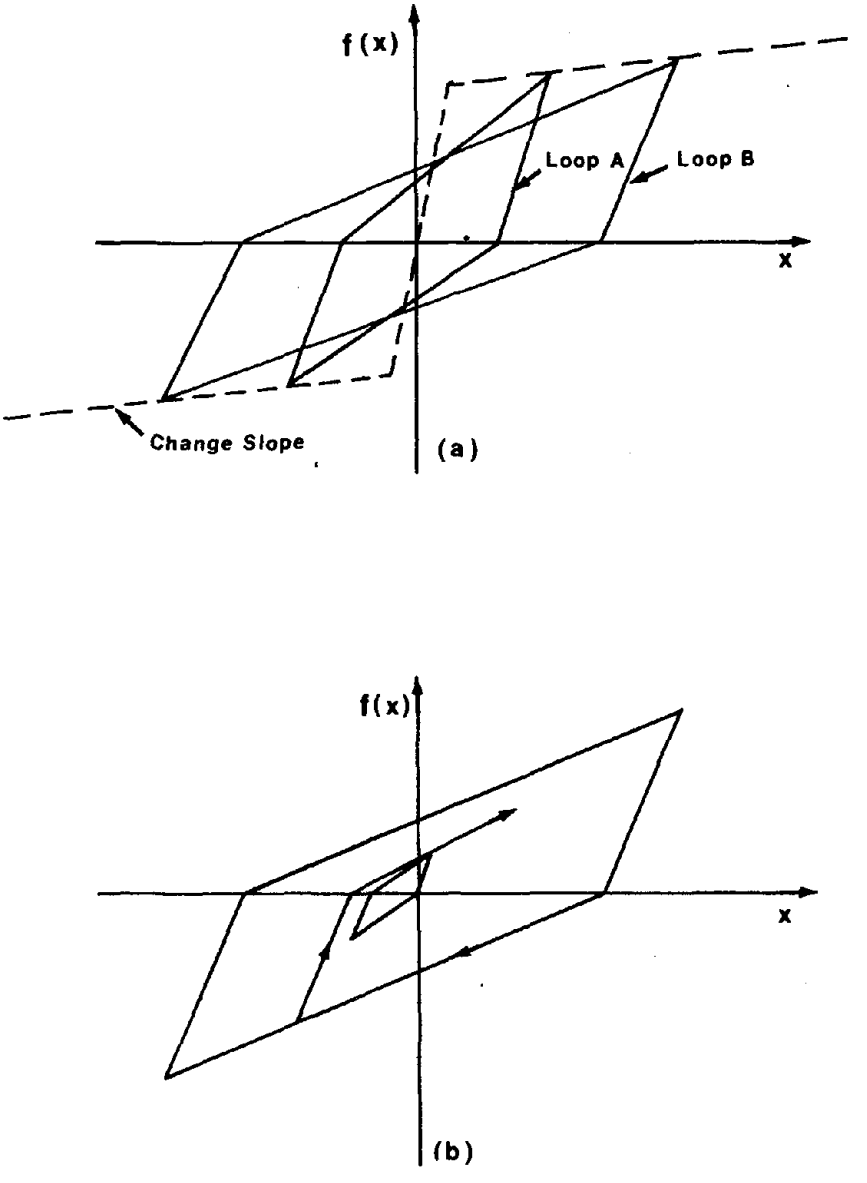

Figure 2.6. Idealized Hysteresis for Reinforced Concrete.

loci of response maxima are used to specify the effective linear system parameters. Let a subscript u denote system parameters based on the upper locus of response maxima and let a subscript ℓ denote system parameters based on the lower locus of response maxima as shown in Fig. 2.4. Thus, $k_u(x_m)$, $H_u(x_m)$, $V_u(x_m)$ denote the secant stiffness, hysteretic energy dissipated and viscous energy dissipated by the nonlinear system which follows the upper locus of response maxima. Similarly, $k_\ell(x_m)$, $H_\ell(x_m)$, $V_\ell(x_m)$ denote the secant stiffness, hysteretic energy dissipated and viscous energy dissipated by the nonlinear system which follows the lower locus of response maxima.

As in the average period and damping method, the equivalent linear system will be defined in terms of the average values of the fundamental parameters. In this method the fundamental system parameters are the stiffness and the energy dissipated. Let $k'(A)$ and $\Delta W'(A)$ be the secant stiffness and the energy dissipated for harmonic oscillations of amplitude A. Then, the average stiffness $k(x_m)$ is given by

$$k(x_m) = \frac{1}{x_m} \int_0^{x_m} k'(A)dA \quad . \tag{2.33a}$$

Likewise, the average energy dissipated $\Delta W(x_m)$ is given by

$$\Delta W(x_m) = \frac{1}{x_m} \int_0^{x_m} \Delta W'(A)dA \quad . \tag{2.33b}$$

The equivalent linear system parameters are obtained by taking the average of the values associated with the upper and lower loci. Hence, the equivalent linear stiffness is given by

$$k_e = \tfrac{1}{2} k_u + \tfrac{1}{2} k_\ell \quad . \tag{2.34}$$

Similarly, the total energy dissipated is given by

$$\Delta W = \tfrac{1}{2}\Delta W_u + \tfrac{1}{2}\Delta W_\ell \quad . \tag{2.35}$$

For a linear system $\Delta W_e'$ is given by (2.18). Substituting (2.18) into (2.33b) yields

$$\Delta W_e(x_m) = V_e(x_m) = \tfrac{2}{3}\pi\zeta_e k_e x_m^2 \quad . \tag{2.36}$$

Thus, the effective viscous damping of the deteriorating system is given by

$$\zeta_e = \frac{\Delta W(x_m)}{\tfrac{2}{3}\pi k_e(x_m) x_m^2} \tag{2.37}$$

where $\Delta W(x_m)$ and $k_e(x_m)$ are given by (2.33) with (2.35) and (2.34), respectively. The effective period may be denoted by (2.22).

This method attempts to account for the significant differences in the stiffness and energy dissipation of the deteriorating system on initial loading to response amplitude x_m greater than x_y and on subsequent loading to that same response amplitude x_m. The contribution to k and ΔW due to the upper locus alone would overestimate the effective stiffness and energy dissipated, while the contribution due to the lower locus alone would underestimate the

effective stiffness and energy dissipated. It is felt that the average of the contributions due to both the upper and lower locus should give a much better estimate of the effective stiffness and energy dissipation of a deteriorating structure.

2.6 Example of Application - Bilinear Hysteresis (BLH)

In this chapter six methods for obtaining an equivalent linear system for a nondeteriorating system with harmonic excitation were discussed. Three methods for obtaining an equivalent linear system for a nondeteriorating system with random or earthquake excitation were also discussed and two methods for obtaining an equivalent linear system for a deteriorating system with earthquake excitation were discussed.

Before moving into the application of the average stiffness and energy method to several deteriorating systems, a comparison of the equivalent linear systems obtained by the application of the various methods in this chapter to the bilinear hysteretic system will be presented.

In Fig. 2.7 the force-displacement diagram for a bilinear hysteretic system is shown. This system has initial slope k_0, post yield slope αk_0, and yield level x_y. The maximum response amplitude is $x_m = \mu x_y$ and in the harmonic methods $x_m = A$.

2.6.1 Harmonic Equivalent Linearization

For the bilinear hysteretic system whose force displacement diagram is shown in Fig. 2.7 the term $f(A \cos \theta)$ in eqn. (2.14) may be written as

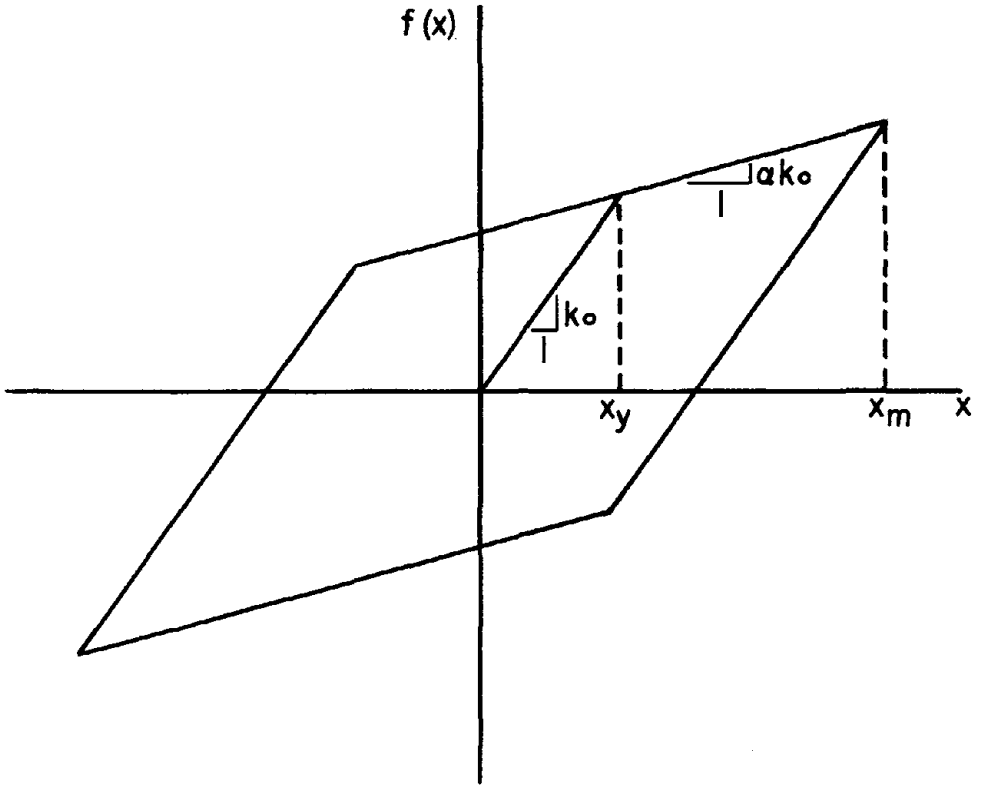

Figure 2.7. Force-Displacement Diagram for Bilinear Hysteretic System.

$$\frac{f(A\cos\theta)}{x_y} = \begin{cases} \alpha\mu\cos\theta - (1-\alpha) & ; \quad \cos\theta < \dfrac{\mu-2}{\mu} \\ \mu\cos\theta - \left(\dfrac{\mu-1}{1-\alpha}\right) & ; \quad \dfrac{\mu-2}{\mu} < \cos\theta < 1 \end{cases} \tag{2.38}$$

where $\mu = A/x_y$. Substituting (2.38) into (2.14) yields

$$\frac{S(A)}{x_y} = \begin{cases} 0 & ; \quad \mu < 1 \\ -\dfrac{\mu}{\pi}(1-\alpha)\sin^2\theta^* & ; \quad \mu > 1 \end{cases} \tag{2.39a}$$

$$\frac{C(A)}{x_y} = \begin{cases} \mu & ; \quad \mu < 1 \\ \dfrac{\mu}{\pi}\left[(1-\alpha)\left(\theta^* - \dfrac{\sin 2\theta^*}{2}\right) + \sigma\pi\right] & ; \quad \mu > 1 \end{cases} \tag{2.39b}$$

where

$$\theta^* = \cos^{-1}\left(\frac{\mu-2}{\mu}\right) . \tag{2.40}$$

Substituting (2.39) into (2.13) and using eqn. (2.8) yields

$$\frac{T_e}{T_0} = \left[\frac{(1-\alpha)}{\pi}\left(\theta^* - \frac{\sin 2\theta^*}{2}\right) + \alpha\right]^{-\frac{1}{2}} \quad ; \quad \mu > 1 \tag{2.41a}$$

$$\zeta_e = \zeta_0 \frac{T_e}{T_0} + \frac{2}{\pi}(1-\alpha)\frac{(\mu-1)}{\mu^2}\left(\frac{T_e}{T_0}\right)^2 \quad ; \quad \mu > 1 . \tag{2.41b}$$

2.6.2 Resonant Amplitude Matching

For the BLH system indicated by Fig. 2.7 the hysteretic energy dissipated per cycle may be written as

$$\frac{H(A)}{x_y^2} = \begin{cases} 0 & ; \quad \mu < 1 \\ 4k_0(1-\alpha)(\mu-1) & ; \quad \mu > 1 \end{cases} . \tag{2.42}$$

The viscous energy dissipated may be written as

$$\frac{V(A)}{x_y^2} = 2\pi\zeta_0 k_e \mu^2 \qquad \forall\ \mu \ . \tag{2.43}$$

Using (2.3) along with (2.42) and (2.43) to express ΔW in (2.19) and using $k_e = k_0$, the resonant amplitude matching method yields

$$\zeta_e(\mu) = \zeta_0 + \frac{2(1-\alpha)(\mu-1)}{\pi\mu^2} \quad ; \qquad \mu > 1 \ . \tag{2.44}$$

T_e is given by (2.16). Note that substituting for T_e from (2.16) into eqn. (2.41b) yields (2.44).

2.6.3 Dynamic Mass

In the dynamic mass method, the effective period shift is given by (2.41a) and the effective viscous damping is given by (2.44).

2.6.4 Constant Critical Damping

The method of constant critical damping gives the same effective period as harmonic equivalent linearization and the effective viscous damping is given by

$$\zeta_e(\mu) = \zeta_0 \frac{T_e}{T_0} + \frac{2}{\pi}(1-\alpha)\frac{(\mu-1)}{\mu^2}\frac{T_e}{T_0} \quad ; \qquad \mu > 1 \ . \tag{2.45}$$

Note that (2.45) differs from (2.41b) only in the exponent of the second T_e/T_0 term. In this method the viscous damping is a linear function of the period shift.

2.6.5 Geometric Stiffness

For the BLH system of Fig. 2.7 the secant stiffness may be written as

$$k_e = \begin{cases} k_0 & ; \quad \mu < 1 \\ k_0 \left(\frac{1-\alpha}{\mu} + \alpha \right) & ; \quad \mu > 1 \end{cases} . \tag{2.46}$$

Substituting this expression for k_e into eqn. (2.21) yields

$$\frac{T_e}{T_0} = \left[\frac{1-\alpha}{\mu} + \alpha \right]^{-\frac{1}{2}} \quad ; \quad \mu > 1 . \tag{2.47}$$

The effective viscous damping is given by (2.41b) with this period shift.

2.6.6 Geometric Energy

The maximum strain energy for the BLH system may be written as

$$\frac{W(A)}{x_y^2} = k_0 \left[(\mu - \tfrac{1}{2}) + \frac{\alpha}{2} (\mu - 1)^2 \right] \quad ; \quad \mu > 1 . \tag{2.48}$$

Thus, the effective viscous damping according to the geometric energy method is given by substituting (2.48) and (2.42) into (2.24) which yields

$$\zeta_e(\mu) = \frac{1}{\pi} \frac{(1-\alpha)(\mu - 1)}{(\mu - \frac{1}{2}) + \frac{\alpha}{2} (\mu - 1)^2} \quad ; \quad \mu > 1 . \tag{2.49}$$

Note that there is no consistent way to treat $\zeta_0 \neq 0$ and no expression for T_e is given by this method.

2.6.7 Stationary Random Equivalent Linearization

Caughey [36] presented the following expressions for the BLH system

$$\beta_e = \beta_0 + \frac{1-\alpha}{\sqrt{\pi}} \frac{\omega_0^2}{\omega_e \sigma^2} \operatorname{erfc}\left(\frac{1}{\sqrt{2}\,\sigma}\right) \tag{2.50a}$$

$$\left(\frac{\omega_e}{\omega_0}\right)^2 = 1 - \frac{8(1-\alpha)}{\pi} \int_1^\infty \sqrt{A-1}\left[\frac{1}{2A\sigma^2} + \frac{1}{A^3}\right] \exp\left(\frac{-A^2}{2\sigma^2}\right) dA \tag{2.50b}$$

where erfc is the complimentary error function.

Using eqn. (2.30) β_e and ω_e may be expressed as functions of x_{rn} or μ. As stated in section 2.5.1, the proper choice of λ in eqn. (2.30) depends on the resulting system parameters. In Fig. 2.8 the effective period shift T_e/T_0 and the effective viscous damping of a BLH system with $\alpha = 0.05$ and $\zeta_0 = 0$ are presented as functions of μ for three values of λ. Note that as λ increases, both the effective period shift and effective viscous damping decrease. For the numerical comparison in the next section λ will be assumed to be 3, even though $\zeta_e \neq \zeta_0$ at $\mu = 1$ for $\lambda = 3$.

2.6.8 Average Period and Damping

As stated in section 2.4.3 the average period and damping method uses the effective period and damping obtained by the geometric stiffness method. Hence, substituting (2.47) and (2.41b) into (2.31) yields

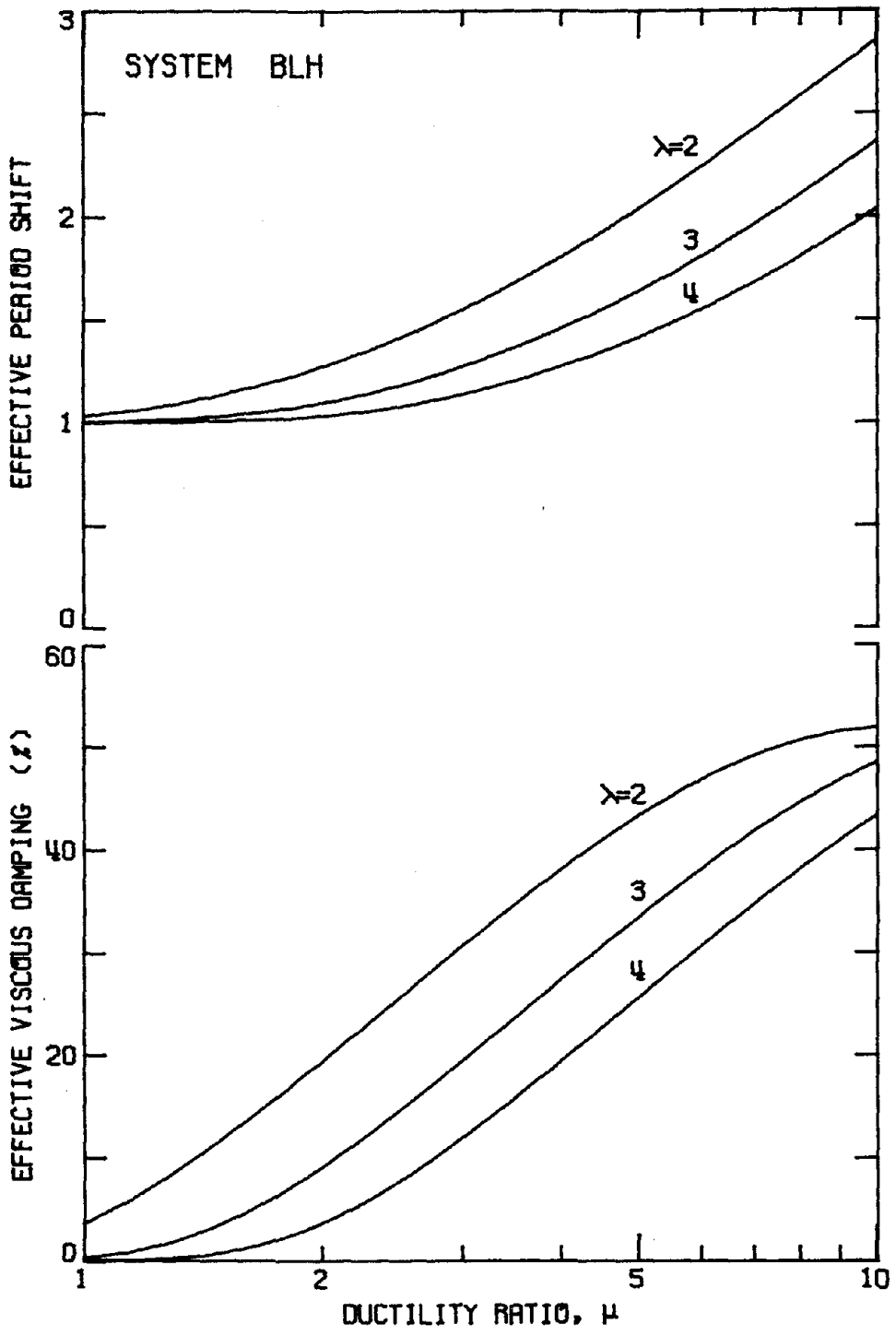

Figure 2.8. Dependence upon $\lambda = x_m/\sigma$ of the SREL Effective Linear System Parameters for the BLH System with $\alpha = 0.05$ and $\zeta_0 = 0$.

$$\frac{T_e}{T_0} = \frac{1}{\mu}\left[1 + \frac{\sqrt{\alpha\mu^2 + (1-\alpha)\mu} - 1}{\alpha} - \frac{1-\alpha}{2\alpha^{3/2}} \ell n\ \xi\right] \quad ; \quad \mu > 1 \qquad (2.51a)$$

where

$$\xi = \frac{2\sqrt{\alpha[\alpha\mu^2 + (1-\alpha)\mu]} + 2\alpha\mu + (1-\alpha)}{\alpha + 2\sqrt{\alpha} + 1}$$

$$\zeta_e(\mu) = \zeta_0 \frac{T_e}{T_0} + \frac{2}{\pi}\frac{1-\alpha}{\mu}\left[\frac{1}{\alpha}\ell n\ (1-\alpha+\alpha\mu) + \frac{1}{1-\alpha}\ell n\left(\frac{1-\alpha}{\mu} + \alpha\right)\right] \quad ; \quad \mu > 1 \ . \qquad (2.51b)$$

These expressions, although lengthy, are easier to evaluate than (2.50) because no numerical integration is involved.

2.6.9 Substitute Damping

The substitute damping method as presented in section 2.5.1 is applicable to Takeda's [9] rule for hysteresis. Hence, no direct comparison with the other methods can be made.

2.6.10 Average Stiffness and Energy

For the BLH system the lower locus of response maxima is identical to the upper locus of response maxima. Hence, substituting (2.46) into (2.33a) and (2.42), (2.43) into (2.33b) yields

$$k_e(\mu) = k_0\left[\frac{1-\alpha}{\mu}(1+\ell n\ \mu) + \alpha\right] \quad ; \quad \mu > 1 \qquad (2.52a)$$

$$\frac{H(x_m)}{x_y^2} = \hat{H}(\mu) = 2k_0(1-\alpha)\frac{(\mu-1)^2}{\mu} \quad ; \quad \mu > 1 \qquad (2.52b)$$

$$\frac{V(x_m)}{x_y^2} = \hat{V}(\mu) = \begin{cases} \frac{2}{3}\pi\zeta_0 k_0 \mu^2 & ; \quad \mu < 1 \\ \frac{\pi\zeta_0 k_0}{\mu}\left[(1-\alpha)\left(\mu^2 - \frac{1}{3}\right) + \frac{2}{3}\alpha\mu\right] & ; \quad \mu > 1 \end{cases} . \quad (2.52c)$$

Thus, the average stiffness and energy method yields

$$\frac{T_e}{T_0} = \left[\frac{1-\alpha}{\mu}(1 + \ell n\ \mu) + \alpha\right]^{-\frac{1}{2}} \quad ; \quad \mu > 1 \quad (2.53a)$$

$$\zeta_e(\mu) = \frac{\hat{H}(\mu) + \hat{V}(\mu)}{\frac{2}{3}\pi k_e(\mu)\mu^2} \quad \forall\ \mu\ . \quad (2.53b)$$

These expressions are easier to evaluate than (2.50) and at least as easy to evaluate as (2.51).

2.7 Numerical Example and Comparison

The results of the various methods for a BLH system with $\alpha = 0.05$ and $\zeta_0 = 0$ are presented in Fig. 2.9. Note that the geometric energy method has no period shift as mentioned earlier. Although the viscous damping for dynamic mass and resonant amplitude matching are identical, the period shift for resonant amplitude matching is unity, while the dynamic mass method yields the largest period shift.

All harmonic methods yield an effective viscous damping with a maxima in the range $1 \leq \mu \leq 10$, while only the average stiffness and energy method of the nonharmonic methods has a maxima in this range.

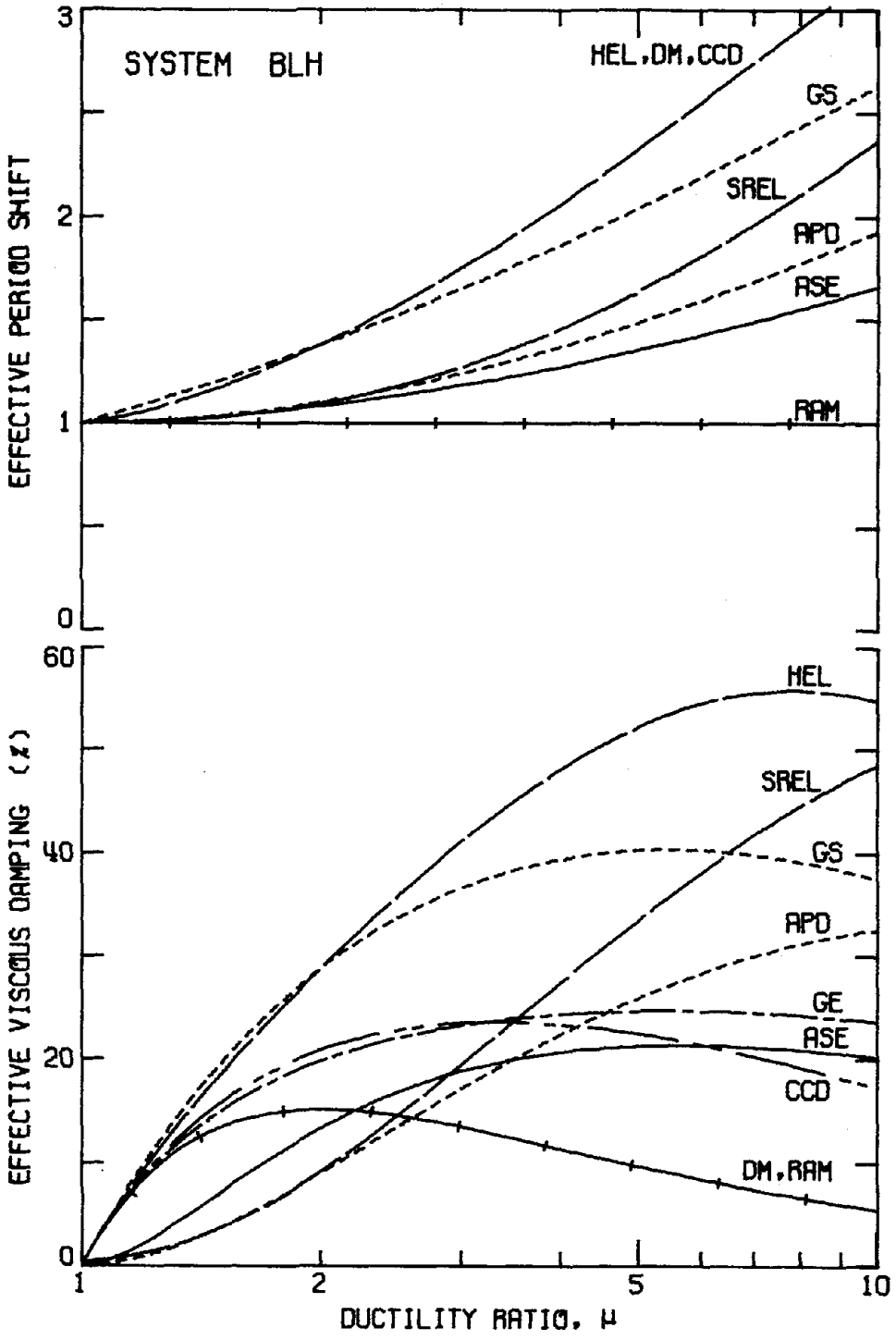

Figure 2.9. Effective Linear System Parameters for the BLH System with $\alpha = 0.05$ and $\zeta_0 = 0$.

All harmonic methods yield an effective period shift which is larger than the nonharmonic methods except resonant amplitude matching and geometric energy. The average stiffness and energy method gives the smallest effective period shift neglecting the $T_e/T_0 = 1$ from the resonant amplitude matching method.

The nonharmonic methods which were applied to the BLH system in the last section are all averaging methods. The SREL method is a weighted average of the HEL method. The APD is an average of the GS method. The ASE is an average of other system parameters, namely stiffness and energy dissipated. A comparison between SREL and HEL or APD and GS demonstrates the effect of averaging. As long as the system parameter due to the harmonic method is monotonically increasing, the system parameter due to the averaging method will be smaller than the system parameter due to the harmonic method.

These approximate methods are discussed further in Chapter V, where comparison is made with the numerical results for a particular BLH system. In Chapter V conclusions are presented regarding the merits of the various methods presented in this chapter.

CHAPTER III

MODEL FOR HYSTERETIC AND DETERIORATING SYSTEMS

3.0 Introduction

Many models for deteriorating or stiffness degrading systems have been proposed. These models fall into three categories. In the first category are highly idealized models which lead to considerable simplification of the mathematics of the dynamic response problem but which only very roughly approximate the behavior of real structures [14, 18]. In the second category are detailed empirical models which very precisely describe a particular system and a particular loading history [9,55] but cannot be easily generalized to other systems or loading histories. In the third category are physically motivated models which are based on phenomenological description of the behavior of deteriorating structures during cyclic loading [23, 24]. At the same time, models in this third category are sufficiently well defined mathematically to make their use in dynamic analysis straightforward.

3.1 The Model

The model which will be used in this investigation falls in the third category. It was first proposed by Iwan [23] and has been demonstrated to be capable of modeling a wide range of deteriorating structures.

The model may be thought of as a subclass of the distributed element model [56]. The gradual changes observed in many force-displacement diagrams may be modeled with distributed

elements. However, in this investigation only one element from each of the three basic types of elements will be used to model the deteriorating system.

3.2 Elements of the Model

The three basic elements of the model for the deteriorating restoring force are: an elastic element (E-type), an elasto-plastic element (Y-type) and an element which exhibits both cracking and crushing like behavior (C-type). In Fig. 3.1 physical analogs of these elements are indicated along with force-deflection diagrams for one cycle of loading from the virgin state.

3.2.1 E-type Element

The E-type element which is completely elastic, contributes a force $k_e x$ to the generalized force for all generalized displacements x.

3.2.2 Y-type Element

The Y-type element is an elasto-plastic element with initial stiffness k_s and generalized yield displacement x_s. Hence, the generalized yield force as shown in Fig. 3.1 is

$$f_s = k_s x_s \quad . \tag{3.1}$$

The Y and E-type elements are frequently used in the analysis of nondeteriorating structures. The bilinear hysteretic system (BLH) can be modeled by a single E-type in parallel with a single Y-type element.

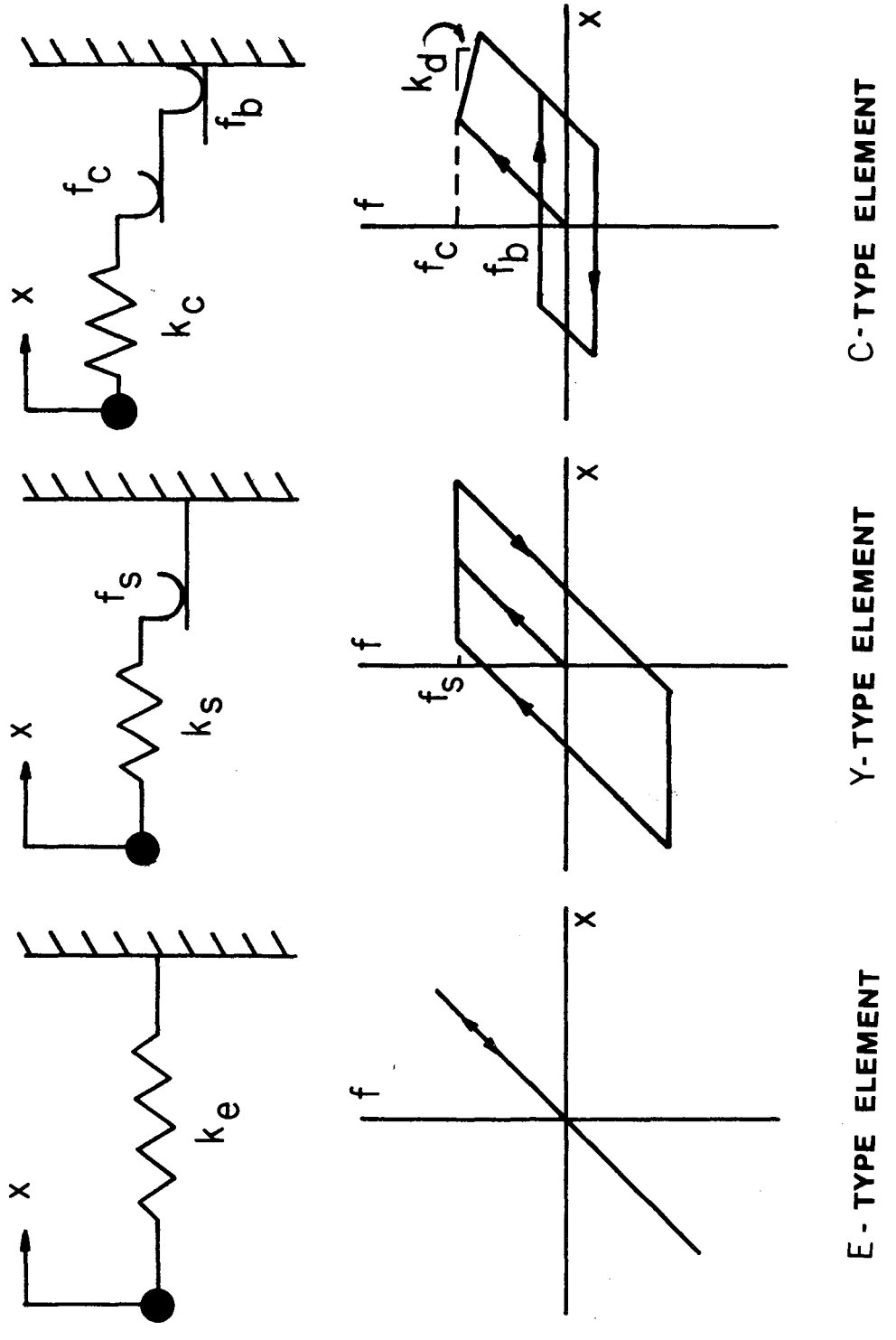
x
k_e
f
x
E- TYPE ELEMENT
x
k_s
f_s
f
f_s
x
Y- TYPE ELEMENT
x
k_c
f_c
f_b
k_d
f
f_c
f_b
x
C- TYPE ELEMENT

Figure 3.1

3.2.3 C-type Element

The effects of deterioration come from the inclusion of the C-type element. As shown in Fig. 3.1 when this element is loaded in a tensile direction it slips or "cracks" at a generalized force level f_b corresponding to a generalized displacement x_b. When the element is loaded in a compressive sense, it yields or "crushes" at a generalized force level f_c corresponding to a generalized displacement x_c. The initial stiffness of this element is given by k_c. The similarity of the behavior of the C-type element to that observed in concrete is apparent. The fact that the generalized force associated with crushing normally decreases with increasing displacement can be accounted for by a negative stiffness after yielding, denoted by k_d ($k_d \leq 0$).

It is easily seen that the cyclic energy dissipation of the C-type element decreases sharply after the first loading excursion to an amplitude greater than that required for compressive failure (i.e. $x > x_c$). Two such elements are used in a back-to-back configuration to model the initially symmetric force-displacement diagrams considered herein.

These three basic elements are the building blocks of the distributed element model. As mentioned earlier, a model composed of one E-type element, one Y-type element and one pair of C-type elements will be used in this investigation to simplify the analysis. An example of how these three elements are combined to give the deteriorating response of the system is shown in Fig. 3.2.

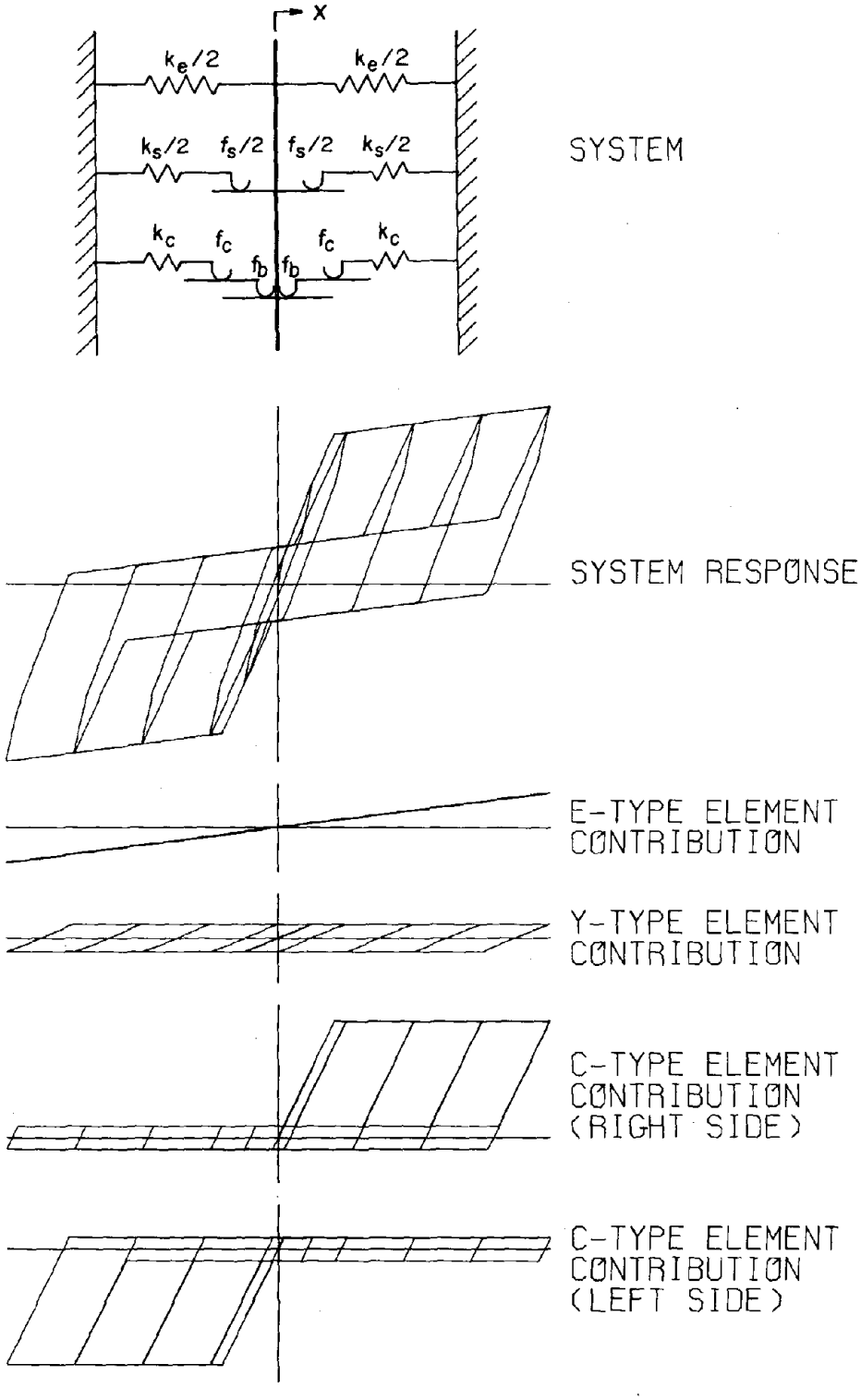

Figure 3.2. Summation of Element Contributions.

3.3 System Parameters

For this simplified model there are five basic system parameters α, β, γ, δ and ν. These five basic system parameters specify the relationships between the spring stiffnesses k_e, k_c, k_s and k_d, and the yield forces f_s, f_b and f_c or the yield displacements x_s, x_b and x_c.

3.3.1 Definition and Description

The five basic system parameters will be defined in terms of the parameters in Fig. 3.1 and in terms of their effect on the shape of the restoring force diagram. The five system parameters are:

$\alpha = \frac{k_e}{k_0}$ = ratio of the stiffness of the elastic element to the nominal stiffness of the system

$\beta = \frac{k_s}{k_c}$ = ratio of the small amplitude stiffness of the simple yielding element to that of one deteriorating element

$\gamma = \frac{x_s}{x_c}$ = ratio of the generalized displacement at which significant yielding occurs to that at which crushing occurs

$\delta = \frac{f_b}{f_c}$ = ratio of cracking to crushing strength for deteriorating elements

$\nu = \frac{k_d}{k_c}$ = ratio of the limiting large amplitude stiffness to the small amplitude stiffness of the deteriorating elements

All of these parameters have a direct physical interpretation and are in some way related to the parameters used in structural

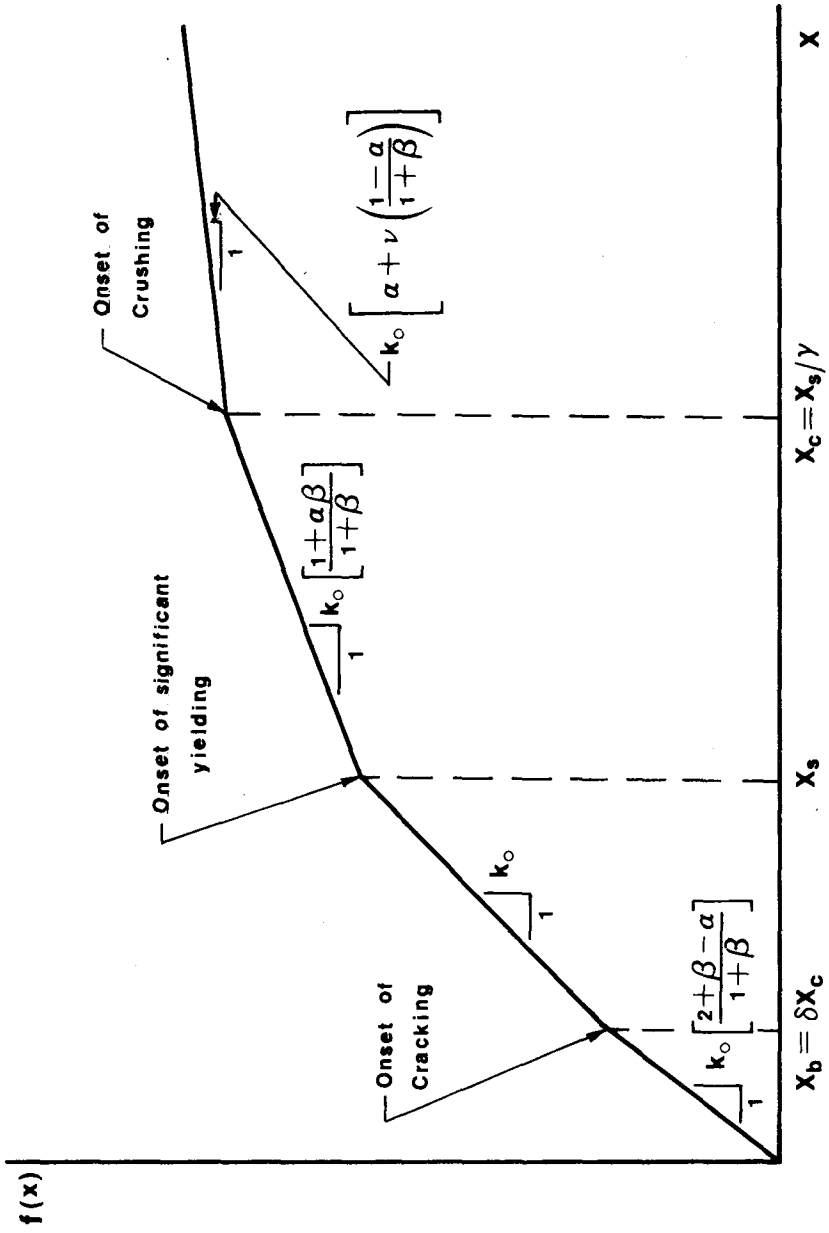

Figure 3.3. Initial Loading Curve.

design. The parameter γ, for example, denotes the degree of ductility of the structure. If $\gamma < 1$, the system is said to be of ductile design with yielding of steel elements occurring before significant crushing of concrete elements.

3.3.2 Effect of Varying the System Parameters

In Fig. 3.3 the initial loading curve for this model is given. The various stiffnesses are indicated in terms of k_0 the nominal stiffness of the system and the system parameters α, β, γ, δ and ν. Note that α and ν control the limiting slope for large amplitude response. The parameter β controls the ratio of the various slopes while γ and δ control the location of the points of slope change.

In Fig. 3.4 the effect on the shape of the hysteresis loop due to variations in β and γ are demonstrated for nine systems specified by $\alpha = 0.05$, $\delta = 0.10$, $\nu = 0.0$, $\beta = 0.2$, 1.0, 50, and $\gamma = 0.2$, 0.6, 1.0. Note that β small indicates a highly deteriorating system.

The effect of varying δ is demonstrated in Fig. 3.5. When $\delta = 0$ the system has no cracking strength, while $\delta = .5$ indicates that the cracking strength is half the crushing strength.

3.3.3 Typical Range of System Parameters

The system parameters β and γ could be deduced directly from an analysis of a given beam or column section according to the rules of normal design practice [57]. This gives a range of values for γ between approximately 0.2 and 0.5 and for β between 5 and 15. However, from tests of full scale structural components it would appear that if the model is used to describe the gross

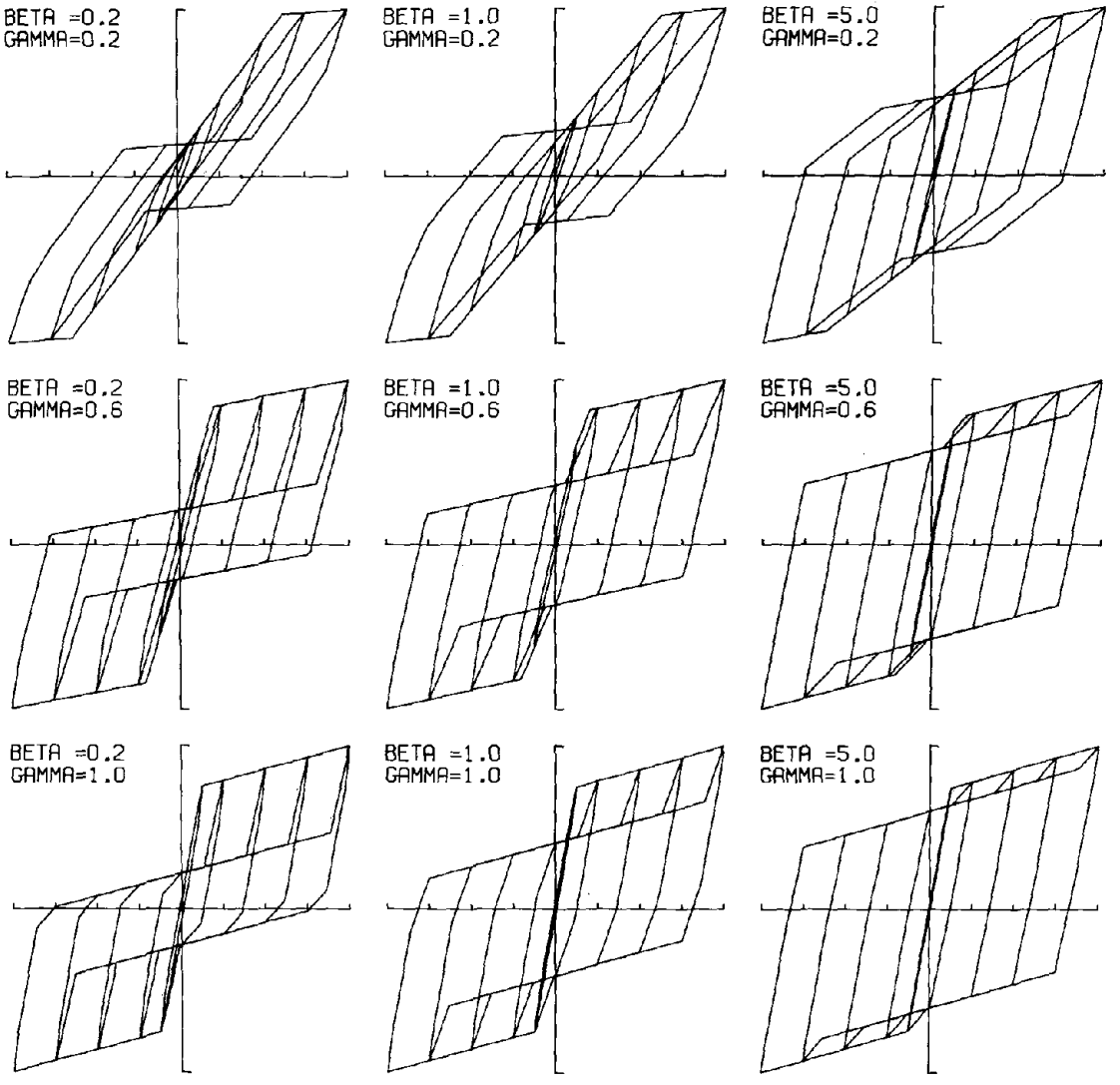

Figure 3.4. The Effect of Varying β and γ.

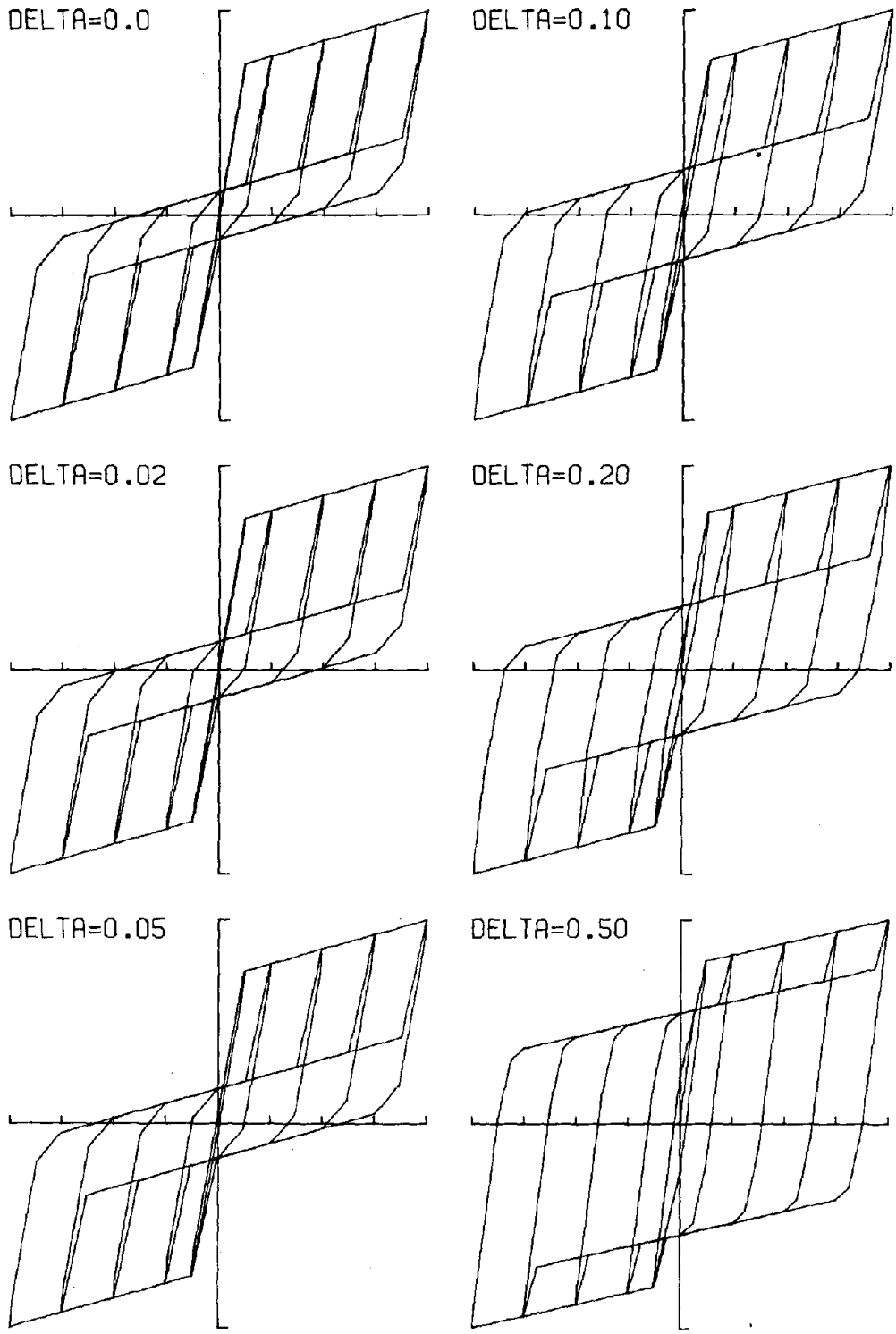

Figure 3.5. The Effect of Varying δ.

behavior of a structure including joints, the parameter γ should be allowed to vary from 0.2 to 1.0 while the meaningful range of β is 0.2 to 5.0.

3.4 Six Particular Systems

In this investigation six systems will be taken as representative of the wide range of systems which can be modeled by the model discussed in this chapter. In all six systems the parameters ν and α will be fixed at 0.0 and 0.05 respectively. Hence, the structural model may be described in terms of the three parameters β, γ and δ. In what follows, the systems will be designated by the code 10β-10γ-100δ. Hence, the code 02-06-10 respresents the system described by the parameters $\beta = 0.2$, $\gamma = 0.6$ and $\delta = 0.10$. The BLH system is the only system among the six investigated which will not be specified by this code.

The force-displacement diagrams of these six systems are shown in Fig. 3.6 for the case of a cyclic loading with monotonically increasing amplitude. It is seen that the systems encompass a wide range of structural behavior. Table 3.1 indicates the nature of the system behavior for the six systems considered as a function of ductility ratio. In this case the ductility ratio is defined as

$$\mu = x_m/x_s \ , \qquad (3.2)$$

where x_m is the maximum amplitude of response. In the table, cracking refers to hysteretic energy dissipation associated with

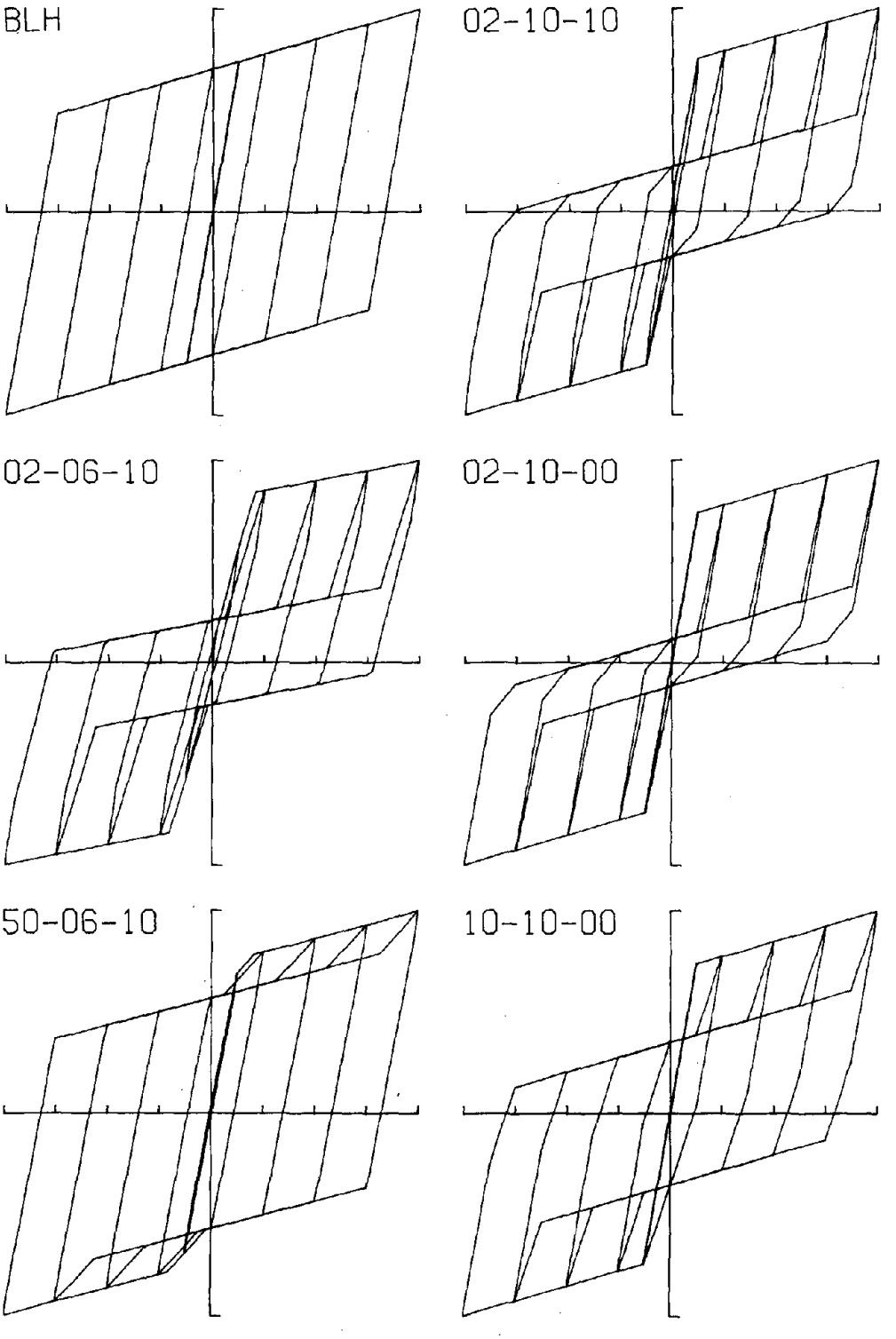

Figure 3.6. The Six Systems Investigated.

TABLE 3.1

SYSTEM	NATURE OF SYSTEM BEHAVIOR			
BLH	Linear		BLH	
10-10-00	Linear		Stiffness degrading	
02-10-00	Linear		Stiffness degrading	
02-10-10	Linear	BLH, cracking only	Stiffness degrading with cracking	
02-06-10	Linear	BLH, cracking only	TLH	Stiff. degrading with cracking
50-06-10	Linear	BLH, cracking only	TLH	Stiff. degrading with cracking
	0.1	0.167	1.0	1.67
	DUCTILITY RATIO, μ			

TABLE 3.2

SYSTEM	SYSTEM PARAMETERS					ELEMENT PARAMETERS						
	α	β	γ	δ	ν	$\frac{k_e}{k_0}$	$\frac{k_s}{k_0}$	$\frac{k_c}{k_0}$	$\frac{k_d}{k_0}$	$\frac{x_s}{x_y}$	$\frac{x_c}{x_y}$	$\frac{x_b}{x_y}$
BLH	0.05	∞	1.0	0.0	0.0	0.050	0.950	0.0	0.0	1.0	1.0	0.0
10-10-00	0.05	1.0	1.0	0.0	0.0	0.050	0.475	0.475	0.0	1.0	1.0	0.0
02-10-00	0.05	0.2	1.0	0.0	0.0	0.050	0.158	0.792	0.0	1.0	1.0	0.0
02-10-10	0.05	0.2	1.0	0.1	0.0	0.050	0.158	0.792	0.0	1.0	1.0	0.1
02-06-10	0.05	0.2	0.6	0.1	0.0	0.050	0.158	0.792	0.0	1.0	1.667	0.167
50-06-10	0.05	5.0	0.6	0.1	0.0	0.050	0.792	0.158	0.0	1.0	1.667	0.167

slip level f_b while stiffness degrading refers to deteriorating energy dissipation associated with the slip level f_c. TLH denotes non-deteriorating trilinear hysteretic behavior.

The BLH system with initial slope k_0 and post yield slope $\alpha k_0 = 0.05k_0$ is included in the six systems of this investigation for comparison with the nondeteriorating methods. This system has been studied by other investigators [35-37] and next to the elasto-plastic system is one of the most commonly used hysteretic models.

The system parameters and the resulting element parameters for the six systems are presented in Table 3.2. The BLH, 10-10-00 and 02-10-00 systems have no cracking strength, while the other three systems all have 10% cracking strength. The 02-10-00, 02-10-10 and 02-06-10 systems all have five times as much stiffness in the C-type element as in the Y-type element. The system 02-10-10 differs from 02-10-00 by the addition of cracking strength. The system 02-06-10 differs from 02-10-10 by the change in yield point for the C-type elements.

Both 10-10-00 and 50-06-10 systems have less deterioration than the three systems with $\beta = 0.2$. The 50-06-10 system is closest to the BLH system of the five deteriorating systems. Thus, it is seen that the smaller β is the greater the contribution of the C-type elements and the more deterioration possible in the system. Likewise, the larger β is the greater the contribution of the Y-type element and the less deterioration possible in the system.

Hence, it is seen that a wide range of system behavior from nondeteriorating to highly deteriorating is represented by the six systems used in this investigation.

CHAPTER IV

NUMERICAL RESULTS

4.0 Introduction

In this chapter the selection and scaling of an ensemble of twelve earthquakes is discussed. The nonlinear equation of motion is restated and the method of numerical integration is discussed. The numerical results of the present investigation are presented in a general form as a function of the parameters of the study. Then, the results are converted to nonlinear response spectra. Finally a method for defining an effective linear system based upon response spectra is discussed and effective linear system parameters are presented.

4.1 Selection and Scaling of Input Accelerograms

In Chapter II the nonlinear equation of motion (2.5) was written as

$$\ddot{x} + \beta_0 \dot{x} + \omega_0^2 f(x) = -a(t) \quad . \tag{4.1}$$

Let the displacement ratio z and the system parameters λ and a_y be defined as

$$z = x/x_y \; ; \qquad \lambda = f_y/(k_0 x_y) \; ; \qquad a_y = f_y/m \quad . \tag{4.2}$$

Then, the equation of motion becomes

$$\ddot{z} + \beta_0 \dot{z} + \omega_0^2 \bar{f}(z) = -\lambda \omega_0^2 a(t)/a_y \tag{4.3}$$

where

$$\bar{f}(z) = f(x)/x_y \quad . \tag{4.4}$$

The magnitude of the excitation in eqn. (4.3) may be specified by some characteristic acceleration a*. This might be taken as the peak acceleration, the rms acceleration, or some other measure of the strength of the excitation. The right-hand side of the equation of motion could then be expressed in terms of the characteristic acceleration as

$$\lambda\omega_0^2 a(t)/a_y = \lambda\omega_0^2 \rho[a(t)/a^*] = \hat{a}(t) \tag{4.5}$$

where

$$\rho = a^*/a_y \quad . \tag{4.6}$$

In this form, $[a(t)/a^*]$ is a dimensionless normalized excitation and the parameter ρ specifies the strength of the excitation relative to that value of steady input acceleration which would just cause significant yielding of the system.

The twelve earthquake accelerograms used in the present investigation are selected so as to be representative of a variety of different types of earthquake. In Table 4.1 the twelve earthquake accelerograms are listed along with their maximum accelerations, a_m and characteristic accelerations, a*. Except for the accelerogram denoted by SGGP all accelerograms may be found among the Caltech digitized accelerograms.

Since the peak acceleration is not necessarily the best measure of the strength of an earthquake [54], the characteristic acceleration used herein is derived from the response spectrum

TABLE 4.1

Symbol	Earthquake Accelerogram	Maximum acceleration a_m (g's)	Characteristic acceleration a^* (g's)
PAC	Pacoima Dam, San Fernando, 1971, S14W	1.170	0.952
HOL	8244 Orion Blvd., 1st Fl., San Fern., 1971, N00W	0.255	0.415
ELC	El Centro, Imperial Valley, 1940, S00E	0.348	0.410
TAF	Taft, Kern Co., 1952, S69E	0.179	0.218
HEL	Helena, Montana, 1935, N90E	0.145	0.123
OLY	Olympia, Washington, 1949, S04E	0.165	0.236
SGGP	Smoothed Golden Gate Park, S80E	0.150	0.264
VER	Vernon, Long Beach, 1933, S82E	0.154	0.169
EUR	Eureka, 1954, N11W	0.168	0.266
PF8	Array No. 8, Parkfield, 1966, N50E	0.237	0.140
BOR	Borrego Mtn., 1968, S90W	0.057	0.125
FIG	445 Figueroa St., San Fernando, 1971, S38W	0.119	0.174

of the earthquake. The characteristic acceleration a^* is the peak acceleration of a reference spectrum which has been scaled so as to minimize the squared error between the log of the 2% damped spectrum of the earthquake and the log of the reference spectrum for periods from 0.2 to 4.0 seconds. Almost any spectrum may be used as the reference spectrum. In the present investigation the reference spectrum is the 2% damped spectrum from the Nuclear Regulatory Guide 1.60 [58] adjusted to mean value. The mean value spectrum is deduced from the published spectrum by subtracting 1σ from this spectrum as discussed in references [59-61]. The peak and mean value design spectra are shown in Fig. 4.1.

The average response spectrum for the twelve earthquakes used herein is shown in Fig. 4.2. This average spectrum is obtained by scaling all of the response spectra of the earthquakes in the ensemble to a 1g characteristic acceleration and taking the ensemble average.

4.2 Method of Numerical Integration

Since the nonlinear restoring force in eqn. (4.3) is piecewise linear for all systems used in the present investigation and since the input accelerograms as available have all been digitized at an equally spaced time interval, an approach based on the exact analytical solution of the Duhamel integral for the successive linear segments of excitation [62] will be used herein.

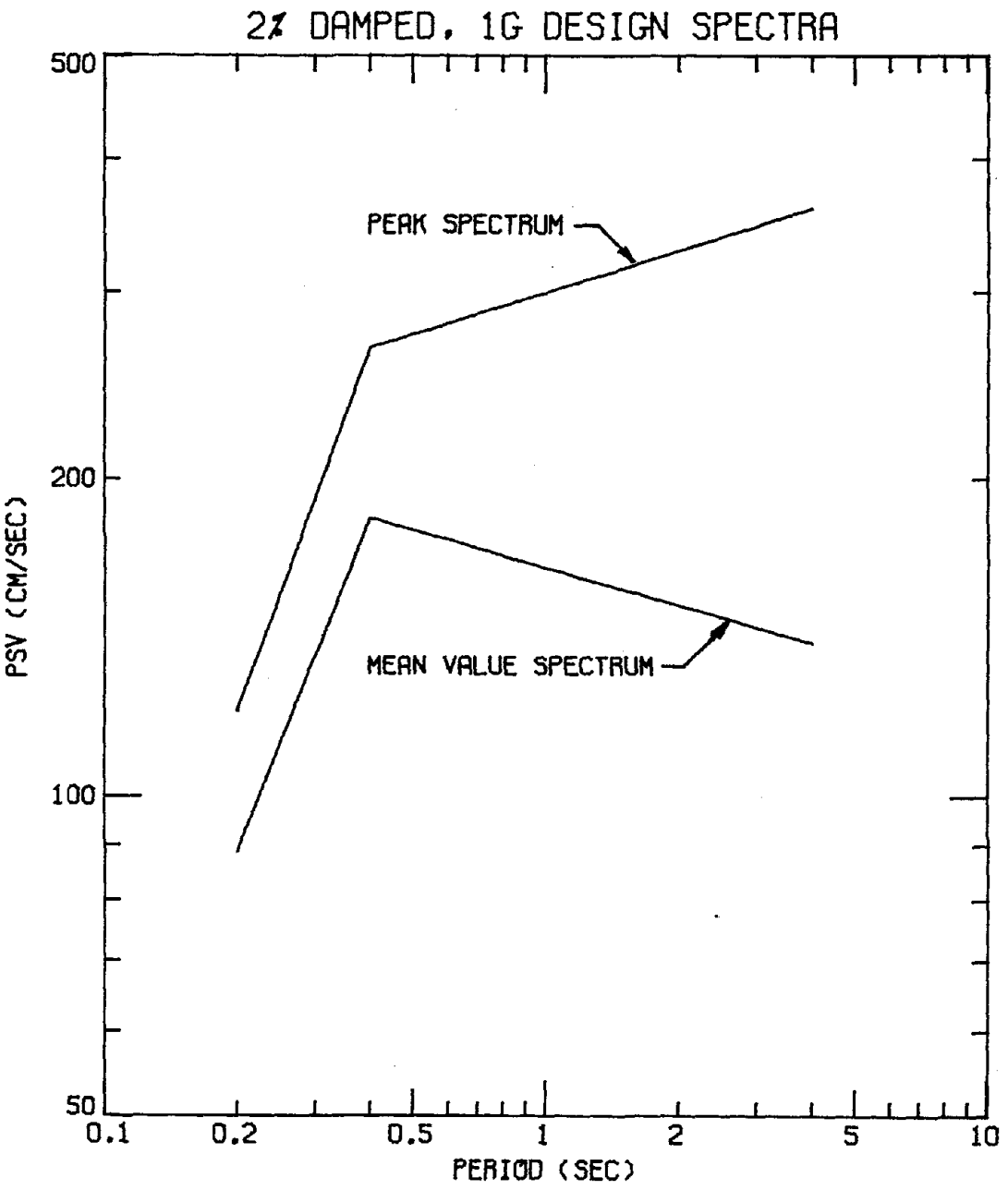

Figure 4.1. Design Spectra - Nuclear Regulatory Guide 1.60.

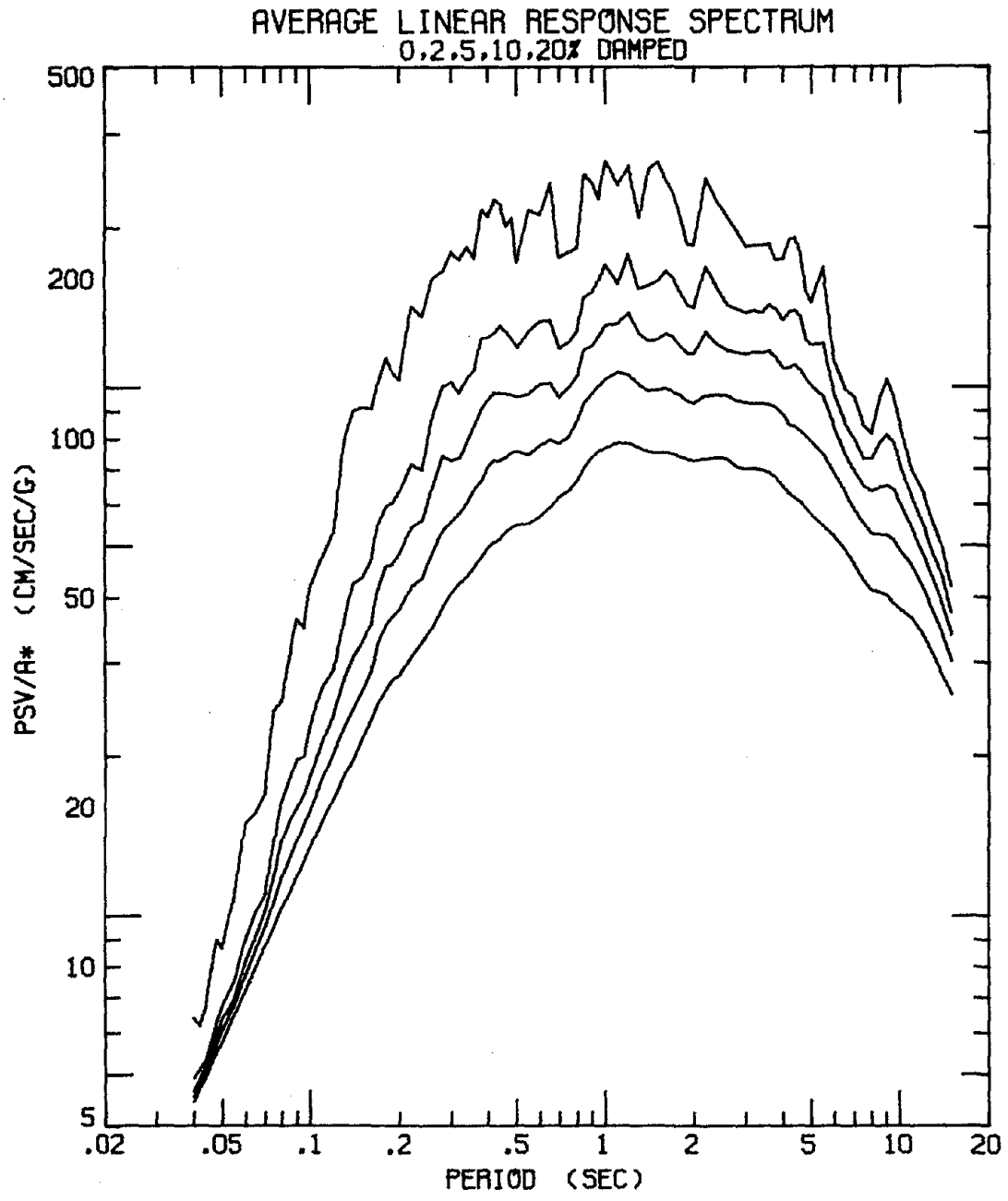

Figure 4.2. Average Spectrum for the Twelve Earthquakes in the Ensemble.

Let Δt be the time interval, k be the local slope of the restoring force curve and ω be the natural frequency based upon the mass m and stiffness k. Let ζ be the fraction of viscous damping of the system and let z_i, $\dot{z}_i$ and $\hat{a}_i$ be the relative displacement ratio, relative velocity ratio and scaled input acceleration at time t_i respectively. As shown in Fig. 4.3, z_0 is the point of intersection between the line with slope k which passes through $[z_i, \bar{f}(z_i)]$ and the displacement ratio axis. Using these definitions the displacement ratio and velocity ratio at time $t_{i+1} = t_i + \Delta t$ are given by

$$\begin{Bmatrix} z_{i+1} - z_0 \\ \dot{z}_{i+1} \end{Bmatrix} = [A(\zeta, \omega, \Delta t)] \begin{Bmatrix} z_i - z_0 \\ \dot{z}_i \end{Bmatrix} + [B(\zeta, \omega, \Delta t)] \begin{Bmatrix} \hat{a}_i \\ \hat{a}_{i+1} \end{Bmatrix} . \quad (4.7)$$

The elements of matrices A and B are

$$\left.\begin{aligned} a_{11} &= e^{-\zeta\omega\Delta t}\left(\frac{\zeta}{\sqrt{1-\zeta^2}} \sin \omega_d\Delta t + \cos \omega_d\Delta t\right) \\ a_{12} &= \frac{e^{-\zeta\omega\Delta t}}{\omega_d} \sin \omega_d\Delta t \\ a_{21} &= -\frac{\omega}{\sqrt{1-\zeta^2}} e^{-\zeta\omega\Delta t} \sin \omega_d\Delta t \\ a_{22} &= e^{-\zeta\omega\Delta t}\left(\cos \omega_d\Delta t - \frac{\zeta}{\sqrt{1-\zeta^2}} \sin \omega_d\Delta t\right) \end{aligned}\right\} \quad (4.8)$$

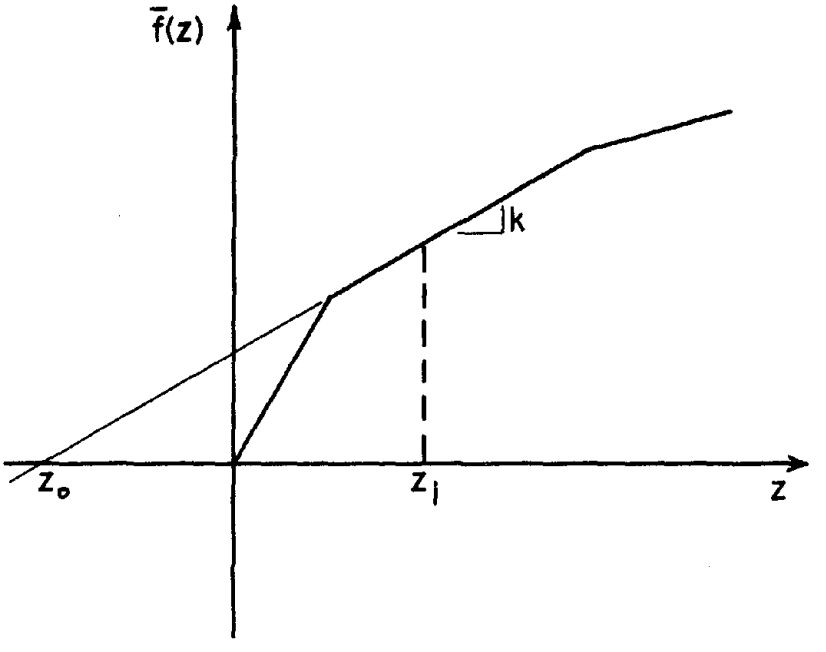

Figure 4.3. Piecewise Linear Restoring Force.

$$
\left.
\begin{aligned}
b_{11} &= e^{-\zeta\omega\Delta t}\left[\left(\frac{2\zeta^2-1}{\omega^2\Delta t}+\frac{\zeta}{\omega}\right)\frac{\sin\omega_d\Delta t}{\omega_d}+\left(\frac{2\zeta}{\omega^3\Delta t}+\frac{1}{\omega^2}\right)\cos\omega_d\Delta t\right]-\frac{2\zeta}{\omega^3\Delta t}\\
b_{12} &= -e^{-\zeta\omega\Delta t}\left[\left(\frac{2\zeta^2-1}{\omega^2\Delta t}\right)\frac{\sin\omega_d\Delta t}{\omega_d}+\frac{2\zeta}{\omega^3\Delta t}\cos\omega_d\Delta t\right]-\frac{1}{\omega^2}+\frac{2\zeta}{\omega^3\Delta t}\\
b_{21} &= e^{-\zeta\omega\Delta t}\left[\left(\frac{2\zeta^2-1}{\omega^2\Delta t}+\frac{\zeta}{\omega}\right)\left(\cos\omega_d\Delta t-\frac{\zeta}{\sqrt{1-\zeta^2}}\sin\omega_d\Delta t\right)\right.\\
&\quad\left.-\left(\frac{2\zeta}{\omega^3\Delta t}+\frac{1}{\omega^2}\right)\left(\omega_d\sin\omega_d\Delta t+\zeta\omega\cos\omega_d\Delta t\right)\right]+\frac{1}{\omega^2\Delta t}\\
b_{22} &= -e^{-\zeta\omega\Delta t}\left[\frac{2\zeta^2-1}{\omega^2\Delta t}\left(\cos\omega_d\Delta t-\frac{\zeta}{\sqrt{1-\zeta^2}}\sin\omega_d\Delta t\right)\right.\\
&\quad\left.-\frac{2\zeta}{\omega^3\Delta t}\left(\omega_d\sin\omega_d\Delta t+\zeta\omega\cos\omega_d\Delta t\right)\right]-\frac{1}{\omega^2\Delta t}
\end{aligned}
\right\} \qquad (4.9)
$$

where

$$\omega_d \equiv \omega\sqrt{1-\zeta^2} \quad . \qquad (4.10)$$

If the displacement and velocity of the oscillator are known at t_i, the complete response can be computed by a step-by-step application of eqn. (4.7). The advantage of this method lies in the fact that for a constant time interval Δt, matrices A and B depend only on ζ and ω which are constant along any linear segment of the restoring force.

4.3 Numerical Results

Solving eqn. (4.3) yields the entire time history of the response. However, only the maximum amplitude of response will

be discussed in this investigation. Let z_m be the maximum displacement ratio as a function of the earthquake, system, nominal period, nominal viscous damping and relative strength of the excitation. Then, the ductility ratio may be expressed as

$$\mu = z_m(\text{Eqk, Sys, } T_0, \zeta_0, \rho) \quad . \tag{4.11}$$

For each ρ as given in eqn. (4.6) there is a corresponding yield displacement x_y. Hence, the maximum displacement response x_m may be expressed as

$$x_m(\text{Eqk, Sys, } T_0, \zeta_0, \rho) = x_y(\text{Sys}, \rho) \cdot z_m(\text{Eqk, Sys, } T_0, \zeta_0, \rho) \quad . \tag{4.12}$$

For a typical earthquake in the ensemble such as HOL the values of x_m/a^* may be plotted versus the corresponding values of μ for monotonically increasing ρ. This is illustrated for the earthquake HOL in Figs. 4.4-4.9.

In Figs. 4.4-4.9 the response of a completely linear system would be a line of constant x_m/a^* for all μ. This is seen in the regions of linear response for the BLH, 02-10-00 and 10-00-00 systems. The method of scaling the system relative to the excitation which was used in the present investigation yields decreasing x_y with increasing ρ. For a linear region of system response, as ρ is increasing x_y is decreasing and μ is increasing such that $x_m = \mu x_y$ remains constant.

Visual inspection of Figs. 4.4-4.9 reveals that x_m/a^* versus μ is not a single valued function of μ. For a typical system such

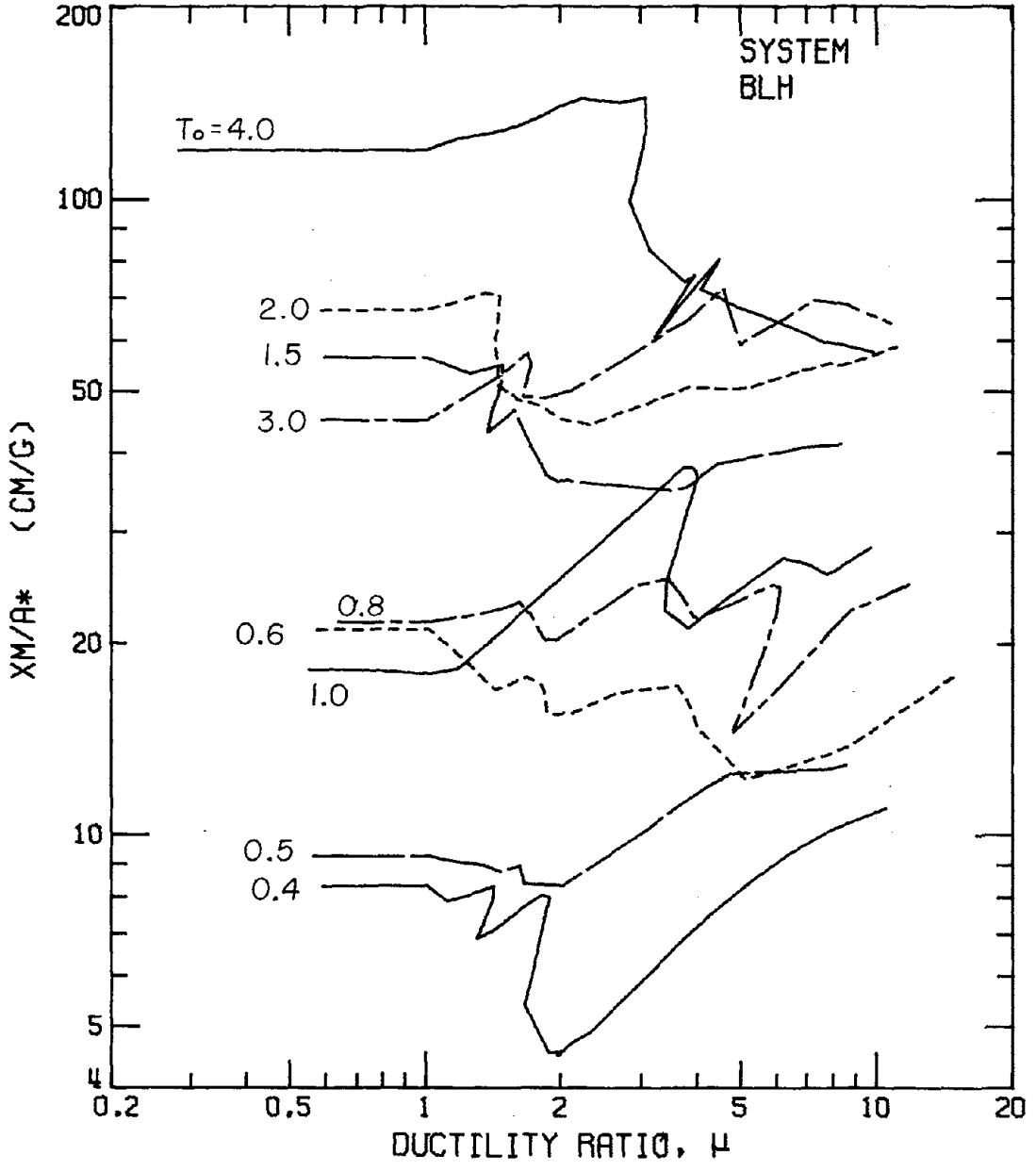

Figure 4.4. Maximum Displacement versus Ductility Ratio for BLH System and HOL Earthquake.

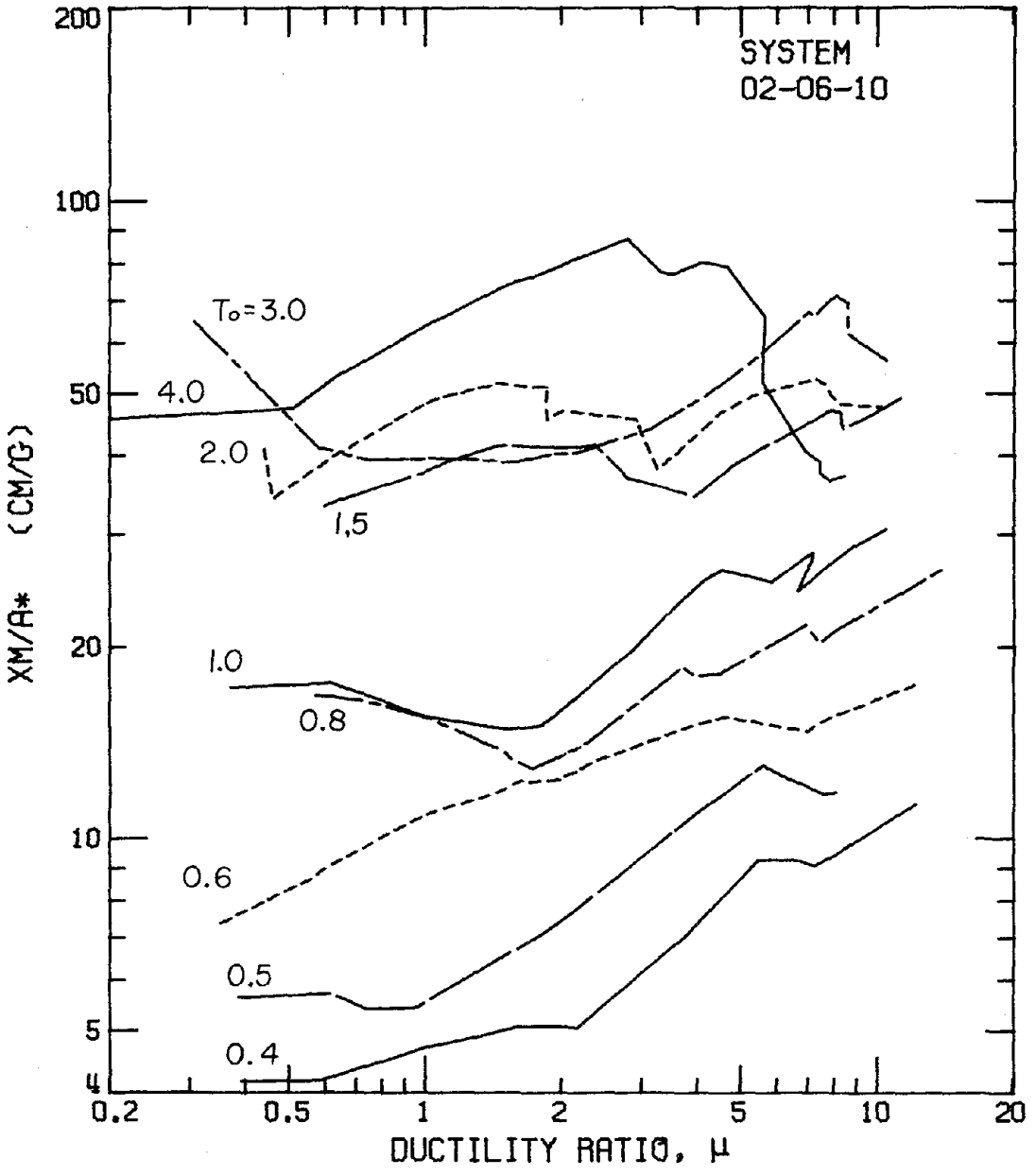

Figure 4.5. Maximum Displacement versus Ductility Ratio for 02-06-10 System and HOL Earthquake.

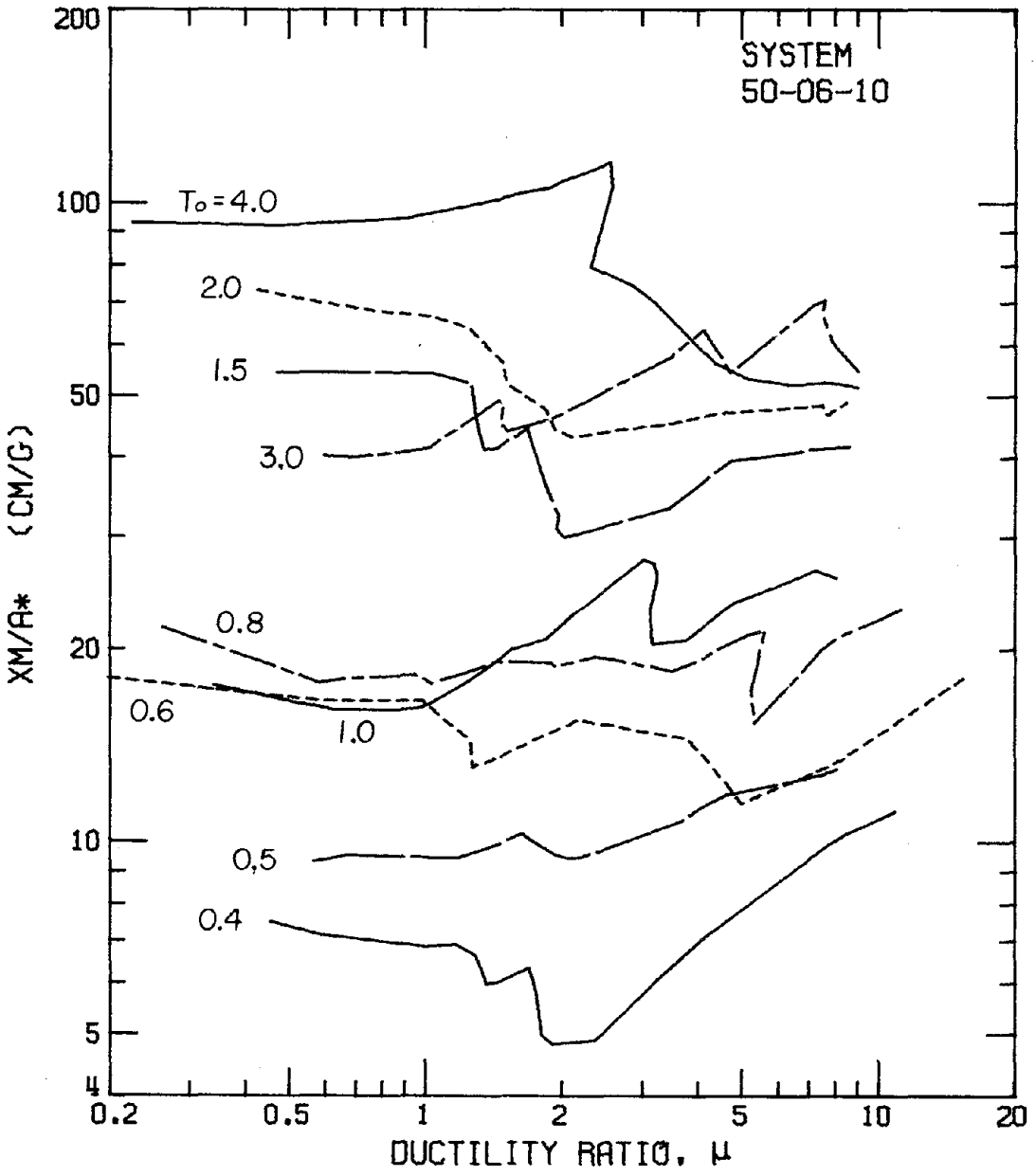

Figure 4.6. Maximum Displacement versus Ductility Ratio for 50-06-10 System and HOL Earthquake.

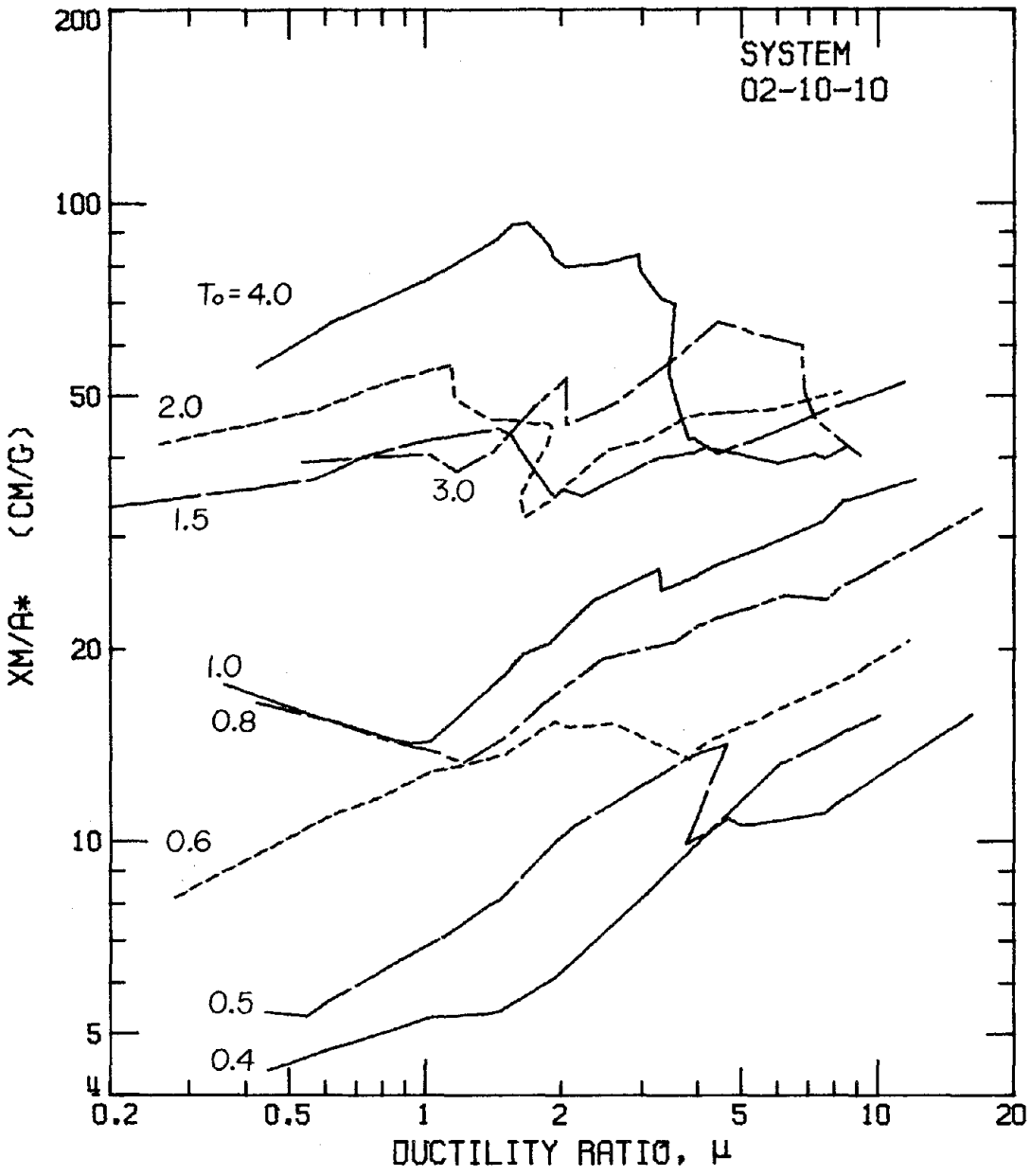

Figure 4.7. Maximum Displacement versus Ductility Ratio for 02-10-10 System and HOL Earthquake.

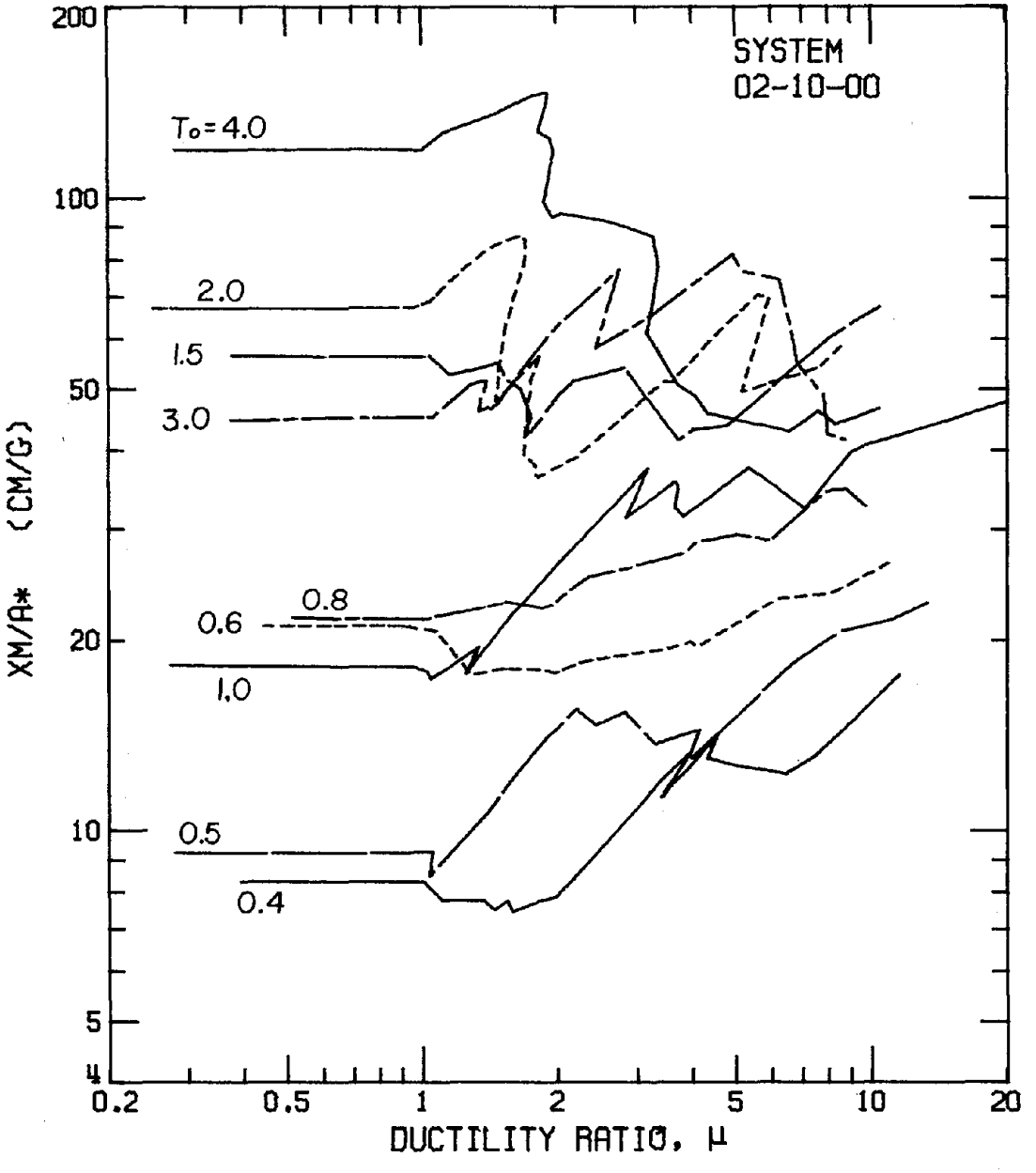

Figure 4.8. Maximum Displacement versus Ductility Ratio for 02-10-00 System and HOL Earthquake.

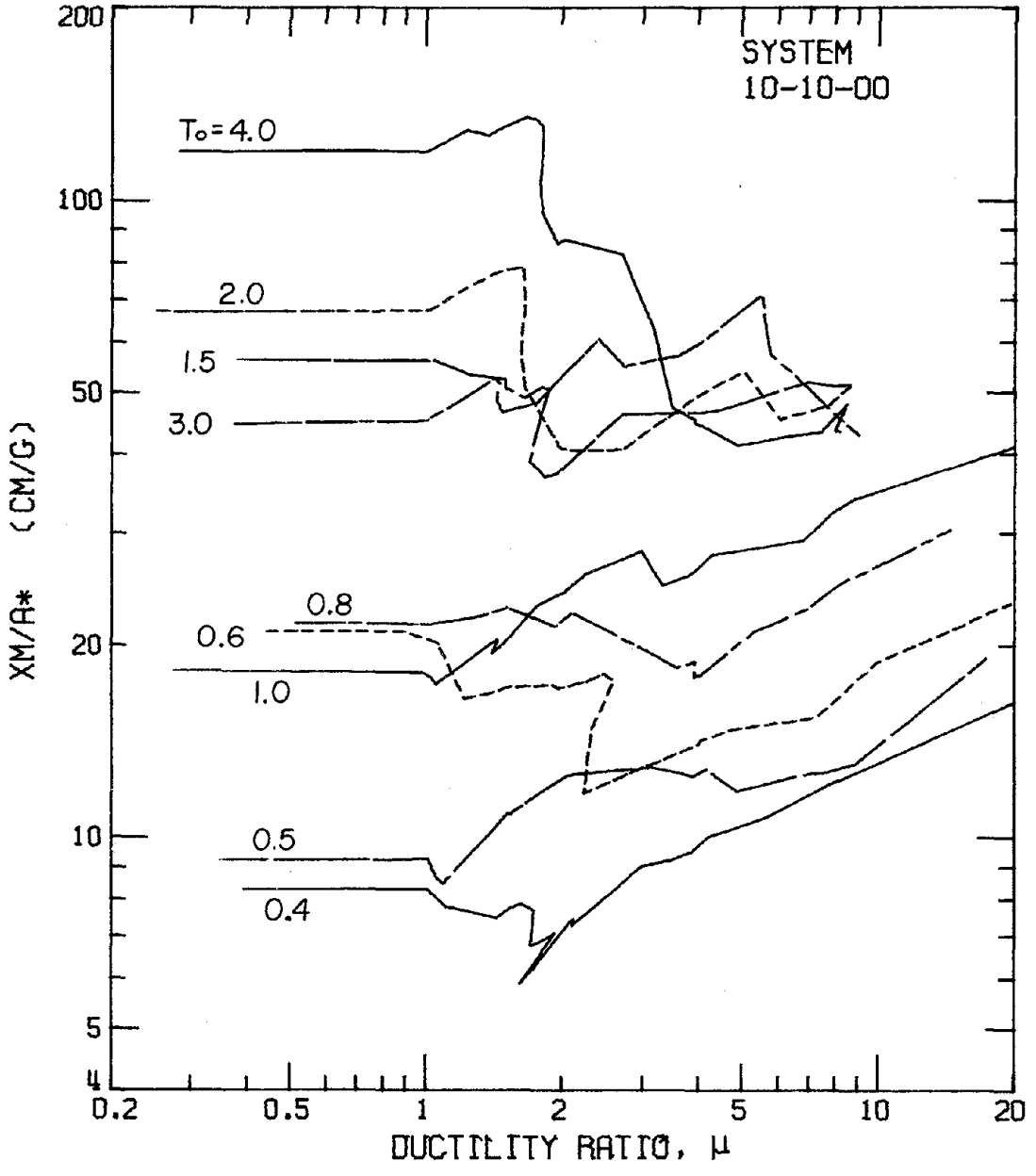

Figure 4.9. Maximum Displacement versus Ductility Ratio for 10-10-00 System and HOL Earthquake.

as 02-10-00 in Fig. 4.8 with nominal period $T_0 = 2.0$ seconds the response as a function of ductility is multivalued in the range of ductilities $1.5 \leq \mu \leq 2.0$.

The time histories for this system corresponding to seven values of ρ are presented in Fig. 4.10. There are two important characteristics of these time histories that help to explain the multivalued nature of the nonlinear system response. First, as ρ increases and x_y decreases the system enters the nonlinear region of response earlier and thus dissipates more energy. Hence, although the system is getting weaker the maximum response may decrease due to the energy dissipation. This decrease in the maximum response may be greater than the corresponding decrease in x_y so that μ actually decreases. In Fig. 4.10 this behavior is evident in comparing $\rho = 2.36$ with $\rho = 1.89$. For $\rho = 1.89$ the response doesn't exceed the yield level until $t = 11$ seconds but for $\rho = 2.36$ the first nonlinear response occurs at $t = 7.5$ seconds. Comparison of $\rho = 4.72$ with $\rho = 2.36$ reveals that more nonlinear behavior is occurring even earlier and the peak response is therefore much earlier as well as being smaller.

The second important characteristic to note from the time histories in Fig. 4.10 is that as the system becomes nonlinear the effective period of the system changes and the system in essence detunes itself from the excitation. Hence, the system may shift its response to a period range where there is less excitation energy and may therefore have a smaller maximum response in spite of the relative increase in the strength of the excitation.

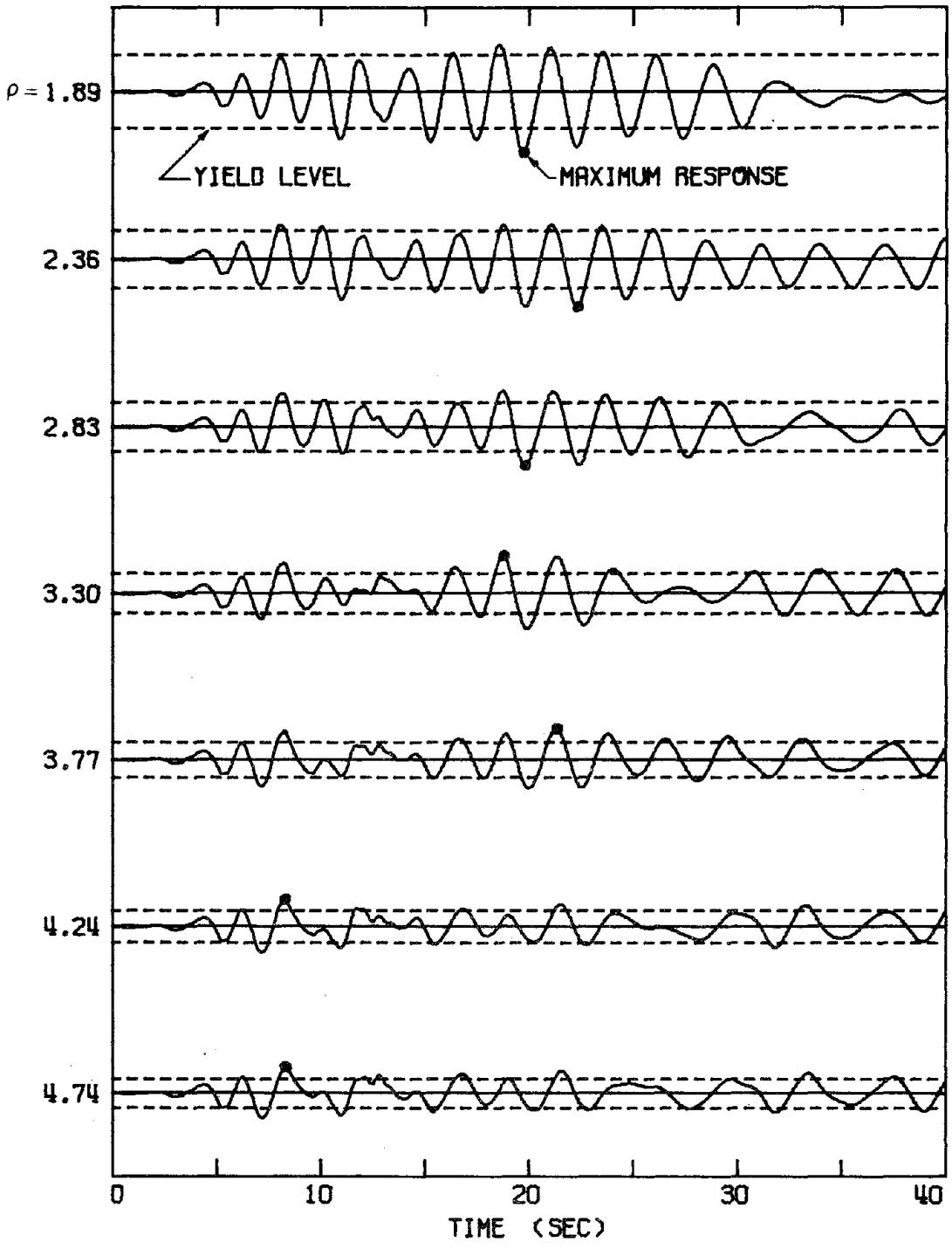

Figure 4.10. Time Histories of Response for HOL Earthquake, 02-10-00 System with T_0 = 2.0 seconds. Vertical Scale is the same in all seven cases.

Again, the decrease in maximum response may be greater than the corresponding decrease in yield level resulting in a decrease in ductility. An example of this detuning is seen in comparing $\rho = 4.72$ with $\rho = 1.89$. For $\rho = 1.89$ the response is nearly the narrowband response of a linear system while $\rho = 4.72$ resembles a broadband response due to the changing period of the nonlinear system.

4.4 Nonlinear Response Spectra

The nonlinear spectral displacement SD_n may be obtained from the maximum response $x_m(\text{Eqk}, \text{Sys}, T_0, \zeta_0, \rho)$ and the ductility μ by letting

$$\left.\begin{aligned} SD_n(\text{Eqk}, \text{Sys}, T_0, \zeta_0, \mu) &= \max_{\rho} x_m(\text{Eqk}, \text{Sys}, T_0, \zeta_0, \rho) \\ \rho \text{ such that } \mu &= z_m(\text{Eqk}, \text{Sys}, T_0, \zeta_0, \rho) \end{aligned}\right\} \quad (4.13)$$

Based on data such as that presented in Figs. 4.4-4.9, displacement response spectra are calculated for each earthquake in the ensemble and each of the six systems at the six ductilities $\mu = 0.6$, 1.0, 1.5, 2.0, 4.0 and 8.0. The ensemble average response spectra for each of the six systems is presented in Figs. 4.11-4.13. The nonlinear displacement response spectra are presented as pseudovelocity spectra using the relationship

$$PSV = \frac{2\pi}{T} SD \quad . \quad (4.14)$$

For the remainder of this chapter the numerical results are based upon the ensemble average rather than one particular earthquake.

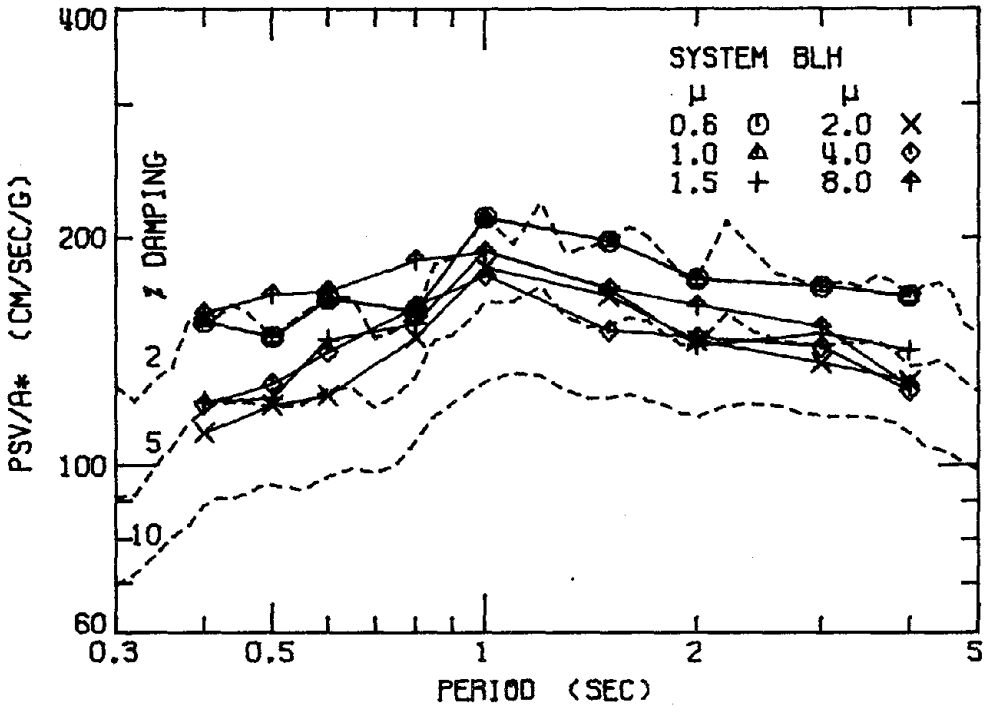

Figure 4.11a. Average Response Spectra BLH System.

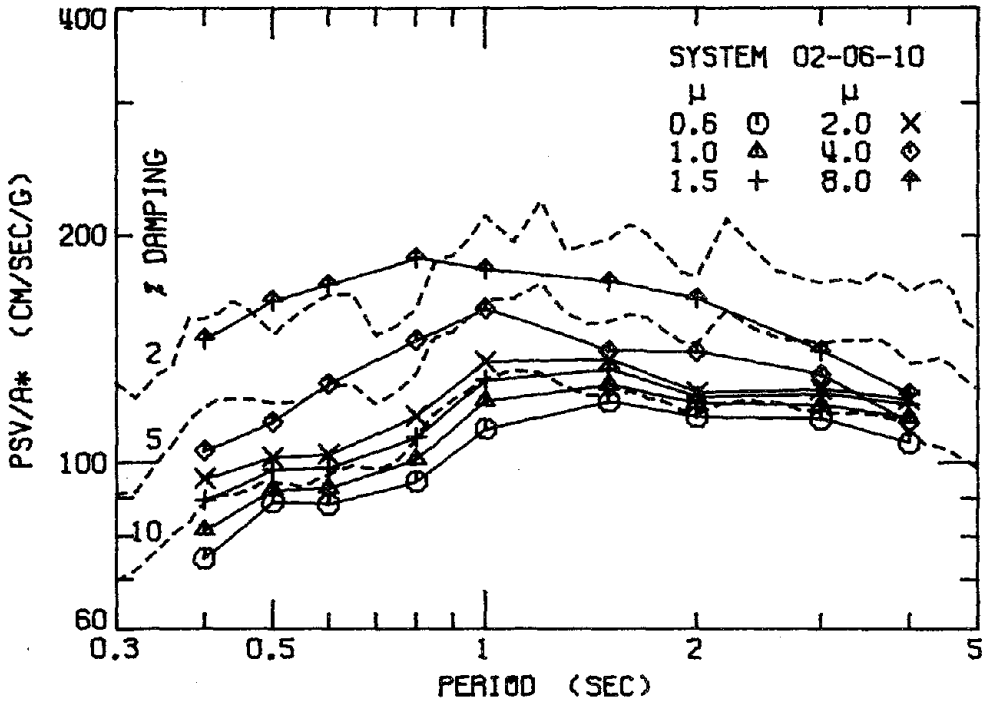

Figure 4.11b. Average Response Spectra 02-06-10 System.

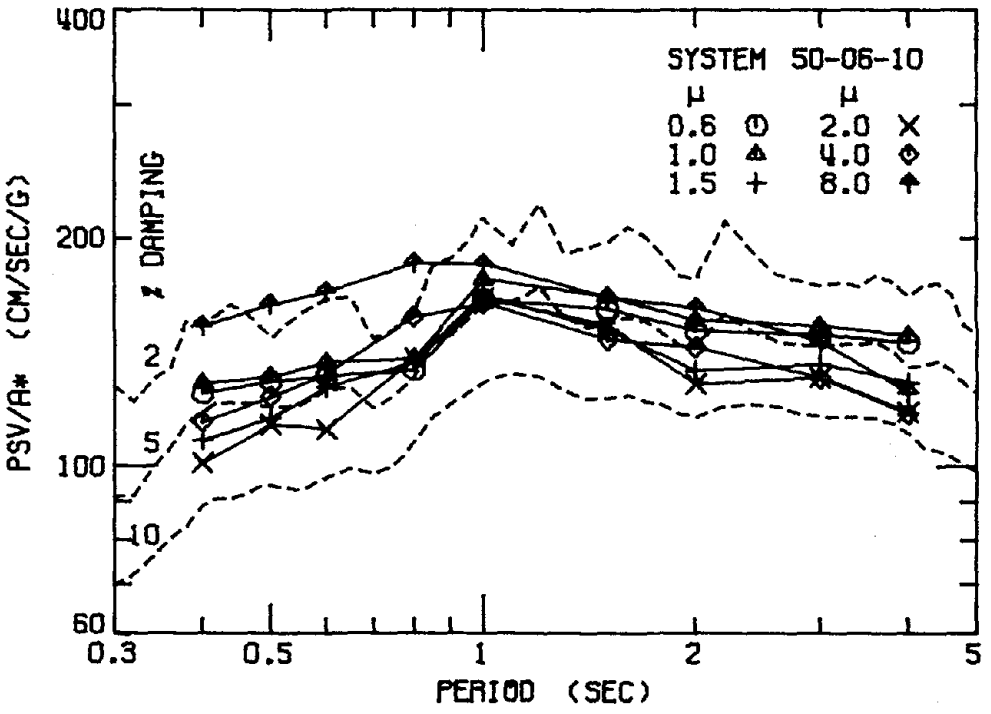

Figure 4.12a. Average Response Spectra 50-06-10 System.

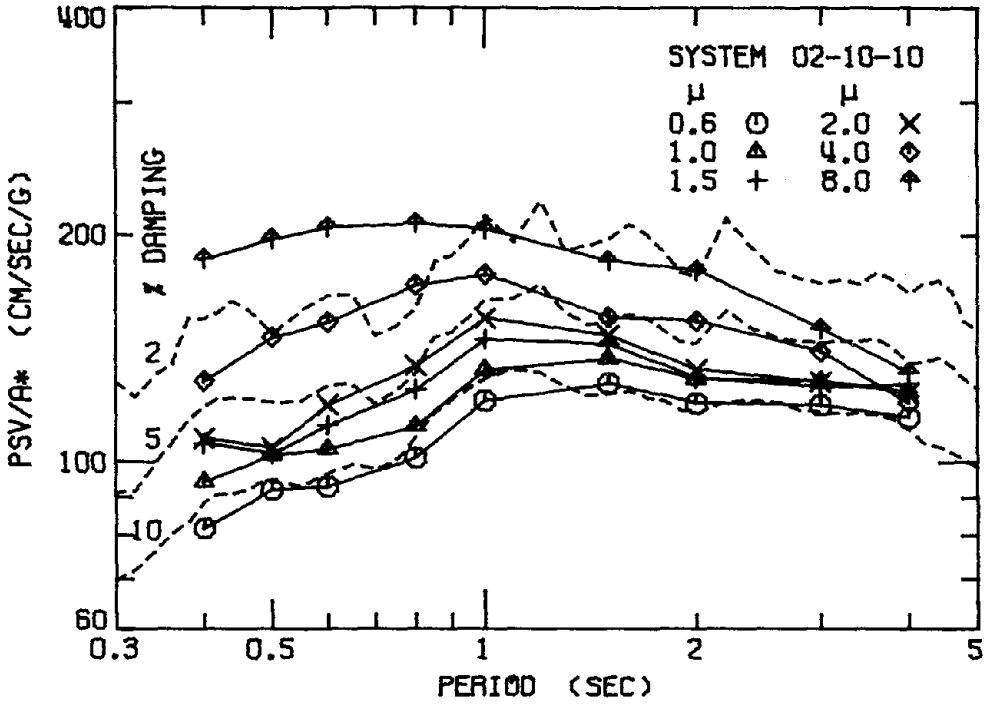

Figure 4.12b. Average Response Spectra 02-10-10 System.

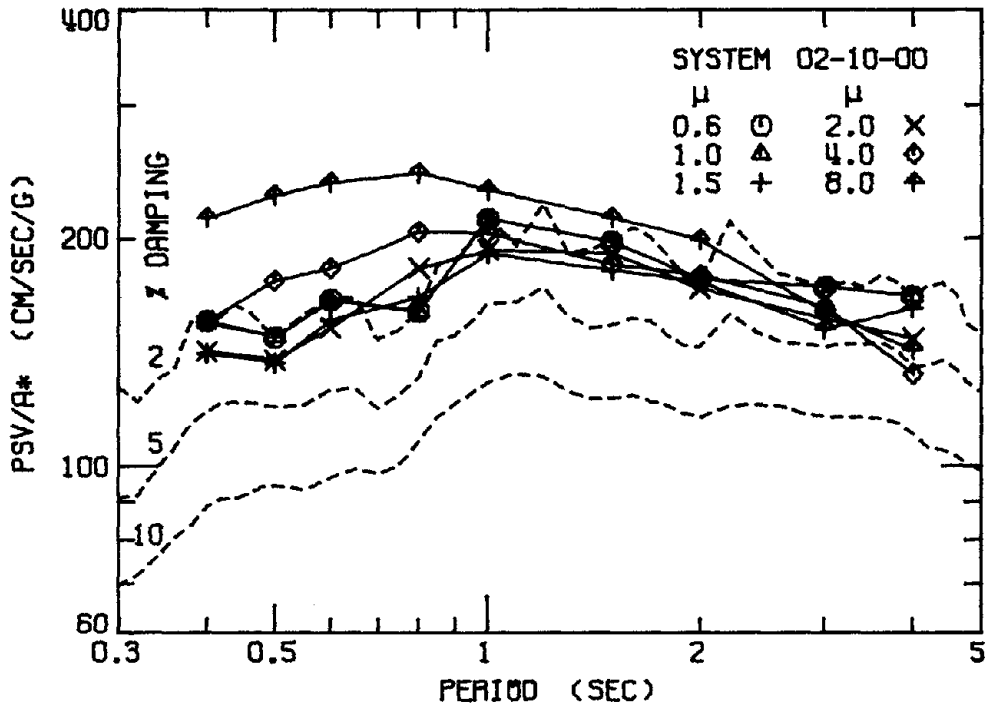

Figure 4.13a. Average Response Spectra 02-10-00 System.

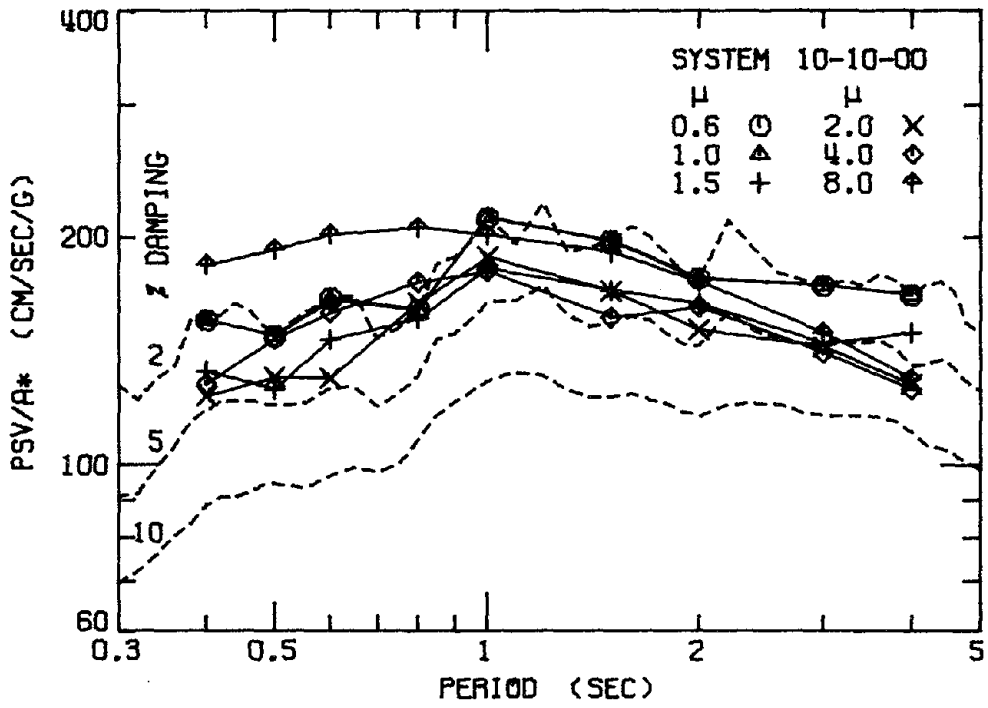

Figure 4.13b. Average Response Spectra 10-10-00 System.

For highly deteriorating systems with cracking such as 02-06-10 and 02-10-10 the nonlinear response spectra generally increase with increasing ductility. On the other hand, for non-deteriorating or slightly deteriorating systems such as BLH and 50-06-10 the response spectra decrease with increasing ductility up to $\mu = 2.0$ then they increase with increasing ductility.

The three systems with no cracking (BLH, 02-10-00 and 10-10-00) have similar response. The $\mu = 0.6$ and 1.0 spectra are the linear response spectrum for these systems. The response decreases then increases with increasing ductility. The spectrum corresponding to $\mu = 8.0$ is larger than the other spectra for small periods. This behavior is predicted by approximate stationary theories [37].

The individual earthquake dependence has been removed from the data presented in Figs. 4.11-4.13 by taking the ensemble average. A measure of the dispersion of the data may be obtained from the ratio of the standard deviation σ and the mean $\bar{x}$ of the nonlinear spectral displacement. In Table 4.2, the ratio $\sigma/\bar{x}$ is presented for all six systems at the six ductilities and the nine nominal periods considered herein.

From visual inspection of the ratio $\sigma/\bar{x}$ in Table 4.2 it appears that there is a significant dependence of $\sigma/\bar{x}$ on the nominal period of the system. Performing two way analyses of variance with replication [63] confirms the observation that period effects have a more significant effect upon $\sigma/\bar{x}$ than ductility or system effects. For a period of 0.4 sec the average value of $\sigma/\bar{x}$ is 22.64% while

TABLE 4.2. $\sigma/\bar{x}$

NOMINAL PERIOD SYSTEM	μ	0.4	0.5	0.6	0.8	1.0	1.5	2.0	3.0	4.0
BLH	0.6	32.19	22.13	32.25	21.57	23.18	35.85	28.86	42.95	48.85
	1.0	32.18	22.11	32.34	21.55	23.33	35.78	28.90	42.91	49.08
	1.5	18.27	25.96	32.27	21.99	25.62	30.44	30.86	36.90	48.04
	2.0	22.86	17.87	17.81	17.63	26.16	27.28	33.01	43.47	43.95
	4.0	16.10	16.35	16.07	13.66	21.34	29.64	26.90	42.69	49.96
	8.0	12.67	16.80	16.04	24.07	29.38	28.63	38.17	50.94	50.30
02-06-10	0.6	22.39	24.72	19.22	27.17	16.65	23.22	26.64	33.36	41.41
	1.0	25.23	25.50	23.40	20.53	17.64	24.91	24.42	36.22	43.64
	1.5	25.81	24.09	26.85	18.16	20.88	25.09	23.60	39.44	44.37
	2.0	26.95	21.71	26.91	15.66	21.12	23.88	23.85	40.54	45.20
	4.0	15.44	20.54	15.72	16.75	24.10	23.32	28.10	41.83	44.22
	8.0	12.61	12.53	16.07	19.59	20.89	27.40	31.07	43.31	53.57
50-06-10	0.6	34.07	23.12	27.47	18.73	20.87	28.07	24.26	40.41	48.34
	1.0	34.52	22.71	27.86	18.40	20.82	30.37	25.95	39.55	48.78
	1.5	20.37	19.69	29.27	18.05	23.06	27.03	23.84	37.15	48.99
	2.0	19.48	19.66	25.05	15.38	24.88	27.86	23.68	43.61	41.05
	4.0	19.54	17.00	13.74	13.01	18.58	31.78	29.14	44.36	50.97
	8.0	13.16	14.66	16.49	18.93	28.99	30.82	37.27	51.41	53.09
02-10-10	0.6	25.29	25.37	23.12	20.72	17.82	24.93	24.31	36.20	43.55
	1.0	29.12	24.52	25.72	19.16	21.76	24.26	22.86	39.15	45.17
	1.5	28.10	19.68	25.07	15.55	20.65	24.85	27.69	38.46	44.80
	2.0	20.85	20.81	25.02	15.01	22.93	24.52	26.62	37.84	45.52
	4.0	16.17	12.89	14.49	18.42	18.20	26.60	26.70	39.45	50.13
	8.0	10.24	14.83	18.68	20.29	28.29	28.34	38.01	49.94	50.98
02-10-00	0.6	32.17	22.20	31.61	21.43	23.24	35.81	28.76	43.01	49.03
	1.0	32.39	22.19	31.42	21.53	23.16	35.83	28.66	42.96	48.87
	1.5	24.79	19.67	24.81	20.78	19.07	21.24	36.69	39.81	44.52
	2.0	18.70	24.87	24.26	18.40	21.88	25.43	41.69	45.89	43.42
	4.0	20.39	13.89	15.00	20.32	23.39	34.33	30.10	40.23	45.63
	8.0	11.62	17.46	20.05	24.60	30.13	32.02	41.69	47.70	55.57
10-10-00	0.6	32.30	22.19	31.61	21.42	23.22	35.80	28.76	43.00	48.84
	1.0	32.34	22.17	31.35	21.53	23.34	35.93	28.62	42.97	48.94
	1.5	24.28	20.43	27.03	20.15	21.34	23.72	31.76	41.28	46.65
	2.0	21.75	24.65	22.29	18.41	22.09	28.84	30.26	44.73	42.76
	4.0	20.55	11.41	12.42	15.54	21.22	24.09	31.86	42.44	50.84
	8.0	10.01	14.79	15.88	20.45	29.77	30.00	39.45	52.64	52.06
MEAN VALUE		22.64	20.03	23.19	19.29	22.75	28.55	29.81	42.19	47.53

for a period of 0.8 sec it is 19.3% and for a period of 4.0 sec it is 47.5%.

4.5 Defining an Effective Linear System

In Figs. 4.11-4.13 it is observed that the averaged nonlinear response spectra resemble the average linear response spectra except for a shift along an axis of constant displacement. For example, it is seen that if the nonlinear spectrum corresponding to the 02-06-10 system at $\mu = 8.0$ is shifted along an axis of constant displacement by a factor corresponding to a period shift of $T/T_0 = 1.59$ then this spectrum lies almost exactly on the linear spectrum corresponding to $\zeta = 13.7\%$. This is illustrated in Fig. 4.14a. Another example of a shifted nonlinear response spectrum is shown in Fig. 4.14b for the 02-10-00 system at $\mu = 8.0$. On the basis of this observation, it is concluded that it is possible to define an effective linear system for each earthquake, system, ductility combination.

The effective linear system may be specified by two parameters T_e/T_0 and ζ_e which minimize the rms error between a linear and shifted nonlinear spectra. The period ratio is used rather than period itself to eliminate the dependence upon nominal period. Let $SD_n(\text{Eqk}, \text{Sys}, T_0, \zeta_0, \mu)$ be the nonlinear spectral displacement as defined in eqn. (4.13) and let $SD_\ell(\text{Eqk}, T, \zeta)$ be the linear spectral displacement corresponding to a linear system with period T and viscous damping ζ. Then, the spectrum error at a particular nominal period T_i is given by

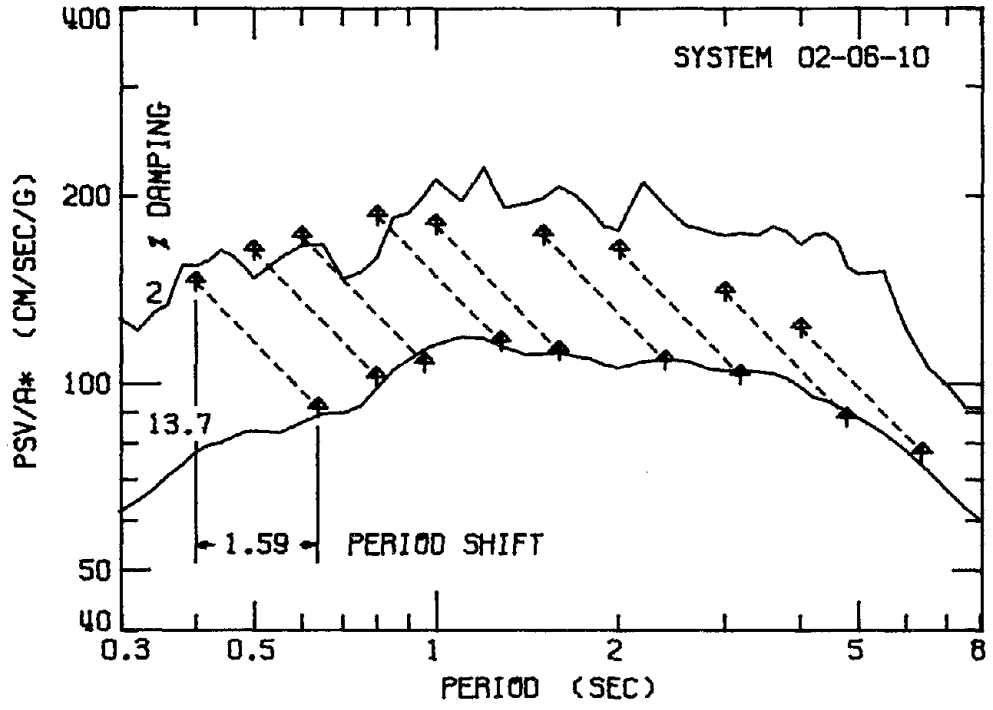

Figure 4.14a. Shifted Nonlinear Response Spectrum, $\mu = 8.0$.

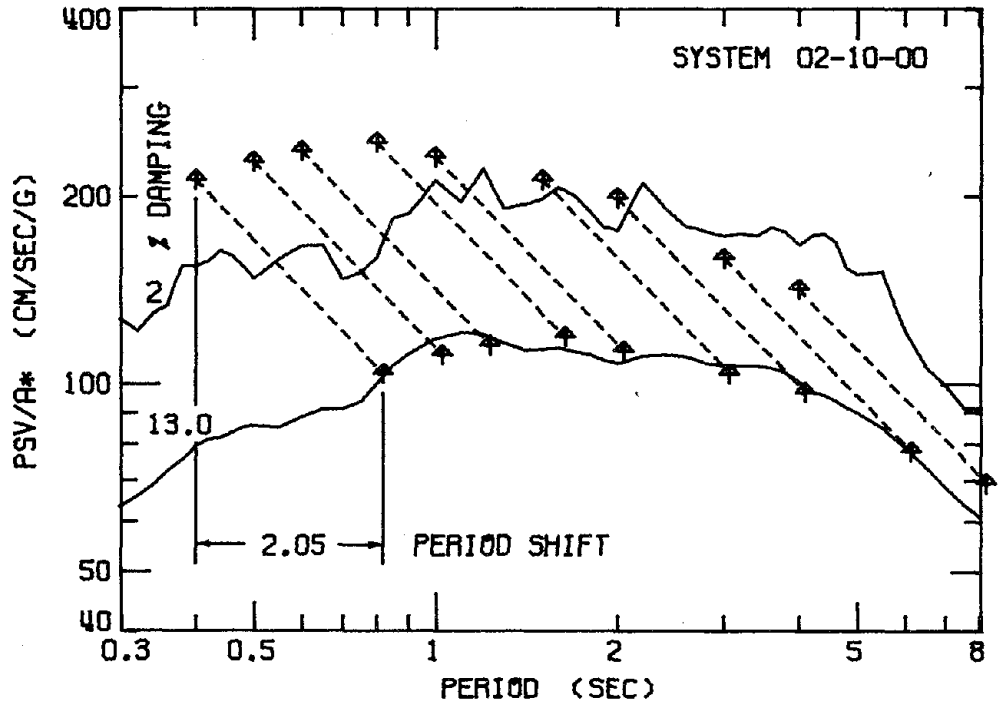

Figure 4.14b. Shifted Nonlinear Response Spectrum, $\mu = 8.0$.

$$\delta_i = \delta(\text{Eqk}, \text{Sys}, T, T_i, \zeta, \zeta_0, \mu)$$

$$= \frac{SD_\ell(\text{Eqk}, T, \zeta)}{SD_n(\text{Eqk}, \text{Sys}, T_i, \zeta_0, \mu)} - 1 \quad . \tag{4.15}$$

The rms spectrum error denoted by ϵ is then taken to be

$$\epsilon(\text{Eqk}, \text{Sys}, T/T_0, \zeta, \zeta_0, \mu) = \sqrt{\sum_{i=1}^{9} \frac{\delta_i^2}{9}} \quad . \tag{4.16}$$

Note that the period shift T/T_0 replaces the dependence upon both T and T_i in eqn. (4.15).

Let ϵ_m be the minimum rms spectrum error and let T_m/T_0 and ζ_m be the linear system parameters corresponding to ϵ_m. Then, the effective linear system for a particular nonlinear system is given by

$$\left.\begin{aligned} T_e &= T_i \cdot T_m/T_0 \\ \zeta_e &= \zeta_m \end{aligned}\right\} \tag{4.17}$$

where T_i is the nominal period of the nonlinear system and T_m/T_0 and ζ_m are functions of earthquake, system, ductility and nominal viscous damping.

All the data presented in the remainder of this chapter are derived from the average linear and average nonlinear spectra. Values of the rms spectral error ϵ for all of the systems considered in this study are shown in Figs. 4.15-4.19 as a function of

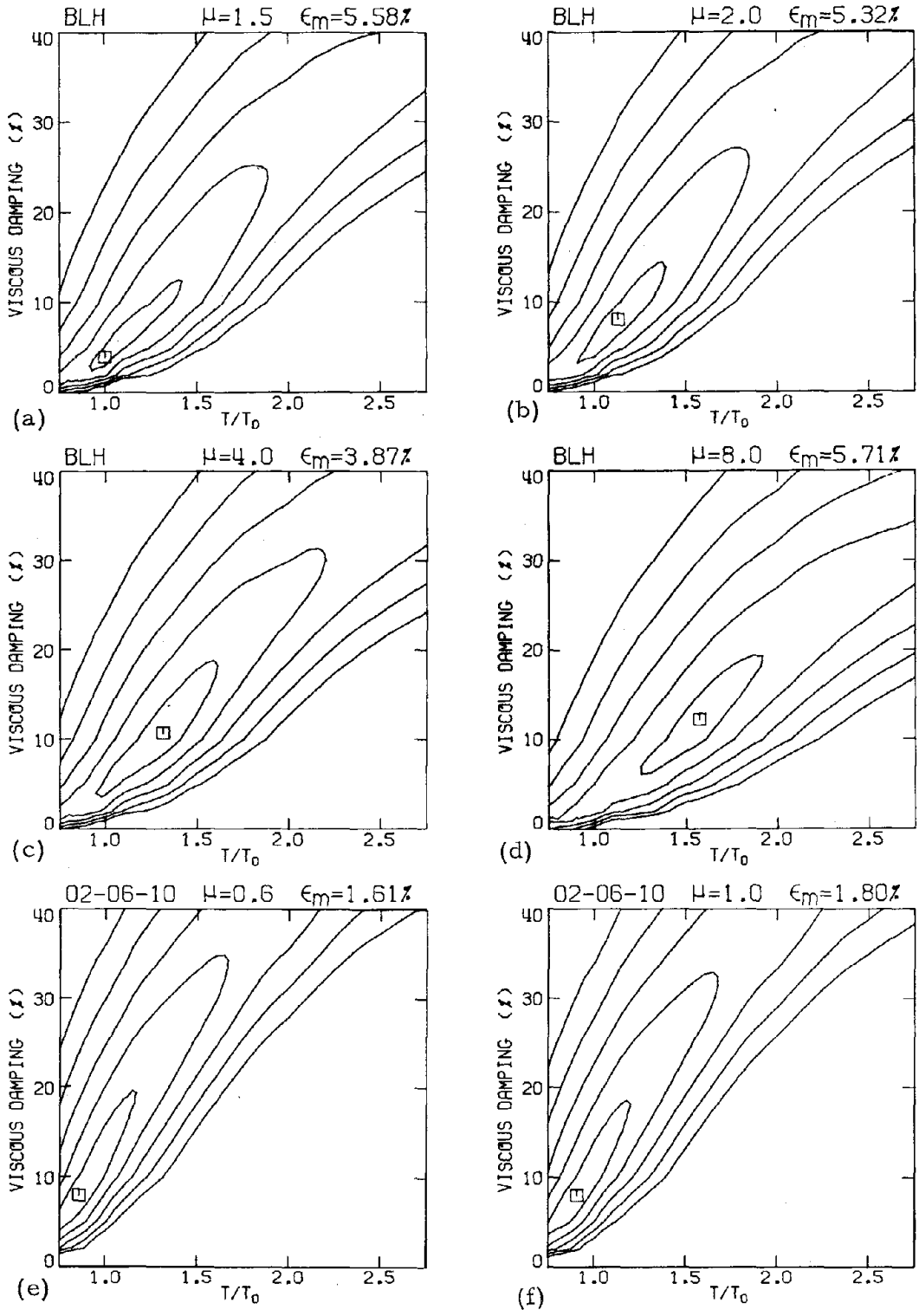

Figures 4.15a-f. RMS Spectral Error.

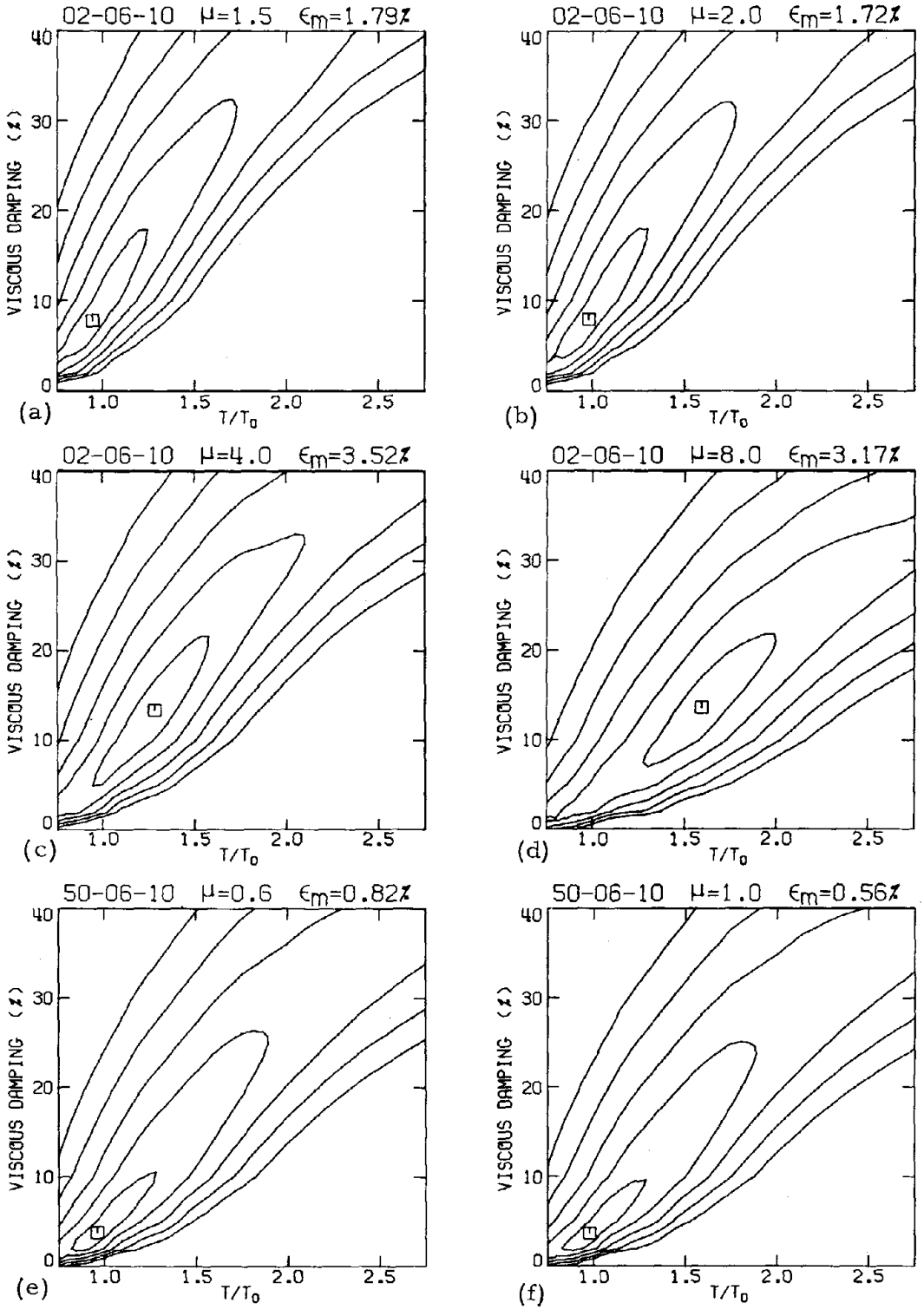

Figures 4.16a-f. RMS Spectral Error.

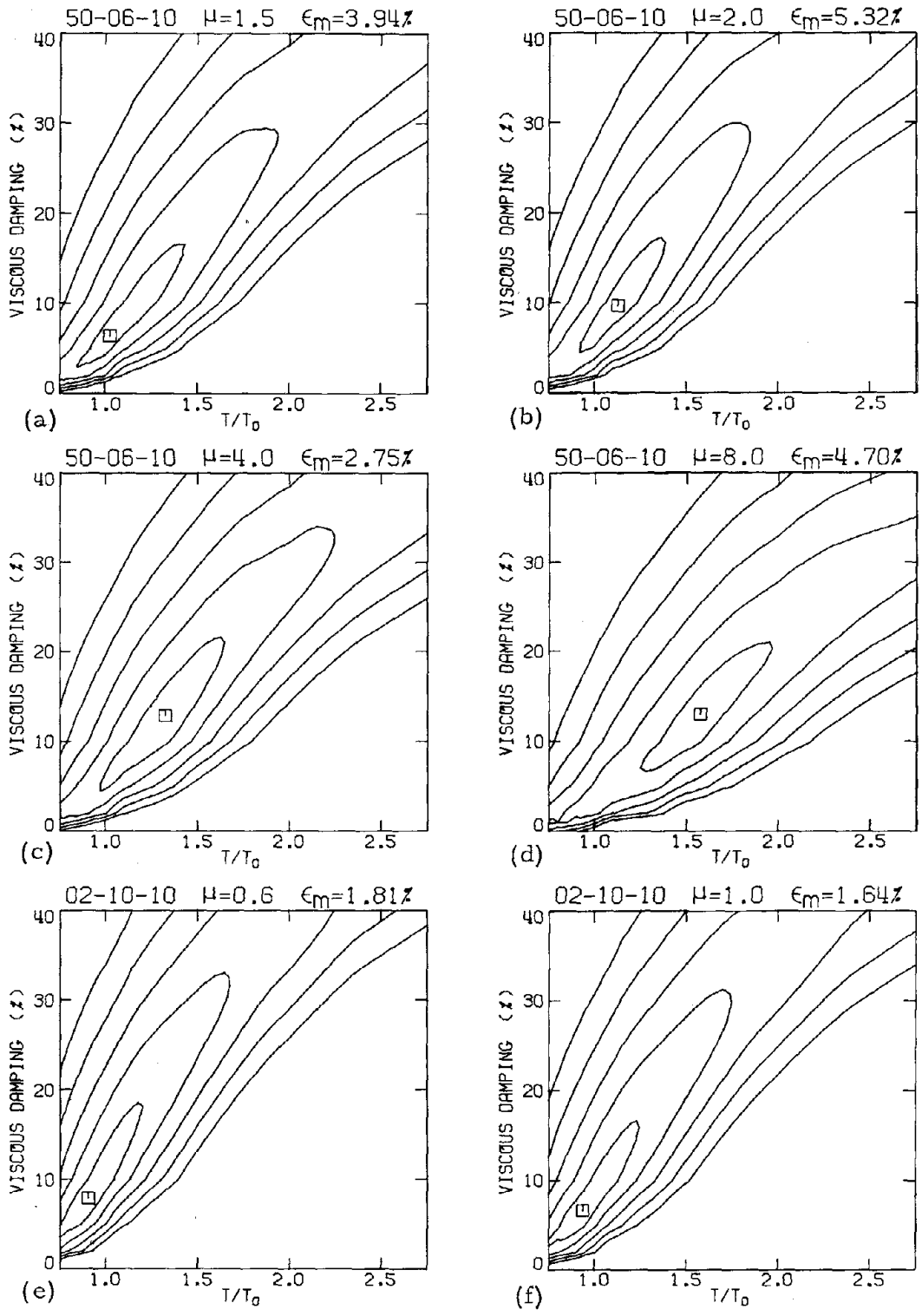

Figures 4.17a-f. RMS Spectral Error.

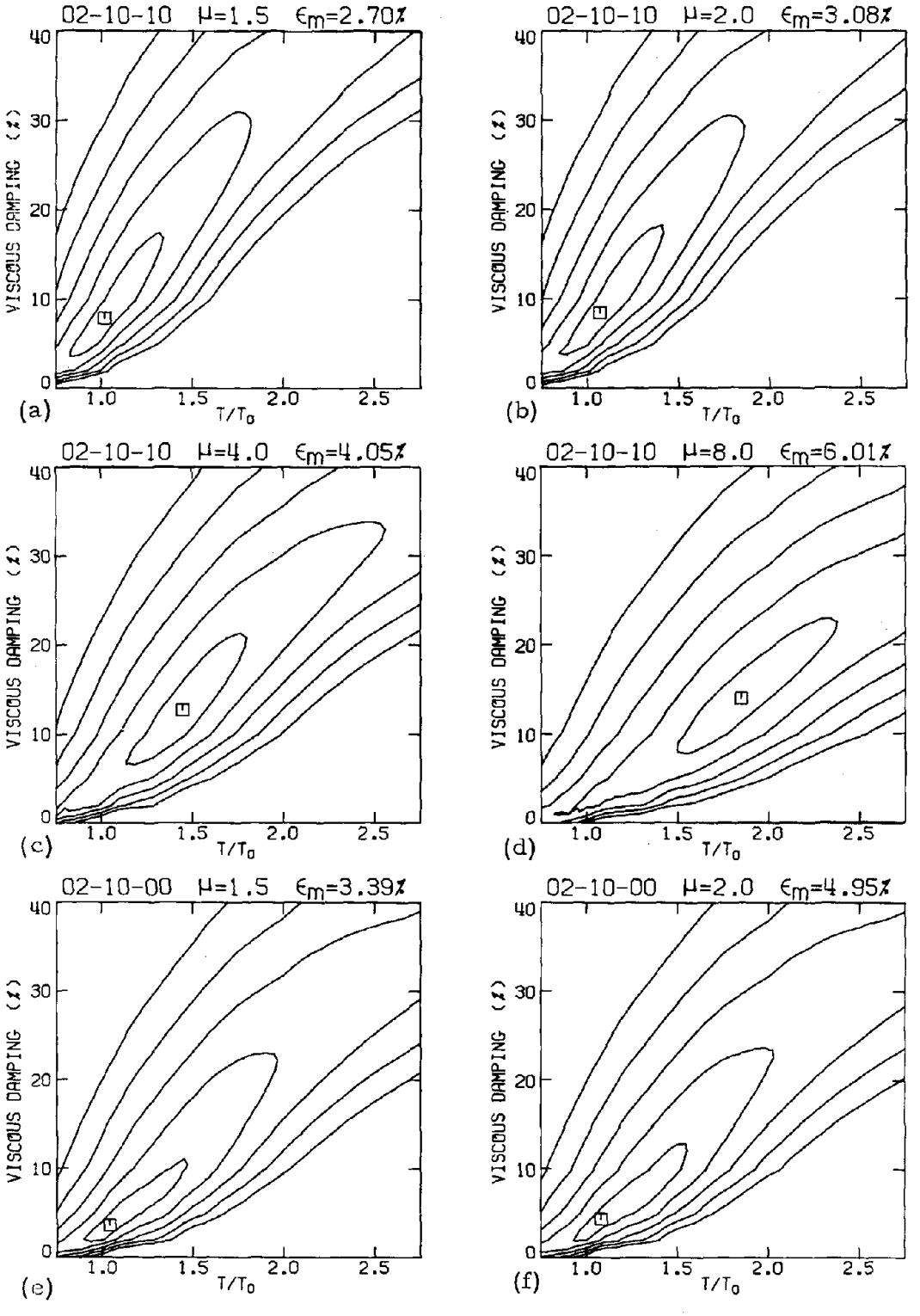

Figures 4.18a-f. RMS Spectral Error.

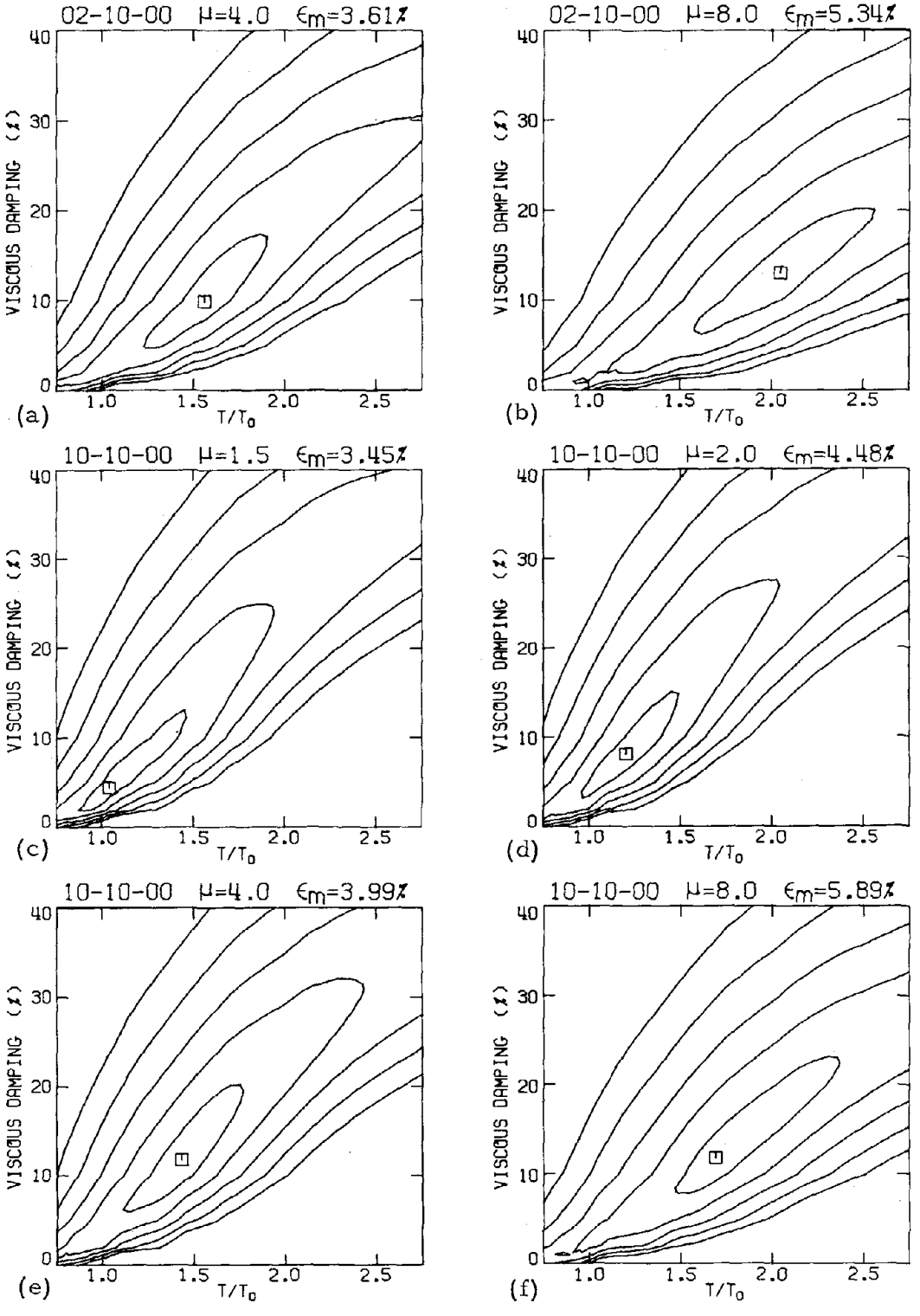

Figures 4.19a-f. RMS Spectral Error.

T/T_0 and ζ. Contour lines for ϵ = 10, 20, 30, 40 and 50 percent are indicated. The location of $(T_m/T_0, \zeta_m)$ corresponding to ϵ_m is denoted by a box. There are thirty contour plots in Figs. 4.15-4.19 corresponding to the rms spectral error for all six systems and all ductilities considered except for combinations which result in purely linear behavior.

In Figs. 4.15-4.19 it can be seen that the gradient of ϵ is a minimum in the direction of an axis passing diagonally through the point $(T_m/T_0, \zeta_m)$ such that $\zeta \propto (T/T_0)$. For example, in the case of system 02-06-10 at μ = 8.0 the minimum rms spectral error is $\epsilon_m = 3.17\%$ at $T_m/T_0 = 1.594$ and $\zeta_m = 13.66\%$. Along the axis of minimum gradient at $T/T_0 = 2.0$ and $\zeta = 21\%$ the error is $\epsilon \simeq 10\%$ while off this axis at $T/T_0 = 1.2$ and $\zeta = 21\%$ the error is $\epsilon \simeq 40\%$. Hence, it is concluded that approximations to T_m/T_0 and ζ_m will give better results if they fall on or near the axis of minimum gradient.

The values of T_m/T_0, ζ_m and ϵ_m are tabulated for the average spectra in Table 4.3. Note that for the three systems with non-zero cracking strength 50-06-10, 02-06-10 and 02-10-10 the period shift is less than one for ductilities less than or equal to one. This is due to neglecting the cracking in defining the nominal stiffness of the system. Hence, the initial stiffness of the system including cracking is greater than the nominal stiffness and the effective stiffness remains greater for all ductilities less than one.

The period shift for the more highly deteriorating systems with cracking such as 02-06-10 and 02-10-10 is smaller at μ = 0.6

TABLE 4.3

μ	T_m/T_0	ζ_m (%)	ϵ_m (%)
SYSTEM BLH			
0.6	1.000	2.00	0.14
1.0	1.000	2.00	0.17
1.5	1.000	4.00	5.58
2.0	1.130	8.06	5.32
4.0	1.317	10.75	3.87
8.0	1.573	12.25	5.71
SYSTEM 02-06-10			
0.6	0.858	7.96	1.61
1.0	0.908	7.96	1.80
1.5	0.946	7.82	1.79
2.0	0.979	7.93	1.72
4.0	1.281	13.44	3.52
8.0	1.594	13.66	3.17
SYSTEM 50-06-10			
0.6	0.963	3.84	0.82
1.0	0.979	3.66	0.56
1.5	1.026	6.44	3.94
2.0	1.128	9.68	5.32
4.0	1.328	12.88	2.75
8.0	1.574	13.06	4.70
SYSTEM 02-10-10			
0.6	0.907	7.90	1.81
1.0	0.938	6.67	1.64
1.5	1.019	7.87	2.70
2.0	1.068	8.53	3.08
4.0	1.449	12.76	4.05
8.0	1.850	14.00	6.01
SYSTEM 02-10-00			
0.6	1.000	2.00	0.23
1.0	1.001	2.06	0.22
1.5	1.043	3.68	3.39
2.0	1.082	4.37	4.95
4.0	1.559	9.88	3.61
8.0	2.050	13.00	5.34
SYSTEM 10-10-00			
0.6	1.001	2.04	0.20
1.0	1.001	2.05	0.28
1.5	1.040	4.44	3.45
2.0	1.202	8.15	4.48
4.0	1.434	11.75	3.99
8.0	1.692	11.80	5.89

than the slightly deteriorating system 50-06-10 due to the greater increase in initial stiffness from the larger C-type element contribution. The effective viscous damping for these three systems with cracking is much larger at small ductilities due mainly to the energy dissipated by cracking and partly due to the effect upon viscous damping factor of period shift. Note that the slightly deteriorating system 50-06-10 has much smaller effective viscous damping at $\mu = 0.6$ than the highly deteriorating systems.

The three systems with zero cracking strength BLH, 02-10-00 and 10-10-00 behave as linear systems up to a ductility of one. For these systems ϵ_m should be zero at $T_m/T_0 = 1.0$ and $\zeta_m = \zeta_0 = 2\%$ but numerical inaccuracies such as round-off errors cause ϵ_m to be as large as 0.28% at values of T_m/T_0 and ζ_m slightly different from their theoretical values.

The effect of cracking is greatest at small ductilities which is clearly demonstrated by comparing the 02-10-10 and 02-10-00 systems. The contribution to the effective viscous damping due to cracking is significant at small ductilities, but at $\mu = 8.0$ its contribution is negligible. The effective period shift continues to reveal some effect of cracking even at ductilities as large as $\mu = 8.0$.

The effect of a more "ductile" design is to increase the energy dissipation as demonstrated by comparing 02-06-10 and 02-10-10. The 02-06-10 system is termed more ductile since the Y-type element yields before the C-type element. At $\mu = 1.0$ and at $\mu = 4.0$ the viscous damping of 02-06-10 exceeds that of 02-10-10.

The period shift for 02-06-10 is less due to the increased post yield stiffness associated with unyielded C-type element.

In Table 4.3 the minimum rms spectral error ϵ_m is generally less than 6%. Hence, the spectral displacement of the nonlinear system can always be estimated to within this error using the effective linear system values T_m/T_0 and ζ_m. Although the error may be larger than the rms value at a particular period, this still provides a very good estimate of the spectral displacement.

CHAPTER V

NUMERICAL COMPARISON WITH ANALYTICAL MODELS

5.0 Introduction

In this chapter the approximate methods of Chapter II are compared to the numerical results of Chapter IV. First, methods applicable to nondeteriorating systems are considered; then, methods applicable to deteriorating systems. Finally, the average stiffness and energy method is used to demonstrate the manner in which a nonlinear response spectrum may be generated from a particular earthquake, system and ductility.

5.1 Nondeteriorating Systems

There are eight approximate methods presented in Chapter II which may be applied to nondeteriorating systems. The five methods which may be used from the harmonic excitation section are harmonic equivalent linearization, resonant amplitude matching, dynamic mass, constant critical damping and geometric stiffness. The geometric energy method is excluded since it gives the effective viscous damping only. The two methods which may be used from the random and earthquake excitation section are stationary random equivalent linearization and average period and damping. Of the two methods in the deteriorating system section, only the average stiffness and energy method may also be applied to nondeteriorating systems.

Each of these eight methods yields a value of the period shift and viscous damping as a function of ductility. This may be

translated into a value for the spectral displacement using the appropriate linear response spectrum.

In this section the eight approximate methods indicated are applied to the BLH system of Chapter III. The approximate linear system parameters and the approximate spectral displacement are compared to the results presented in Chapter IV.

5.1.1 Effective Period Shift and Effective Viscous Damping

Applying the eight methods just mentioned to the BLH system with $\alpha = 0.05$ and $\zeta_0 = 2\%$ yields the values of T_e/T_0 and ζ_e indicated in Fig. 5.1. The effective viscous damping is larger than that indicated in Fig. 2.9 since $\zeta_0 = 2\%$ in this case. Also indicated in Fig. 5.1 are the numerical results for the period shift and viscous damping which minimize the rms spectral error between the average linear and nonlinear response spectra. These results are tabulated in Table 4.3.

The following observations may be made about the approximate methods. All of the approximate methods except resonant amplitude matching and dynamic mass overestimate the effective viscous damping at all ductilities. For ductilities less than 5 the RAM and DM methods also overestimate the viscous damping. Generally speaking, the effective period shift is overestimated by all the methods except RAM and ASE methods. At $\mu = 1.5$ the SREL and APD methods also underestimate the effective period shift.

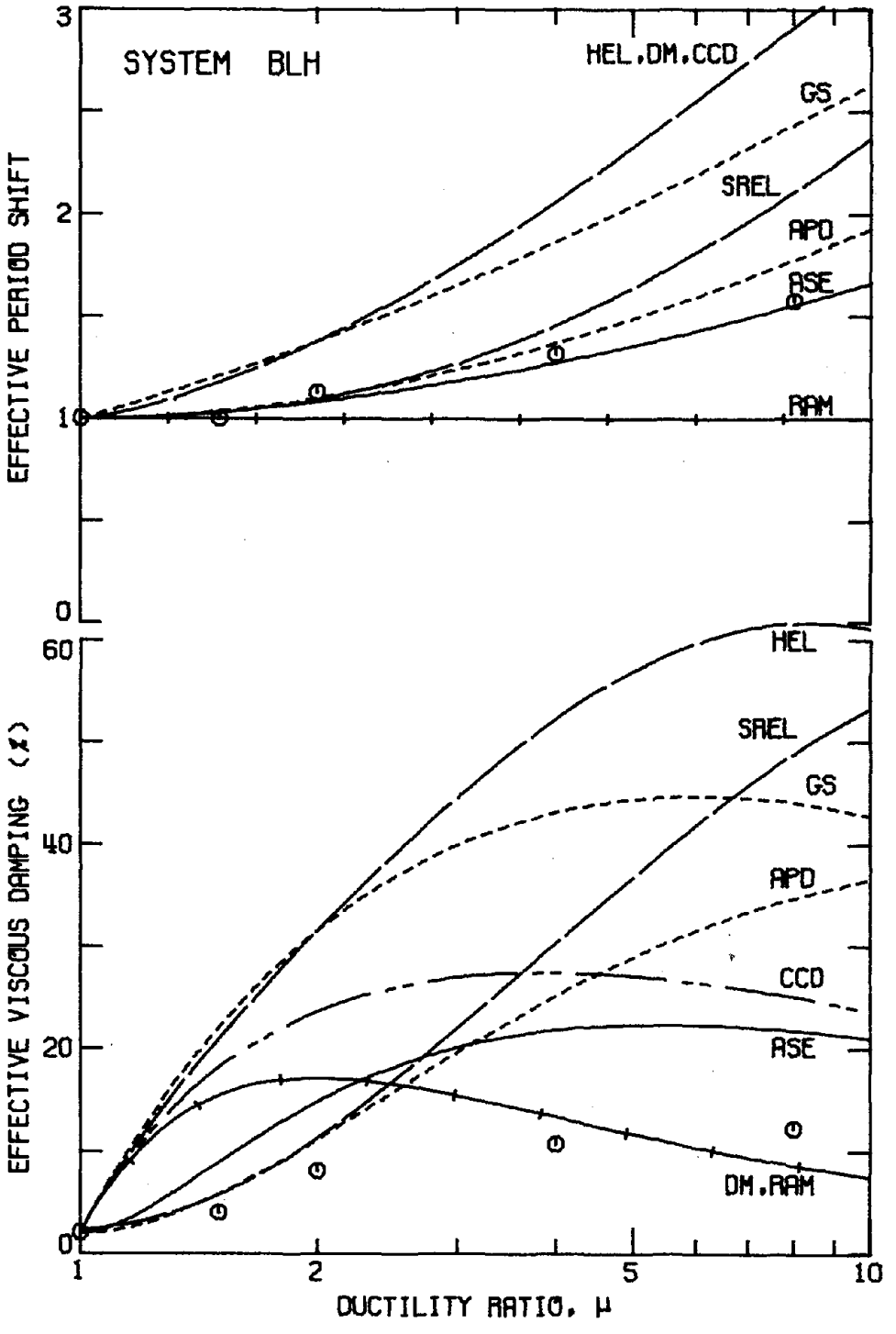

Figure 5.1. Approximate Linear System Parameters for the BLH system with $\alpha = 5\%$ and $\zeta_0 = 2\%$.

As mentioned in Chapter II and indicated by the numerical results, the effective viscous damping increases much more gradually with ductility on the range $1 \leq \mu \leq 2$ than indicated by the harmonic methods.

Generally speaking the three methods SREL, APD and ASE appear to give values for the effective linear system parameters which show better agreement with numerical results than do those from the harmonic methods. Furthermore, for large ductilities ($\mu \geq 4$) the ASE method gives effective linear system parameters which show better agreement than either the SREL or APD methods.

5.1.2 Spectral Displacement

The fact that an approximate method gives better values for the linear system parameters may or may not imply that it also gives a better value for the spectral displacement. As mentioned in section 4.5 the location of the point $(T_e/T_0, \zeta_e)$ with respect to the axis of minimum gradient has an important effect upon the accuracy of the approximate spectral displacement.

To evaluate the accuracy of the approximate spectral displacement, the rms spectral error $\mathcal{E}$ as defined by eqn. (4.16) is used. In Table 5.1 $\mathcal{E}$ is tabulated along with T_e/T_0 and ζ_e for each of the eight approximate methods considered in this section.

As mentioned earlier, the location of point $(T_e/T_0, \zeta_e)$ as well as its distance from $(T_m/T_0, \zeta_m)$ has an important effect on the rms spectral error. In the case of the CCD method at $\mu = 4$ the rms spectral error is 18.3% even though T_e/T_0 is 56.4% greater

TABLE 5.1

Comparison of Approximate Methods
BLH System with $\alpha = 5\%$ and $\zeta_0 = 2\%$

		DUCTILITY RATIO, μ			
		1.5	2.0	4.0	8.0
RAM	T_e/T_0 =	1.000	1.000	1.000	1.000
	ζ_e (%) =	15.44	17.12	13.34	8.61
	$\mathcal{E}$ (%) =	37.7	36.9	31.8	30.8
HEL	T_e/T_0 =	1.176	1.380	2.060	2.904
	ζ_e (%) =	20.95	31.56	52.23	61.61
	$\mathcal{E}$ (%) =	36.0	41.0	52.2	57.3
DM	T_e/T_0 =	1.176	1.380	2.060	2.904
	ζ_e (%) =	15.44	17.12	13.34	8.61
	$\mathcal{E}$ (%) =	25.2	13.5	52.0	98.8
CCD	T_e/T_0 =	1.176	1.380	2.060	2.904
	ζ_e (%) =	18.16	23.63	27.48	25.02
	$\mathcal{E}$ (%) =	30.7	26.5	18.3	28.7
GS	T_e/T_0 =	1.210	2.380	1.865	2.434
	ζ_e (%) =	22.09	31.56	43.17	44.07
	$\mathcal{E}$ (%) =	36.2	41.0	43.9	40.3
SREL	T_e/T_0 =	1.030	1.095	1.458	2.105
	ζ_e (%) =	5.72	11.30	30.31	48.79
	$\mathcal{E}$ (%) =	8.6	16.8	37.1	53.1
APD	T_e/T_0 =	1.036	1.102	1.372	1.775
	ζ_e (%) =	5.82	11.20	25.17	34.76
	$\mathcal{E}$ (%) =	8.4	16.0	31.8	40.6
ASE	T_e/T_0 =	1.031	1.082	1.273	1.551
	ζ_e (%) =	8.92	14.83	21.83	21.74
	$\mathcal{E}$ (%) =	20.3	25.9	30.2	25.6

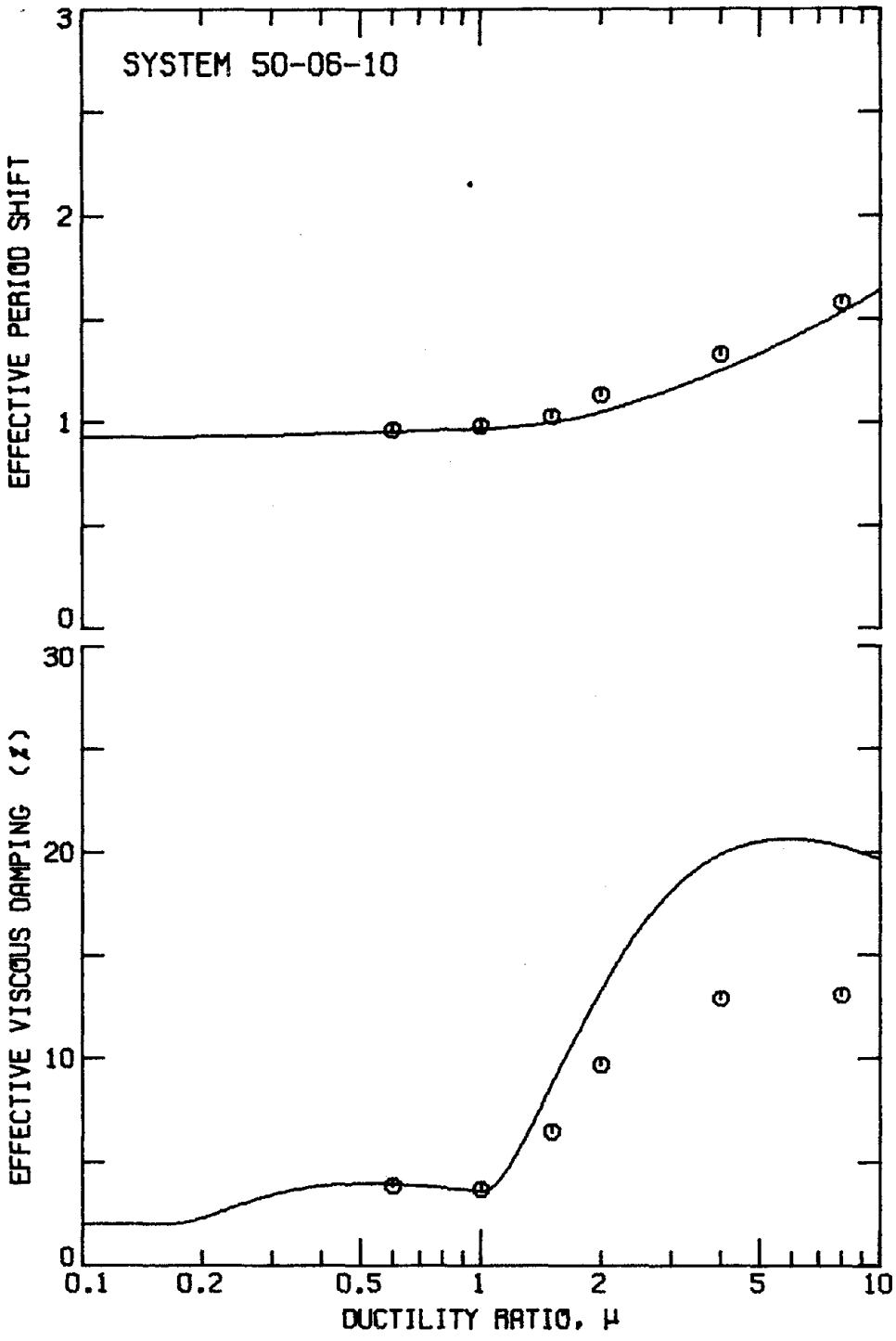

Figure 5.4. ASE Method Linear System Parameters for the 50-06-10 System with $\alpha = 5\%$ and $\zeta_0 = 2\%$.

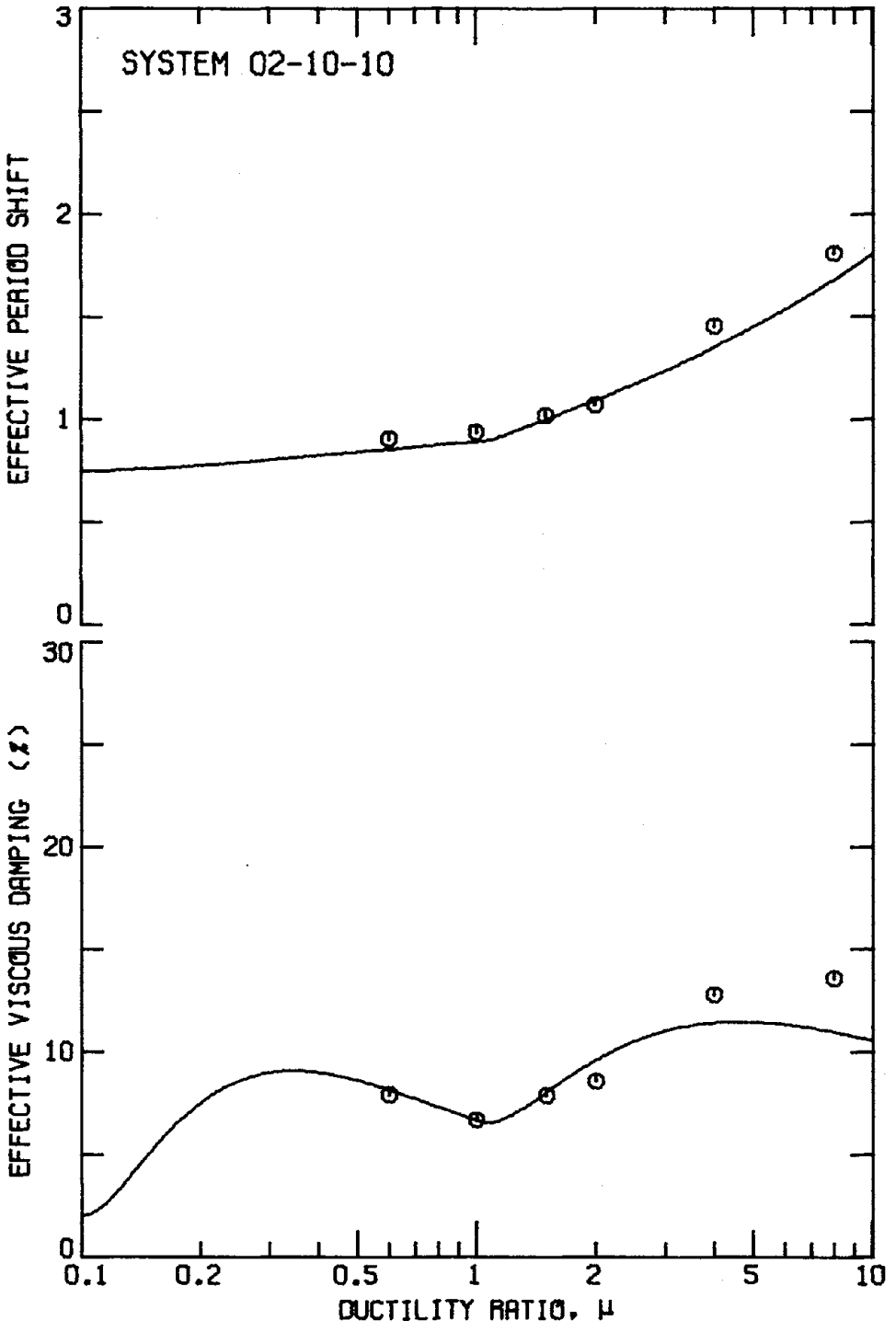

Figure 5.5. ASE Method Linear System Parameters for the 02-10-10 System with $\alpha = 5\%$ and $\zeta_0 = 2\%$.

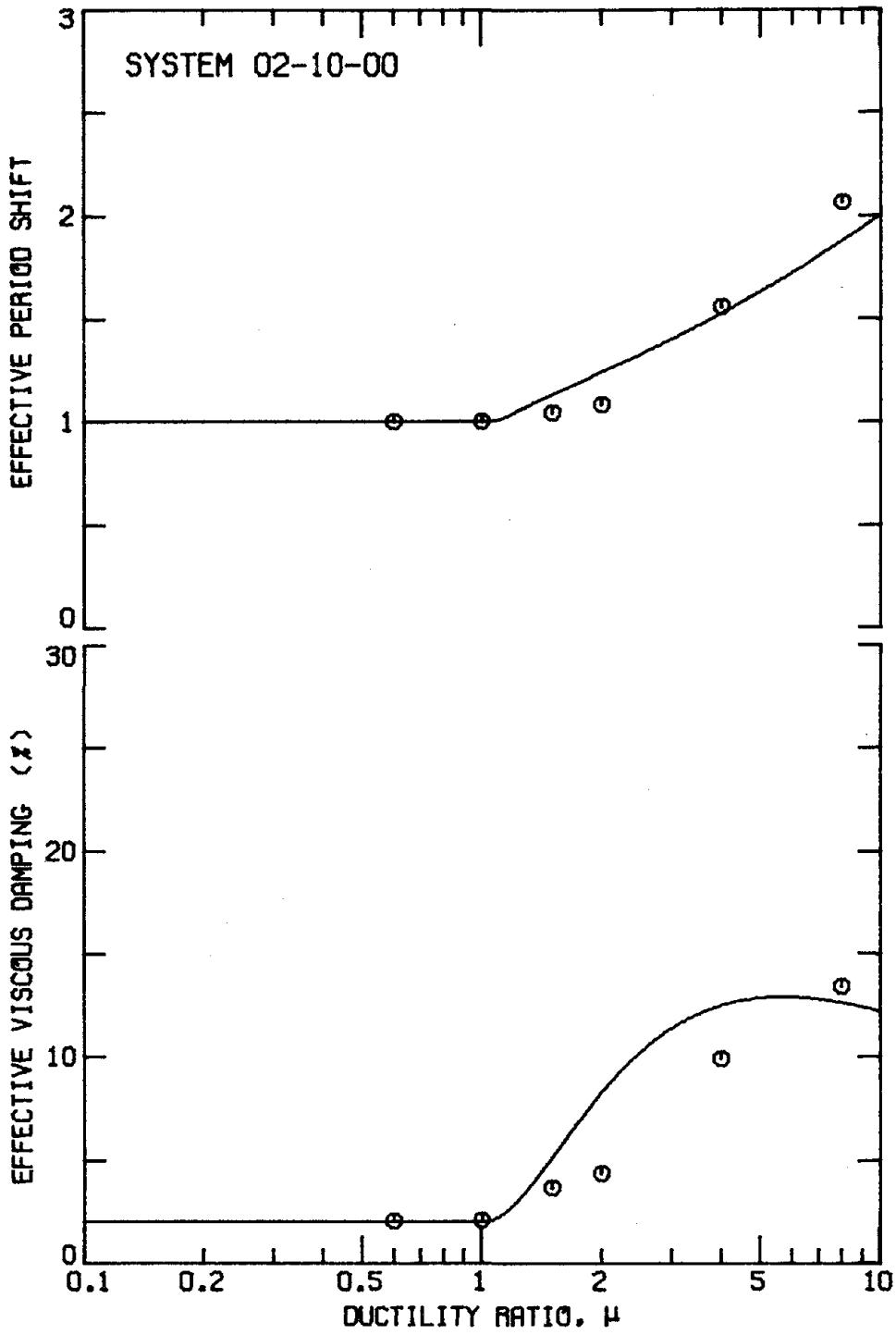

Figure 5.6. ASE Method Linear System Parameters for the 02-10-00 System with $\alpha = 5\%$ and $\zeta_0 = 2\%$.

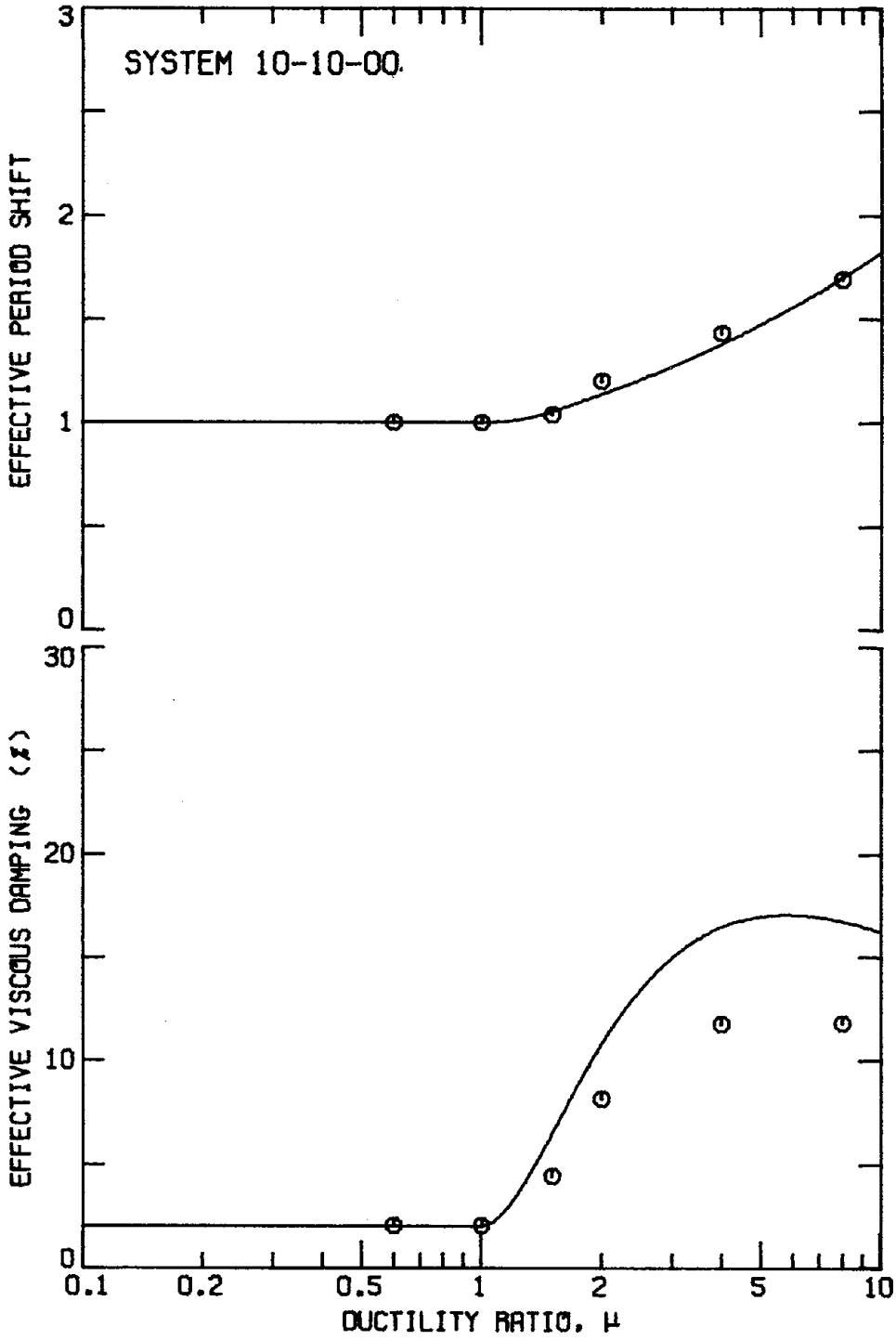

Figure 5.7. ASE Method Linear System Parameters for the 10-10-00 System with $\alpha = 5\%$ and $\zeta_0 = 2\%$.

5.2.2 Spectral Displacement

As in section 5.1.2 for the BLH system, the effective linear system parameters are used to calculate the rms spectral error for the six systems considered in the present investigation. In Table 5.2 the effective period shift, the effective viscous damping and the rms spectral error are tabulated for the ASE method applied to the six systems considered at the six ductilities investigated. As noted in the last section, the ASE method does a much better job of estimating the effective linear system parameters and hence the spectral displacement for highly deteriorating systems than for non-deteriorating or slightly deteriorating systems. This is seen in the fact that $\mathcal{E}$ is generally less than 10% for the systems 02-06-10, 02-10-10 and 02-10-00 while it is as great as 30% for the BLH system. This may be due to the fact that the actual system behavior of nondeteriorating systems favors smaller amplitude oscillations. Hence, the weighting factor used in calculating the average stiffness and average energy dissipated should not be uniform but should decrease with increasing amplitude of response.

The rms value of the error does not provide any information about the sign of the error in estimating the spectral displacement. As mentioned in section 5.2.1, overestimating ζ_e should imply a nonconservative estimate of the spectral displacement. In Figs. 5.8-5.10 the spectral error, δ_i, is indicated for each nominal period for each ductility considered and for all six systems.

As mentioned previously, the ASE method almost always over-estimates the effective viscous damping and hence the estimated

TABLE 5.2

Comparison of ASE Method for Six Systems

		DUCTILITY RATIO, μ					
		0.6	1.0	1.5	2.0	4.0	8.0
BLH	T_e/T_0 =	1.000	1.000	1.0031	1.0082	1.274	1.551
	ζ_e (%) =	2.00	2.00	8.97	14.91	21.97	21.97
	$\mathcal{E}$ (%)	0.1	0.2	20.5	26.0	30.4	26.0
02-06-10	T_e/T_0 =	0.816	0.855	0.887	0.951	1.190	1.479
	ζ_e(%)	9.05	8.14	7.84	8.75	13.43	14.61
	$\mathcal{E}$ (%)	11.1	7.8	7.8	7.8	8.3	11.1
50-06-10	T_e/T_0 =	0.953	0.965	0.997	1.046	1.249	1.530
	ζ_e (%) =	3.93	3.57	8.69	13.28	19.87	20.23
	$\mathcal{E}$ (%) =	2.2	1.5	14.2	19.1	23.5	21.6
02-10-10	T_e/T_0 =	0.855	0.890	0.998	1.090	1.350	1.678
	ζ_e (%) =	8.14	6.63	8.01	9.57	11.40	10.93
	$\mathcal{E}$ (%) =	7.8	6.3	4.6	4.6	6.0	6.3
02-10-00	T_e/T_0 =	1.000	1.000	1.130	1.240	1.526	1.876
	ζ_e (%) =	2.00	2.00	5.11	8.25	12.48	12.59
	$\mathcal{E}$ (%) =	0.2	0.3	5.3	9.4	10.3	9.4
10-10-00	T_e/T_0 =	1.000	1.000	1.055	1.138	1.381	1.698
	ζ_e(%) =	2.00	2.00	6.47	10.80	16.48	16.73
	$\mathcal{E}$ (%) =	0.2	0.3	9.8	16.4	16.8	14.3

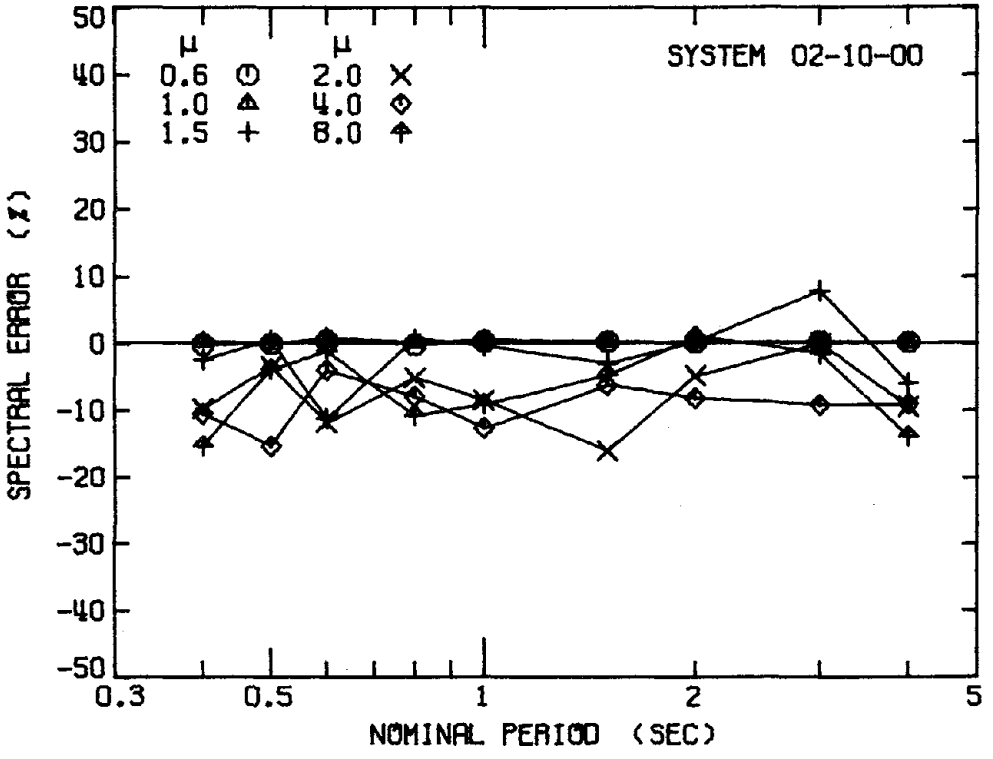

Figure 5.10a. Spectral Error - Average Spectra.

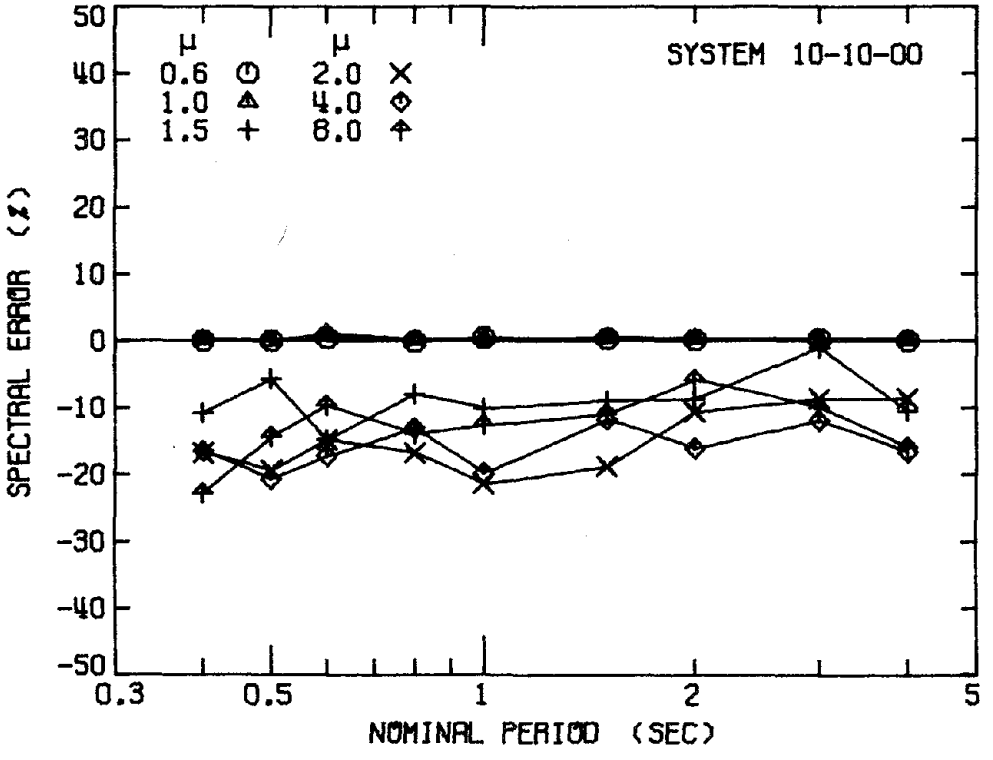

Figure 5.10b. Spectral Error - Average Spectra.

spectral displacement is almost always nonconservative. This is especially true for the nondeteriorating and slightly deteriorating systems such as BLH, 50-06-10 and 10-10-00.

The rms spectral error may disguise a strong period dependence of the spectral error but in this case the spectral error is generally independent of the nominal period. As indicated in Table 5.2 the spectral errors shown in Figs. 5.8-5.10 are less for highly deteriorating than for nondeteriorating or slightly deteriorating systems.

Up to this point the spectral error has been calculated using the relatively smooth average spectra. One might ask, how well the ASE method estimates the spectral displacement for a particular earthquake whose spectrum is not particularly smooth.

In Figs. 5.11-5.13 the spectral errors for the ELC earthquake are presented for all nominal periods, for all ductilities considered and for all six systems investigated. The increased scatter in the spectral error and the increased period dependence are the most obvious changes from the average spectrum cases of Figs. 5.8-5.10. However, the magnitude of the spectral error is still less than 50% in these cases.

Comparing Figs. 5.8-5.10 with Figs. 5.11-5.13 respectively, one can clearly see that the amplitude of the spectral error and the scatter of the spectral error about the rms spectral error is larger in the case of the ELC spectrum than the average spectrum. Generally speaking, the approximate spectral displacement will be more accurate when using a smooth linear response spectrum such

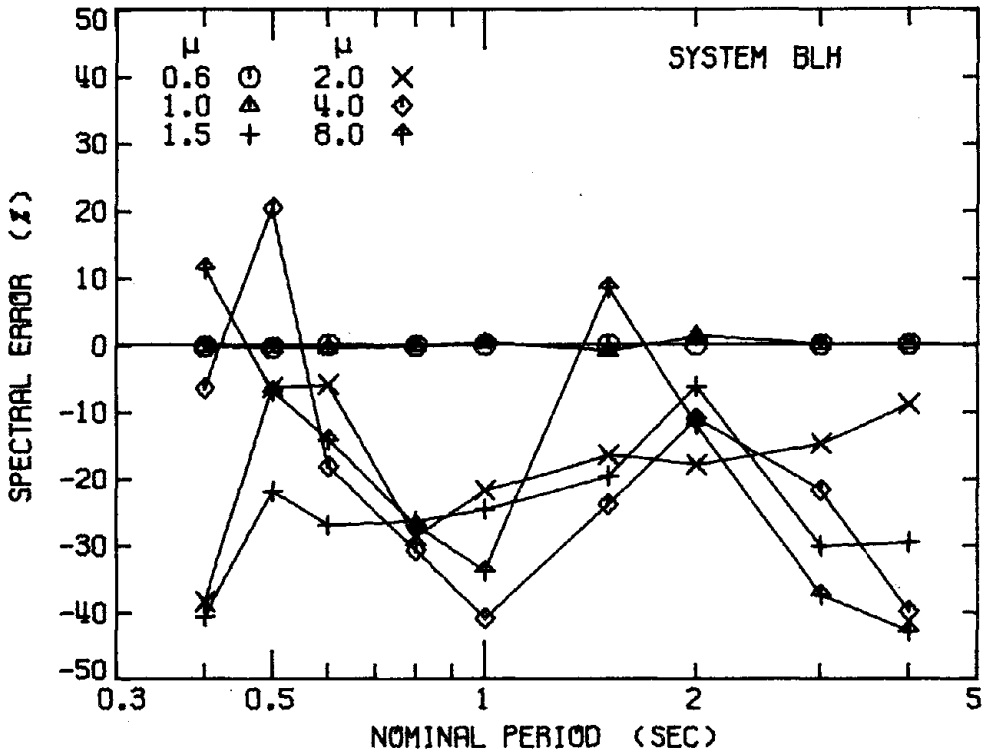

Figure 5.11a. Spectral Error - El Centro Spectra.

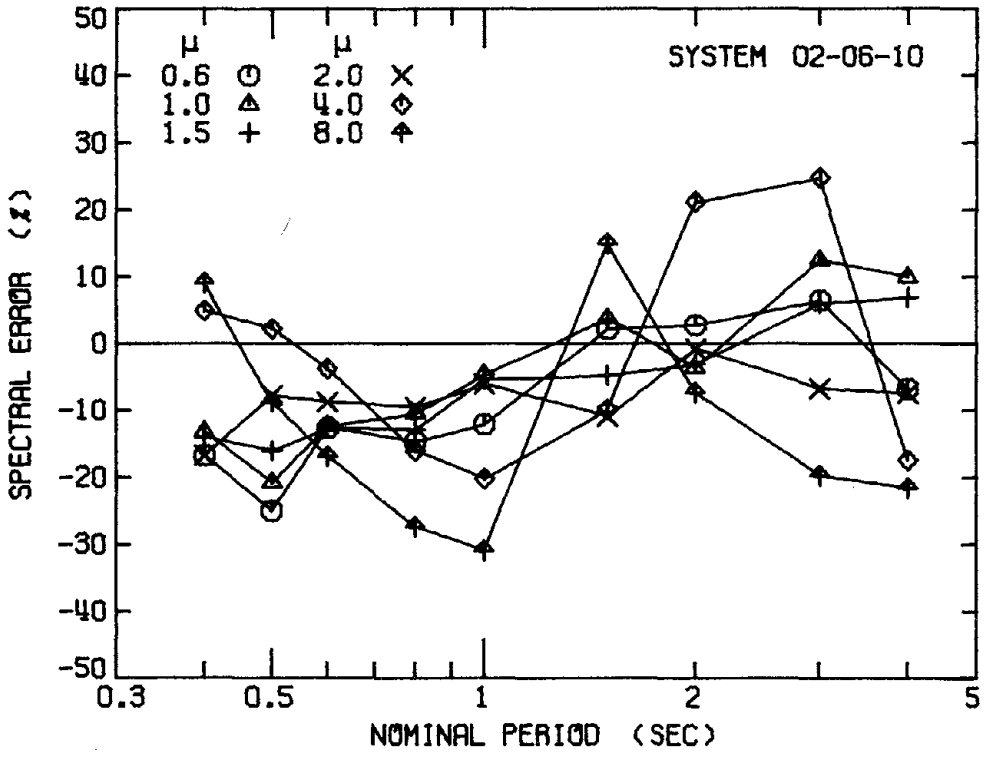

Figure 5.11b. Spectral Error - El Centro Spectra.

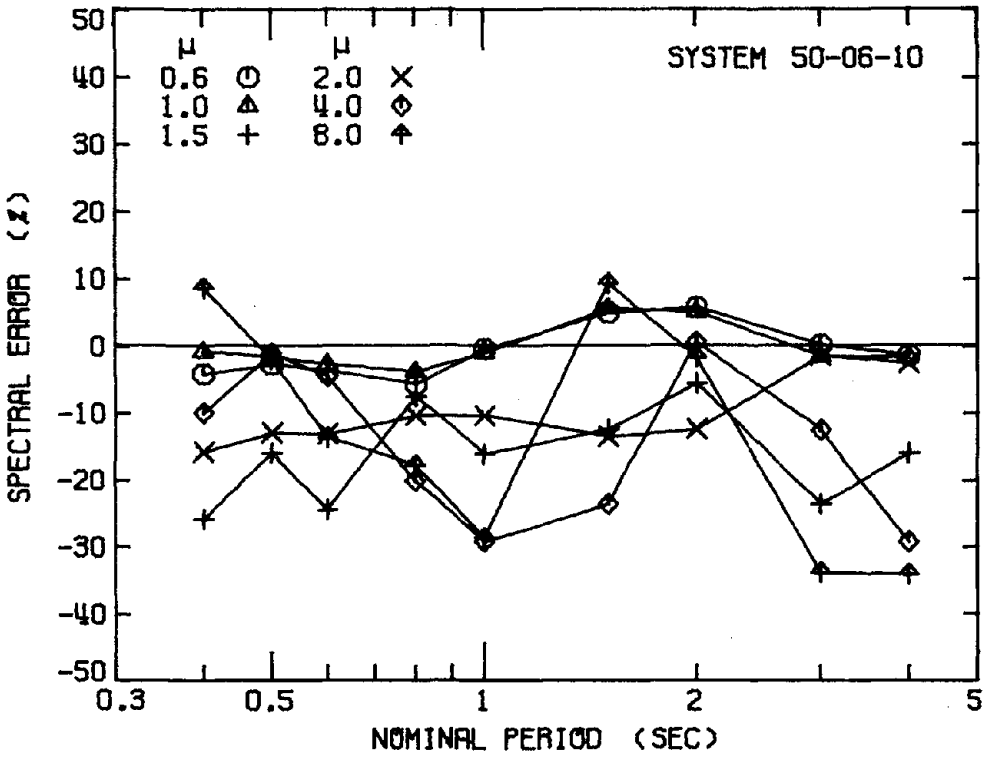

Figure 5.12a. Spectral Error - El Centro Spectra.

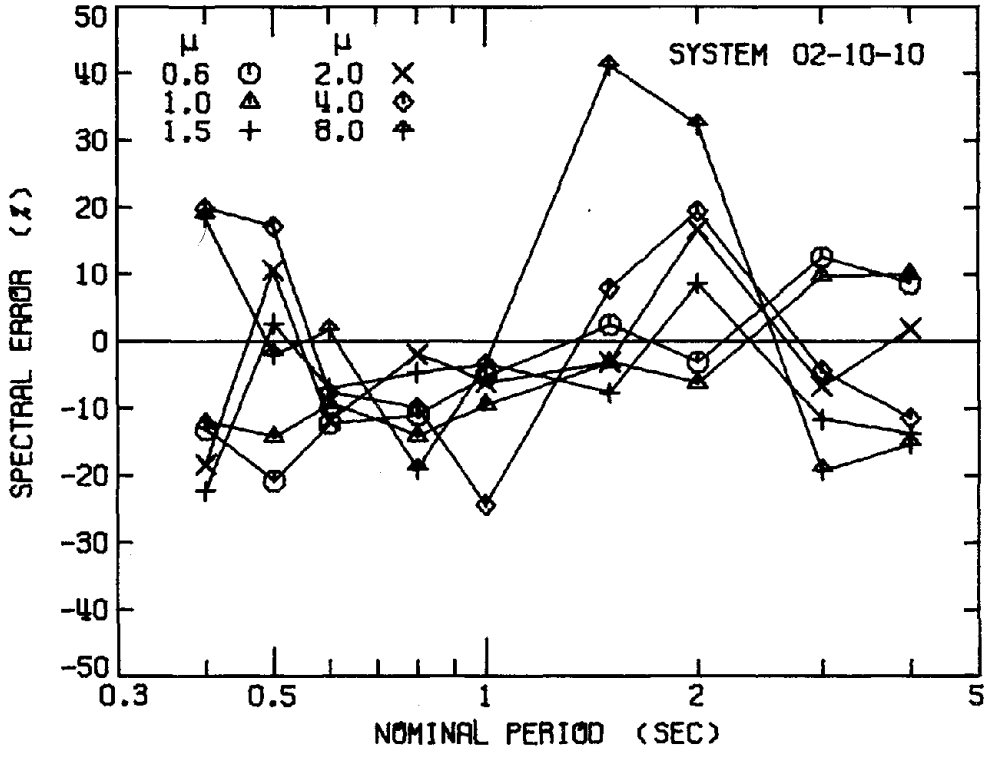

Figure 5.12b. Spectral Error - El Centro Spectra.

that maximum error in estimating the spectral displacement is less than 29%.

The fact that a nonlinear response spectrum can be generated from a linear response spectrum is more clearly indicated in Figs. 5.14a and b. In Fig. 5.14a the nonlinear response spectra corresponding to $\mu = 1, 2$ and 4 are indicated along with the linear response spectra corresponding to $\zeta = 2, 5$ and 10 percent damping. Shifting the linear response spectrum corresponding to the appropriate ζ_e by the appropriate T_e/T_0 from Table 5.3 the nonlinear response spectrum may be obtained for each value of μ as indicated in Fig. 5.14b. There is clearly a strong similarity between the analytically predicted and numerically determined response spectra. The approximate nonlinear response spectra and the numerical results for $\mu = 1$ and 2 show much better agreement than those for $\mu = 4$. However, even for $\mu = 4$ the numerical results show trends similar to a shifted linear response spectrum. It is encouraging to note that the strong peaks and valleys of the numerical results are matched reasonably well by the approximate nonlinear response spectra.

5.4 Comparison with Newmark-Hall Procedure

The Newmark-Hall procedure [33] for calculating an inelastic response spectrum from a linear response spectrum strictly speaking applies only to an elasto-plastic system. However, this method is sometimes applied to other systems for lack of a better method.

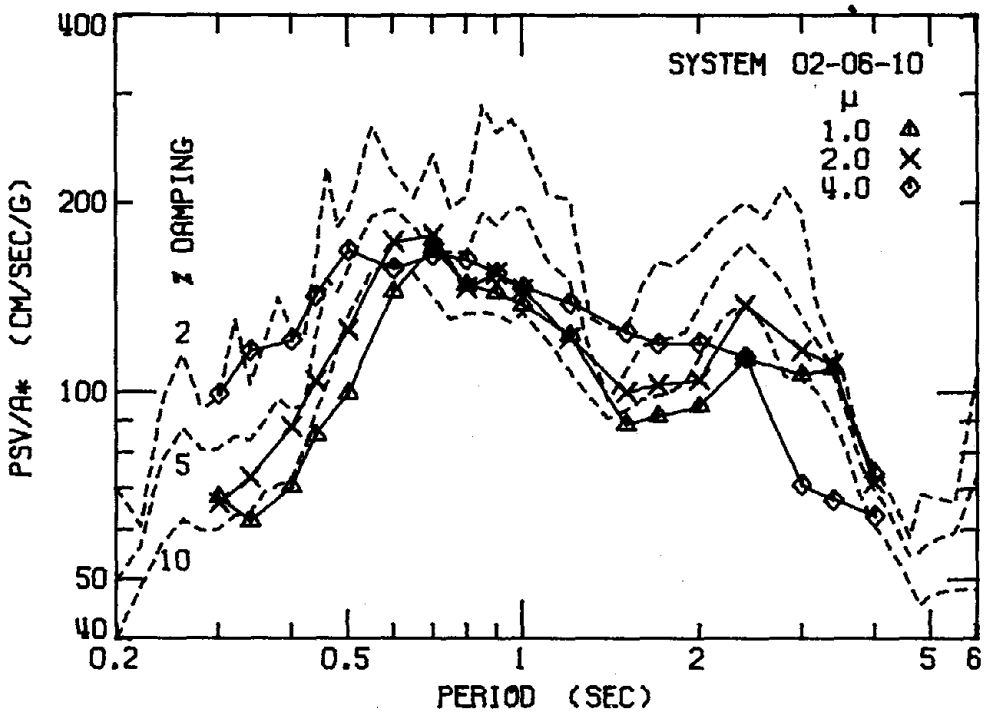

Figure 5.14a. Nonlinear and Unshifted Linear Spectra - El Centro.

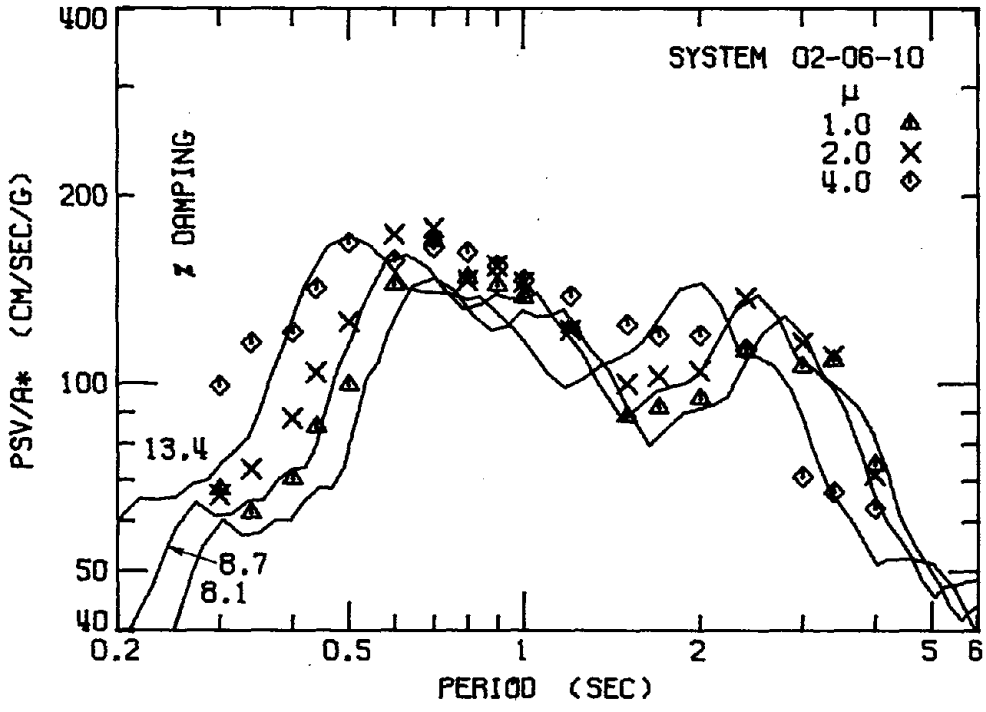

Figure 5.14b. Nonlinear and Shifted Linear Spectra - El Centro.

Comparison of the Newmark-Hall inelastic response spectrum with the numerical results for the six systems investigated herein indicates that the spectral error may be as great as 125% based on the average spectrum. The rms spectral error may exceed 88%. For the bilinear hysteretic system, the maximum error is 100%, but the rms error is less than 38%.

All nominal periods used in this investigation except $T_0 = 0.4$ seconds are in the region where the Newmark-Hall spectral displacement for the inelastic response spectrum is identical to that of the linear response spectrum for all ductilities. Hence, using the Newmark-Hall inelastic response spectrum, while it may be conservative, gives no information regarding the variation of response amplitude with ductility. In all cases, the results of the ASE method represent a significant improvement over the predictions of the Newmark-Hall inelastic spectrum.

CHAPTER VI

SUMMARY AND CONCLUSIONS

6.0 Summary

In Chapter II the existing approximate analytical methods for linearizing nonlinear systems are surveyed. Six methods are considered which are applicable to nondeteriorating systems with harmonic excitation. Three methods are discussed which are applicable to nondeteriorating systems with stationary random or earthquake excitation. Two methods are presented which are applicable to deteriorating systems with earthquake excitation. Of all of the methods considered only the average stiffness and energy method is applicable to both deteriorating and nondeteriorating systems.

Comparison of those methods which may be applied to nondeteriorating systems is made with reference to a bilinear hysteretic system with ratio of upper to lower slope of 0.05 and no viscous damping.

It is observed that the nonharmonic methods (SREL, APD and ASE) give effective period shifts which are smaller than the values obtained from the harmonic methods except RAM whose period shift is unity. It is also observed that the effective viscous dampings obtained from the harmonic methods increase more rapidly in the range $1 \leq \mu \leq 2$ than do the values obtained from the nonharmonic methods.

Presented in Chapter III is a model for general deteriorating and nondeteriorating systems. The model is physically motivated and based on a phenomenological description of the behavior of the

system during cyclic loading. The model is sufficiently well defined mathematically to make its use in dynamic analysis straightforward. Also the model is easily generalized and adapted to a variety of dynamic loading histories.

The model consists of three basic elements. The nature of the behavior of these three basic elements is discussed. The relationship between the element parameters and the system parameters is presented and six particular systems are discussed in detail. These six systems are used throughout the remainder of the investigation.

In Chapter IV the results of a numerical investigation are presented. First, the selection and scaling of the input earthquake accelerograms are discussed. Then, the method of numerical integration is presented. This method utilizes the special character of the piecewise linear restoring forces and uniformly digitized accelerograms to simplify the computer calculations.

The numerical results presented in Chapter IV are first presented as functions of the relative strength of the system excitation. Then, simple linear interpolation is used to obtain nonlinear response spectra for six values of ductility. It is observed that the nonlinear response spectra have the same trends as do linear response spectra of higher damping and shifted period. This fact is used to define effective linear system parameters T_m/T_0 and ζ_m which minimize the rms value of the error between the linear and nonlinear response spectra.

The absolute minimum values of the rms spectral error are generally less than 6%. Examination of the rms spectral error as a function of period shift and viscous damping indicates that there is an axis of minimum gradient (valley in the contour plots). Along the direction of the axis of minimum gradient the spectral error is minimized relative to any other direction.

Presented in Chapter V is a comparison of the approximate analytical methods of Chapter II and the numerical results of Chapter IV. First, the eight methods which may be applied to the BLH system are compared. Comparison of the effective linear system parameters reveals that the nonharmonic methods (SREL, APD and ASE) yield parameters which show better agreement with the numerical results than do the harmonic methods (HEL, DM, CCD, GS and RAM). Comparison of the spectral displacement also supports this conclusion. The fact that the error between the approximate response spectrum and the numerical results is dependent upon the relative position of effective linear system parameters with respect to the axis of minimum gradient is also demonstrated.

Also presented in Chapter V is a comparison of the average stiffness and energy method and the numerical results for all six systems considered in the present investigation. Comparison of the effective linear system parameters indicates that the ASE method overestimates the damping for nondeteriorating and slightly deteriorating systems. For highly deteriorating systems the effective linear system parameters obtained from the ASE method

show good agreement with the numerical results. Comparison of the spectral displacement shows that overestimating the viscous damping generally implies underestimating the spectral displacement. Although the approximate spectral displacement is generally smaller than the numerically calculated spectral displacement, in no case is the error greater than 40% for the average response spectrum and for highly deteriorating systems the error is less than 20%.

The effect of the smoothness of the linear response spectrum upon the accuracy of the approximate nonlinear response spectrum is also considered in Chapter V. Generally speaking, the smoother the linear response spectrum the better the agreement between the approximate nonlinear response spectrum and the actual response of the nonlinear system. Smoothness of the linear response spectrum minimizes the effect of inaccuracies in estimating the effective period shift.

An example of how the ASE method may be applied to obtain a nonlinear response spectrum is presented in Chapter V. Three nonlinear response spectra are presented and numerical results corresponding to eighteen nominal periods of oscillation are compared to these spectra. Even though the linear response spectrum is not very smooth the approximate response spectra show good agreement with the numerical results. Even in the case where agreement between the approximate response spectrum and the numerical results is poorest, it is obvious that the numerical results have trends similar to a shifted linear response spectrum.

The procedure proposed by Newmark and Hall for obtaining an inelastic response spectrum from a linear response spectrum is used to estimate the spectral displacement for the systems investigated. It is observed that large errors in the spectral displacement occur when this procecure is used to calculate the spectral displacement for deteriorating systems.

6.2 Conclusions

Based on the results of this investigation, it is concluded that the ASE method is a useful tool in estimating the peak earthquake response of deteriorating systems. This method is useful in estimating the peak earthquake response of nondeteriorating systems, even though it somewhat overestimates the effective viscous damping and hence underestimates the spectral displacement.

Further study should be done in the area of understanding why this method overestimates the effective viscous damping for non-deteriorating systems. Perhaps the weighting factor in calculating the average stiffness and average energy dissipated should be a function of the amplitude rather than a constant. Also the weighting of the contribution due to upper locus of response maxima relative to lower locus of response maxima might be investigated further. At the present there is no obvious reason to weight either contribution higher than the other.

Another area for further investigation is applying the ASE method to more deteriorating and nondeteriorating systems. The present model for the system may be used or an extension of the

present model to include more than one element from each of the three types of elements in the model. The ASE method is not restricted to the model used for the system. Hence, further investigation might include applying this method to other models for deteriorating systems.

The region of greatest variation in response as a function of system parameters occurs at short periods. There is relatively less variation for long periods. Hence, it would be instructive to extend the range of numerical results to nominal periods below $T_0 = 0.4$ seconds.

REFERENCES

1. Aoyama, H., Umemura, H., and Minamino, H., "Tests and Analyses of SRC Beam-Column Subassemblages," Proc. of the Sixth World Conference on Earthquake Engineering, New Delhi, India, 1977, Preprints, vol. 11, pp. 93-98.

2. Bertero, V.V., Popov, E.P., Wang, T.Y., and Vallenas, J., "Seismic Design Implications of Hysteretic Behavior of Reinforced Concrete Structural Walls," Proc. of the Sixth World Conference on Earthquake Engineering, New Delhi, India, 1977, Preprints, vol. 5, pp. 159-165.

3. Corley, W.G., and Hanson, N.W., "Design of Beam-Column Joints for Seismic Resistant Reinforced Concrete Frames," Proc. of the Fourth World Conference on Earthquake Engineering, Santiago, Chile, 1969, vol. 2, B-3, pp. 69-82.

4. Hanson, N.W. and Connor, H.W., "Seismic Resistance of Reinforced Concrete Beam Column Joint," Journal of the Structural Division ASCE, vol. 93, no. ST5, Proc. Paper 5537, Oct. 1967, pp. 533-560.

5. Gulkan, P. and Sozen, M.A., "Inelastic Response of Reinforced Concrete Structures to Earthquake Motions," Journal of ACI, vol. 71, no. 12, Dec. 1974, pp. 601-609.

6. Karlson, B.I., Aoyama, H., and Sozen, M.A., "Spirally Reinforced Concrete Columns Subjected to Loading Reversals Simulating Earthquake Effects," Proc. of the Fifth World Conference on Earthquake Engineering, Rome, Italy, 1973, pp. 803-810.

7. Krawinkler, H., and Popov, E.P., "Hysteretic Behavior of Reinforced Concrete Rectangular and T-Beams," Proc. of the Fifth World Conference on Earthquake Engineering, Rome, Italy, 1973, pp. 249-258.

8. Park, R., and Paulay, T., "Behavior of Reinforced Concrete External Beam-Column Joints under Cyclic Loading," Proc. of the Fifth World Conference on Earthquake Engineering, Rome, Italy, 1973, pp. 722-781.

9. Takeda, T., Sozen, M.A., and Nielson, N.N., "Reinforced Concrete Response to Simulated Earthquakes," Journal of the Structural Division ASCE, vol. 96, no. ST12, Dec. 1970, pp. 2557-2573.

10. Townsend, W.H., and Hanson, R.D., "Hysteresis Loops for Reinforced Concrete Beam-Column Connections," Proc. of the Fifth World Conference on Earthquake Engineering, Rome, Italy, 1973, pp. 1131-1134.

11. Umemura, H., Aoyama, H., and Takizawa, H., "Analysis of the Behavior of Reinforced Concrete Structures during Strong Earthquakes based on Empirical Extimation of Inelastic Restoring Force Characteristics of Members," Proc. of the Fifth World Conference on Earthquake Engineering, Rome, Italy, 1973, pp. 2201-2210.

12. Anagnostopoulos, S.A., "Nonlinear Dynamic Response and Ductility Requirements of Building Structures Subjected to Earthquakes," Department of Civil Engineering Research Report R72-54, M.I.T., Sept. 1972.

13. Chopra, A.K., and Kan, C., "Effects of Stiffness Degradation on Ductility Requirements for Multi-Story Buildings," International Journal of Earthquake Engineering and Structural Dynamics, vol. 2, no. 1, July-Sept. 1973, pp. 35-45.

14. Clough, R.W., and Johnston, S.B., "Effect of Stiffness Degradation on Earthquake Ductility Requirements," Proc. Japan Earthquake Engineering Symposium, Tokyo, 1966, pp. 227-232.

15. Imbeault, F.A., and Nielsen, N.N., "Effect of Degrading Stiffness on the Response of Multi-Story Frames Subjected to Earthquakes," Proc. of the Fifth World Conference on Earthquake Engineering, Rome, Italy, 1973, pp. 1756-1765.

16. Otani, S., "Inelastic Analysis of R/C Frame Structures," Journal of the Structural Division ASCE, vol. 100, no. ST7, 1974, pp. 1433-1449.

17. Ozaki, M., Ishizama, Y., and Yamazaki, Y., "Earthquake Response Prediction of Reinforced Concrete Buildings," Proc. of the Fifth World Conference on Earthquake Engineering, Rome, Italy, 1973, pp. 118-128.

18. Penzien, J., and Liu, S.C., "Nondeterministic Analysis of Nonlinear Structures Subjected to Earthquake Excitations," Proc. of the Fourth World Conference on Earthquake Engineering, Santiago, Chile, 1969, vol. 1, A-1, pp. 114-129.

19. Shibata, A., "Equivalent Linear Models to Determine Maximum Inelastic Response of Nonlinear Structures for Earthquake Motions," Proc. of the Fourth Japan Earthquake Engineering Symposium, 1975.

20. Shibata, A., and Sozen, M. A., "Substitute Structure Method for Seismic Design in R/C," Journal of the Structural Division ASCE, vol. 102, no. ST1, Jan. 1976, pp. 1-18.

21. Shibata, A., and Sozen, M.A., "Use of Linear Models in Design to Reflect the Effect of Nonlinear Response," Proc. of the Review Meeting, U.S.-Japan Cooperative Research Program in Earthquake Engineering with Emphasis on the Safety of School Buildings, Honolulu, Aug. 1975.

22. Shibata, A., and Sozen, M.A., "Substitute-Structure Method to Determine Design Forces in Earthquake-Resistant Reinforced Concrete Frames," Proc. of the Sixth World Conference on Earthquake Engineering, New Delhi, India, 1977, Preprints, vol. 5, pp. 167-172.

23. Iwan, W.D., "A Model for the Dynamic Analysis of Deteriorating Structures," Proc. of the Fifth World Conference on Earthquake Engineering, Rome, Italy, 1973, pp. 1782-1791.

24. Iwan, W.D., "The Response of Simple Stiffness Degrading Structures," Proc. of the Sixth World Conference on Earthquake Engineering, New Delhi, India, 1977, Preprints, vol. 3, pp. 121-126.

25. Bertero, V.V., Mahin, S.A., and Herra, R.A., "Problems in Prescribing Reliable Design Earthquakes," Proc. of the Sixth World Conference on Earthquake Engineering, New Delhi, India, 1977, Preprints, vol. 5, pp. 13-18.

26. Mahin, S.A., and Bertero, V.V., "Nonlinear Seismic Response Evaluation - Charaima Building," Journal of the Structural Division ASCE, vol. 100, no. ST6, June 1974.

27. Applied Technology Council, "An Evaluation of a Response Spectrum Approach to Seismic Design of Buildings," A Study Report for the N.B.S., Washington, D.C., Sept. 1974.

28. Anagnostopoulos, S.A., and Biggs, J.M., "An Evaluation of Response Spectra Design Procedures through Inelastic Analysis," Proc. of the Sixth World Conference on Earthquake Engineering, New Delhi, India, 1977, Preprints, vol. 5, pp. 103-108.

29. Blume, J.A., "Elements of a Dynamic-Inelastic Design Code," Proc. of the Fifth World Conference on Earthquake Engineering, Rome, Italy, 1973, pp. 2256-2265.

30. Isbell, J.E., and Biggs, J.M., "Inelastic Design of Building Frames to Resist Earthquakes," Department of Civil Engineering Research Report R74-36, M.I.T., May, 1974.

31. Veletsos, A.S., Newmark, N.M., and Chelapati, C.V. "Deformation Spectra for Elastic and Elastoplastic Systems Subjected to Ground Shock and Earthquake Motions," Proc. of the Third World Conference on Earthquake Engineering, Aukland and Wellington, New Zealand, 1965, vol. 12, pp. 663-682.

32. Veletsos, A.S., "Maximum Deformations of Certain Nonlinear Systems," Proc. of the Fourth World Conference on Earthquake Engineering, Santiago, Chile, 1969, vol. 2, A-4, pp. 155-170.

33. Newmark, N.M., and Hall, W.J., "Procedures and Criteria for Earthquake Resistant Design," Building Practices for Disaster Mitigation, Building Science Series 46, NBS, Feb. 1973, pp. 209-237.

34. Berg, Glen V., "A Study of the Earthquake Response of Inelastic Systems," Proc. of the 34th Convention of the Structural Engineers Association of California, Coronado, Calif., Oct. 1965, pp. 63-67.

35. Caughey, T.K., "Sinusoidal Excitation of a System with Bilinear Hysteresis," Journal of Applied Mechanics, vol. 27, Trans. ASME, vol. 82, Series E, 1960, pp. 640-643.

36. Caughey, T.K., "Random Excitation of a System with Bilinear Hysteresis," Journal of Applied Mechanics, vol. 27, no. 4, Dec. 1960, pp. 649-652.

37. Iwan, W.D., and Lutes, L.D., "Response of the Bilinear Hysteretic System to Stationary Random Excitation," Journal of the Acoustical Society of America, vol. 43, no. 3, March 1968, pp. 545-552.

38. Guerra, O.R., and Esteva, L., "Equivalent Properties and Ductility Requirements in Seismic Dynamic Analysis of Nonlinear Systems," Proc. of the Sixth World Conference on Earthquake Engineering, New Delhi, India, 1977, Preprints, vol. 5, pp. 263-268.

39. Hudson, D.E., "Equivalent Viscous Friction for Hysteretic Systems with Earthquake-Like Excitations," Proc. of the Third World Conference on Earthquake Engineering, Auckland and Wellington, New Zealand, 1965.

40. Iwan, W.D., "On Defining Equivalent Systems for Certain Ordinary Nonlinear Differential Equations," International Journal of Nonlinear Mechanics, vol. 4, 1969, pp. 325-334.

41. Iwan, W.D., and Yang, I.M., "Application of Statistical Linearization Techniques to Nonlinear Multi-Degree of Freedom Systems," Journal of Applied Mechanics, vol. 39, 1972, pp. 545-550.

42. Iwan, W.D., "A Generalization of the Concept of Equivalent Linearization," International Journal of Nonlinear Mechanics, vol. 8, no. 3, June 1973, pp. 279-287.

43. Jacobsen, L.S., "Steady Forced Vibration as Influenced by Damping," Transactions, ASME, vol. 52, Part 1, 1930, pp. APM 169-181.

44. Jacobsen, L.S., "Damping in Composite Structures," Proc. of the Second World Conference on Earthquake Engineering, Tokyo and Kyoto, Japan, vol. 2, 1960, pp. 1029-1044.

45. Jennings, P.C., "Periodic Response of a General Yielding Structure," Proc. of the American Society of Civil Engineers, vol. 90, no. EM2, 1964, pp. 131-166.

46. Jennings, P.C., "Equivalent Viscous Damping for Yielding Structures," Journal of the Engineering Mechanics Division ASCE, vol. 94, no. EM1, Feb. 1968, pp. 103-116.

47. Lutes, L.D., and Shah, V.S., "Transient Random Response of Bilinear Oscillators," Journal of the Engineering Mechanics Division ASCE, vol. 99, no. EM4, Aug. 1973, pp. 715-734.

48. Lutes, L.D., and Takemiya, H., "Random Vibration of Yielding Oscillator," Journal of the Engineering Mechanics Division ASCE, vol. 100, no. EM2, April 1974, pp. 343-358.

49. Rosenblueth, E., and Herrera, I., "On a Kind of Hysteretic Damping," Journal of the Engineering Mechanics Division ASCE, vol. 90, no. EM4, Aug. 1964, pp. 37-48.

50. Booton, R.C., Jr., "Nonlinear Control Systems with Random Inputs," IRE Transactions Circuit Theory, CT-1, 1954, pp. 9-18.

51. Caughey, T.K., "Equivalent Linearization Techniques," Journal of the Acoustical Society of America, vol. 35, no. 11, Nov. 1963, pp. 1706-1711.

52. Liu, S.C., "Earthquake Response Statistics of Nonlinear Systems," Journal of Engineering Mechanics Division ASCE, no. EM2, 1969, pp. 397-419.

53. Kobori, T., Minai, R., and Suzuki, Y., "Statistical Linearization Techniques of Hysteretic Structures to Earthquake Excitations," Bulletin of Disaster Prevention Research Institute, Kyoto University, vol. 23, no. 215, Dec. 1973, pp. 111-135.

54. Newmark, N.M., and Rosenblueth, E., Fundamentals of Earthquake Engineering, Prentice Hall, Inc., Englewood Cliffs, New Jersey, 1971.

55. Park, R., "Theorization of Structural Behavior with a View to Defining Resistance and Ultimate Deformability," Bulletin of the New Zealand Society for Earthquake Engineers, vol. 6, no. 2, June, 1973, pp. 52-70.

56. Iwan, W.D., "The Distributed Element Concept of Hysteretic Modeling and Its Application to Transient Response Problems," Proc. of the Fourth World Conference on Earthquake Engineering, Santiago, Chile, 1969, vol. 2, A-4, pp. 45-47.

57. Blume, J.A., Newmark, N.M., and Corning, L.H., Design of Multi-Story Reinforced Concrete Buildings for Earthquake Motion, Portland Cement Assn., Chicago, 1971, pp. 92-113.

58. U.S. Atomic Energy Commission Regulatory Guide 1.60, "Design Response Spectra for Seismic Design of Nuclear Power Plants," 1973.

59. Newmark, N.M., Blume, J.A., and Kanwar, K.K., "Design Response Spectra for Nuclear Power Plants," ASCE Structural Engineering Meeting, San Francisco, April 1973.

60. Newmark, N.M., Consulting Engineering Services, "A Study of Vertical and Horizontal Earthquake Spectra," Urbana, Ill. USAEC Contract No. AT(49-5)-2667, WASH-1255, April 1973.

61. Blume, J.A. and Associates, "Recommendations for Shape of Earthquake Response Spectra," San Francisco, Ca., USAEC Contract No. AT(49-5)-3011, WASH-1254, Feb. 1973.

62. Iwan, W.D., "Digital Calculation of Response Spectra and Fourier Spectra," unpublished note, California Institute of Technology, Pasadena, Ca.

63. Guttman, I., Wilkes, S.S., and Hunter, J.S., Introductory Engineering Statistics, John Wiley & Sons, Inc., New York, 1965, pp. 384-391.